Jens Langelage

Phase transitions in finite temperature lattice QCD from strong coupling expansions

-2009-

Theoretische Physik

Phase transitions in finite temperature lattice QCD from strong coupling expansions

Inaugural-Dissertation
zur Erlangung des Doktorgrades
der Naturwissenschaften im Fachbereich Physik
der Mathematisch-Naturwissenschaftlichen Fakultät
der Westfälischen Wilhelms-Universität Münster

vorgelegt von
Jens Langelage
aus Mettingen
-2009-

Dekan:	Prof. Dr. Johannes P. Wessels
Erster Gutachter:	Prof. Dr. Owe Philipsen
Zweiter Gutachter:	Prof. Dr. Gernot Münster
Tag der mündlichen Prüfung:	.....
Tag der Promotion:	.....

Selbständigkeitserklärung

Hiermit versichere ich, die vorliegende Doktorarbeit selbständig angefertigt und keine anderen als die angegebenen Hilfsmittel verwendet zu haben.

Jens Langelage

Münster, Oktober 2009

The Force is strong with this one...
Darth Vader

Contents

Abstract

In this thesis we investigate finite temperature phase transitions in lattice gauge theories using strong coupling expansions. Matter of particular interest is the deconfinement transition from a hadronic phase to a plasma phase consisting of quarks and gluons. Beginning with pure $SU(N)$ gauge theories, we finally investigate full lattice QCD and calculate strong coupling series expansions of observables like the free energy density and the Polyakov loop susceptibility. Using series extrapolation techniques we obtain estimates for the critical parameters of the phase transition in good agreement with Monte Carlo results. Of particular significance is the calculation of an effective Polyakov loop action.

Besides this we are able to derive the validity of the hadron resonance gas model in the strong coupling and heavy quark mass region from a first principles calculation. Another result which we obtain from a strong coupling expansion is the full β correction to the strong coupling limit of lattice QCD. This could be used in future investigations to make a step towards a calculation of thermodynamic properties of QCD at finite density μ, even when it is not small compared to the temperature.

Zusammenfassung

In dieser Arbeit untersuchen wir Phasenübergänge in Gittereichtheorien bei endlichen Temperaturen. Von besonderer Bedeutung ist dabei der Deconfinement-Übergang der hadronischen Phase in ein aus Quarks und Gluonen bestehendes Plasma. Beginnend mit reinen $SU(N)$ Eichtheorien, werden wir schließlich die volle Gitter-QCD untersuchen und Starkkopplungsentwicklungen von Observablen wie der freien Energiedichte and der Polyakov-Loop-Suszeptibilität berechnen. Unter Benutzung von Reihenextrapolationstechniken erhalten wir Näherungswerte für die kritischen Parameter des Phasenübergangs, die gut mit Monte Carlo Resultaten übereinstimmen. Von besonderer Bedeutung ist dabei die Berechnung einer effektiven Polyakov-Loop-Wirkung.

Des Weiteren haben wir die Gültigkeit des Hadron-Resonanz-Gas Modells in der Region starker Kopplung und schwerer Quarks abgeleitet. Ein weiteres Resultat, aus einer Starkkopplungsentwicklung ist die volle β-Korrektur zum Starkkopplunglimes der Gitter-QCD. Dieser Ausdruck könnte in späteren Untersuchungen einen Schritt in Richtung der Berechnung von thermodynamischen Eigenschaften bei endlicher Dichte μ darstellen, wenn μ nicht klein im Vergleich zur Temperatur ist.

1 Introduction

The current understanding of elementary particle physics is based on the standard model. Matter fields are described by three families of quarks and leptons, which interact with strong, weak and electromagnetic forces, depending on the particle. The latter two forces can be unified to the electroweak interaction, where the $SU(2)_L \otimes U(1)_Y$ gauge symmetry is broken down to the $U(1)_{EM}$. This is believed to happen via the Higgs mechanism and the search for the necessary Higgs boson is one of the most famous physical problems of today. In principle one also has to consider gravitation, but this can be neglected at the energy scales currently reachable in particle physics.

In this thesis we are dealing with the strong interaction, especially at finite temperature. Strong interactions are described by an $SU(3)_c$ gauge symmetry, mediated by 8 gauge bosons, so-called gluons. The corresponding theory is named Quantum Chromodynamics (QCD) [1]. At zero and small temperatures all matter must form singlets under the corresponding gauge transformations. This is due to the experimental non-observation of coloured states in nature. Nevertheless, another property of QCD called asymptotic freedom [2, 3] leads to the suggestion that at higher temperatures the binding of quarks and gluons into hadrons weakens and that there exists some deconfinement mechanism, which results in the formation of the quark-gluon plasma [4–6]. In this new state of matter we can have unbounded quarks and gluons. With several experiments being built to observe this exotic matter (e.g. at RHIC, LHC, FAIR), it is also of importance to investigate the underlying theory. One of the most successful approaches to obtain this is to discretize spacetime and to formulate the theory on a lattice [7]. Then, one can try to solve the theory numerically and indeed in the last years one has reached the stage where lattice QCD simulations are able to make predictions [8].

In this work, we want to present a different approach to finite temperature lattice QCD, that is purely analytical and well tested in spin models: series expansions and extrapolation techniques [9]. High and low temperature expansions have a long history, e.g. for the Ising model, where some of the best estimates for critical parameters are obtained from them. This is due to the relatively simple generation of the series expansion. In QCD this is much more difficult. Nevertheless we will show how to derive series expansions for some quantities of interest and that these really lead to some qualitatively, and in some cases quantitatively good results.

We will start investigating the pure $SU(2)$ gauge group, which, although not the gauge group of QCD, shares some important properties like asymptotic freedom with it and can be seen as a model suitable for testing the series

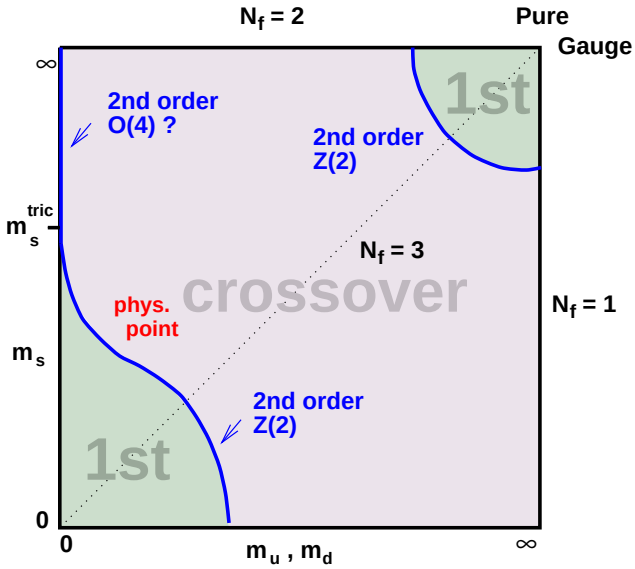

Figure 1: Schematic overview of the $N_f = 2 + 1$ phase diagram for finite temperature QCD, from [10].

expansion approach. Later we will continue with $SU(3)$, that corresponds to a theory with static quarks and finally we will study full QCD with the proper gauge group and dynamical quarks. Of particular interest is the QCD phase diagram, which can be seen in fig. (1). At the order of the QCD phase transitions $\mathcal{O}(200\text{MeV})$, the heavier quarks c, b, t can be neglected to a very good approximation, thus one is interested in the $N_f = 2+1$ phase diagram. Here one sets $m_u = m_d = m$ since both are very light compared to the QCD scale of about several hundred MeV. In the phase diagram there are two regions with first order phase transitions, one at large and one at small quark masses. It is the first one, the deconfinement transition which is interesting to us in this context. The latter one is the chiral phase transition.

As one can see in fig. (1), when decreasing the quark masses m or m_s one gets from the first order region to a crossover region, where all thermodynamic quantities stay finite. The boundary between these two regions is a critical line with second order phase transitions in the universality class of the 3D Ising model [11]. In the following chapters we will introduce methods to investigate this region with series expansions.

2 Quantum field theory in the continuum

In this chapter we want to present some aspects of quantum field theory. More precisely, we deal with its Euclidean formulation, which is suitable for a later lattice conversion. After shortly introducing zero temperature field theory [12], we want to consider thermodynamic properties of quantum field theories and especially of QCD. The topics of the finite temperature sections include the definition of thermodynamic observables, calculational methods and a section about phase transitions. More details about finite temperature field theory in general can be found in [13], and we have adjusted our notations to this textbook.

2.1 Partition function at zero temperature

Important quantities to calculate in quantum field theory are vacuum expectation values, which can be written in the path integral formalism as

$$\langle \mathcal{O} \rangle = \frac{1}{Z} \int \mathcal{D}\left[\overline{\psi}, \psi, A_\mu\right] \mathcal{O} \exp\Big(- S\left[\overline{\psi}, \psi, A_\mu\right] \Big), \tag{1}$$

where the partition function Z is given as

$$Z = \int \mathcal{D}\left[\overline{\psi}, \psi, A_\mu\right] \exp\Big(- S\left[\overline{\psi}, \psi, A_\mu\right] \Big). \tag{2}$$

The integration variables are bosonic gauge fields A_μ and fermionic fields $\psi, \overline{\psi}$. The latter ones are Grassmann variables, which means they are anti-commuting

$$\{\psi, \psi\} = 0 = \left\{\overline{\psi}, \overline{\psi}\right\}. \tag{3}$$

The properties of the physical system are encoded in these degrees of freedom and their interactions, which enter the calculation via the action

$$S\left[\overline{\psi}, \psi, A_\mu\right] = \int d^4x \mathcal{L}. \tag{4}$$

We are interested in QCD and consequently consider the Lagrangian

$$\mathcal{L} = \overline{\psi}_{c_1,f} \big(\gamma_\mu D_\mu^{c_1 c_2} + m_f\big) \psi_{c_2,f} + \frac{1}{4} F^a_{\mu\nu} F^a_{\mu\nu}. \tag{5}$$

Colour indices of the fundamental representation c_1 and c_2 run from 1 to 3 and those of the adjoint representation from $a = 1$ to 8. Spacetime indices μ and ν run from 0 to 3, where 0 stands for the temporal direction. Flavour

indices run from $f = 1$ to 6. An important limit is pure Yang-Mills theory, which can be obtained from QCD by increasing all quark masses to infinity

$$\mathcal{L}_{YM} = \frac{1}{4} F^a_{\mu\nu} F^a_{\mu\nu}. \tag{6}$$

The field strength tensor and the covariant derivative depend on the gauge field A_μ as follows

$$\begin{aligned} F^a_{\mu\nu} &= \partial_\mu A^a_\nu - \partial_\nu A^a_\mu + g f^{abc} A^b_\mu A^c_\nu, & (7) \\ D_\mu &= \partial_\mu - i g A^a_\mu T^a. & (8) \end{aligned}$$

The matrices T^a are the generators of the gauge group and satisfy

$$\begin{aligned} \left[T^a, T^b\right] &= i f^{abc} T^c \\ \text{tr}\left(T^a T^b\right) &= \frac{1}{2}\delta^{ab}, & (9) \end{aligned}$$

where the f^{abc} are the real and antisymmetric structure constants of the gauge group. The factor g is the coupling constant and describes the strength of the interaction.

2.2 Finite-temperature field theory

Among the physical systems where strong interactions at finite temperature and density play a role are heavy ion collision experiments (e.g. at RHIC, LHC, FAIR), the early universe and compact stars. Thus it is important to gain theoretical knowledge about observables like the equation of state which can be compared to experiments. Here we want to present the basics of the theoretical access.

2.2.1 Thermodynamic variables

In thermodynamics one usually considers a physical system consisting of a macroscopic number of particles N in a volume V, which is in contact with a heat bath at some temperature T. To describe this situation theoretically one can use the canonical ensemble, where V and N are fixed and the system exchanges energy with the heat bath. If we also allow for particle exchange with the heat bath, it is the grand canonical ensemble that is used to describe the system. In the following we will consider the grand canonical partition function

$$Z = \text{tr}\, \exp\left[-\frac{\left(\hat{H} - \mu_i \hat{N}_i\right)}{T}\right], \tag{10}$$

where $\hat{H}$ is the quantum Hamiltonian of the underlying theory, $\hat{N}_i$ stands for every conserved number operators and the μ_i are corresponding to chemical potentials. Thermal expectation values of physical observables can be calculated as follows

$$\langle \mathcal{O} \rangle = \frac{\mathrm{tr}\rho\mathcal{O}}{\mathrm{tr}\rho}, \tag{11}$$

where ρ is the density matrix

$$\rho = \exp\left[-\frac{(\hat{H} - \mu_i N_i)}{T}\right]. \tag{12}$$

From the partition function, which depends on the microscopic degrees of freedom, we can deduce the macroscopic properties of the physical system by

$$\begin{aligned} P &= \frac{\partial}{\partial V}\big(T \ln\, Z\big), & (13)\\ N_i &= \frac{\partial}{\partial \mu_i}\big(T \ln\, Z\big), & (14)\\ S &= \frac{\partial}{\partial T}\big(T \ln\, Z\big), & (15)\\ E &= -PV + TS + \mu_i N_i. & (16) \end{aligned}$$

That means knowledge of the partition function is the crucial feature to gain information about thermal properties. In the following from these quantities, we will only need the pressure P, which in homogeneous systems can be written as

$$P = \frac{T}{V} \ln\, Z = -f. \tag{17}$$

We see that the pressure is just the negative free energy density f. Hence our task is to calculate the partition function. Usually this cannot be done exactly and approximation schemes have to be used.

2.2.2 Partition function at finite temperature

In the last section we introduced the grand canonical partition function of QCD. Its path integral representation reads

$$Z = \int \mathcal{D}\left[(A_\mu)_p(\overline{\psi}\psi)_a\right] \exp\left(-\int_0^{1/T} d\tau \int d^3x \Big(\mathcal{L} - \overline{\psi}\mu\gamma^0\psi\Big)\right). \tag{18}$$

This formula needs some explanation. As in the zero temperature case the integration covers all field configurations of the gauge fields A_μ as well as the quark and antiquark fields ψ and $\overline{\psi}$. At finite temperature these fields are constrained by periodic boundary conditions for bosons and antiperiodic boundary conditions for fermions, which is indicated by indices in the integration measure. In the exponential function we recognize the action, which is a functional of the QCD Lagrangian. We remark that we have not fixed a gauge, which is usually done with the method of Faddeev and Popov [14]. This is a necessity when calculating a perturbative expansion.

We also notice that the Euclidean time integral is restricted to the compact interval $[0, 1/T]$. This is the reason why we call the quantity in eq. (2) a partition function. It is just the $T, \mu = 0$ limit of (18). (Anti-)periodic boundary conditions come into play due to the trace operation in

$$Z = \text{tr } \exp\left(-\frac{\hat{H}}{T}\right), \tag{19}$$

and to get correct statistics for bosons and fermions. They read

$$\text{periodic:} \quad A_\mu(\tau, \vec{x}) = A_\mu(\tau + 1/T, \vec{x}), \tag{20}$$

$$\text{anti-periodic:} \quad \psi(\tau, \vec{x}) = -\psi(\tau + 1/T, \vec{x}). \tag{21}$$

Although it is not a topic in this thesis, we want to say a few words about the shortcomings of weak coupling perturbation theory at finite temperature, as this motivates us to consider strong coupling expansions. Naively one would suggest perturbation theory at very high temperatures to work well because of asymptotic freedom. Indeed, this is the case, but only for asymptotic high temperatures, much larger than the order $\mathcal{O}(200 \text{ MeV})$, where the QCD transitions are supposed to take place. The application of perturbative results to intermediate temperatures is further conceptually hampered by the Linde problem [15]. Also perturbation series are just asymptotic expansions, whereas strong coupling expansions on the lattice have been shown to have a finite radius of convergence.

2.3 Phase transitions

In this subsection we want to present those facts about phase transitions, that are important for the understanding of this work. At first we would like to classify first and second order phase transitions and the implications for series expansions. Afterwards we give some information about the deconfinement transition, which is the one we are investigating within this thesis.

2.3.1 Classification of phase transitions

Usually one distinguishes between a first and a second order phase transition, which are also called discontinuous and continuous. Whereas the former show discontinuities in the first partial derivatives of thermodynamic potentials like the free energy density, the latter are continuous and only higher partial derivatives are discontinuous [16]. In our context the more interesting phase transitions are the second order ones. They have a diverging correlation length, leading to power law behaviour for several quantities, like e.g. for a ferromagnetic system

$$\text{specific heat:} \qquad C(T) = -T^2 \left(\frac{\partial^2 F}{\partial T^2} \right) \sim |t|^{-\alpha}, \tag{22}$$

$$\text{susceptibility:} \qquad \chi(T) = -\frac{1}{V} \left(\frac{\partial^2 G}{\partial H^2} \right) \sim |t|^{-\gamma}, \tag{23}$$

where F is the free energy density, G is the Gibbs free enthalpy and H is an external magnetic field. There exist more observables displaying such behaviour [17], but in the following we will only need these two. The parameter t is called the reduced temperature and is defined as

$$t \equiv \frac{T_c - T}{T_c}, \tag{24}$$

with T_c being the critical temperature. These power laws show universal behaviour. This means different physical systems that undergo second order phase transitions behave in the same way near their critical parameters if they are defined in the same number of spacetime dimensions, share the same global symmetries and their order parameters have the same number of components. The importance for our work lies in the fact that equations (22) and (23) give us important knowledge of the behaviour of the functions near the phase transition.

There is a third type of transition where all thermodynamic variables stay finite and analytic. Thus it is actually no real phase transition and called a crossover. Nevertheless even for a crossover there can be rapid changes in the order parameter and other thermodynamic variables, which can be used to define pseudocritical temperatures. A typical example for this situation is the water-vapour transition at pressures beyond that of the critical point.

2.3.2 Deconfinement phase transition

The deconfinement transition means a change from a hadronic phase to a plasma phase, dominated by quarks and gluons, which in this case is induced

by increasing temperature. A crucial property of QCD, asymptotic freedom, is thought to be responsible for this mechanism. At low temperatures, quarks and gluons are confined into hadrons, which are colour singlets. Asymptotic freedom, on the other hand, states that for very large temperatures, the running coupling should be very small and quarks and gluons should behave as an ideal gas of quasi-free particles.

From Monte Carlo simulations [8] it is known that QCD undergoes no real phase transition at zero chemical potential, but a rapid crossover and there are signs that this remains true for chemical potentials up to $\mu_B \sim 500$ MeV [18]. On the contrary, pure Yang-Mills theories are supposed to have second order (in the case of $SU(2)$) or first order (for $SU(N > 3)$) deconfinement transitions [19, 20].

3 Lattice field theory

In this chapter we introduce Euclidean lattice field theory as far as needed in the context of this thesis. We mostly use the notations as in [21], to which we also refer as a more detailed guide to lattice field theory.

3.1 The lattice

Lattice gauge theories were first considered by Wilson [7] in 1974. In the path integral formulation they have the advantage of giving a mathematically rigorous definition to the expectation value

$$\langle \mathcal{O} \rangle = \frac{1}{Z} \int \mathcal{D}\left[\overline{\psi}, \psi, A_\mu\right] \mathcal{O} \exp\Big(- S\left[\overline{\psi}, \psi, A_\mu\right] \Big), \tag{25}$$

which in the continuum has a formal meaning and is indeed formulated as the limit of a time-discretized version of the path integral.

We formulate the theory on a $(3+1)$ dimensional hypercubic lattice with lattice spacing a. The lattice volume is given by $\Omega = L_s^3 L_\tau = N_s^3 N_\tau a^4$, where $L_s^3 = V$ is the spatial volume and L_τ is the temporal lattice extent. The corresponding numbers of lattice points are given by N_s and N_τ. Usually, we set $a = 1$ and do not distinguish between L and N. With a discretized spacetime lattice we have to define a lattice derivative operation which becomes the usual derivative in the continuum. This can be done by considering finite differences instead of the derivative. After introducing proper lattice gauge and fermion fields and expressing ordinary derivatives as finite differences, one ends with a lattice action that should go to its continuum version when $a \to 0$. This correct naive continuum limit is the first condition to be ensured when discretizing the physical system.

An important feature of introducing a spacetime lattice is that it provides a valid regularization scheme. That means for non-zero lattice spacing a all momenta have an ultraviolet cut-off $\Lambda = \frac{\pi}{a}$. The most important fact is that this scheme is not tied to perturbation theory. In fact the lattice is so far the only known non-perturbative regulator. Nevertheless one can also use lattice perturbation theory. Although other schemes like dimensional regularization are more convenient for such calculations, lattice perturbation theory is able to provide insights for calculations near the continuum limit [22].

If one wants to use Monte Carlo simulations, introducing the lattice is crucial in order to have a finite number of degrees of freedom in a finite volume. The more computer power one can spend, the finer lattices and the larger volumes one can simulate. Fine lattices are important to arrive at

the continuum limit and large volumes are necessary to have a large enough physical system size.

3.2 Gauge action

We have already seen that the dynamics of pure gauge fields in the continuum are determined by the Yang-Mills action

$$S_{YM} = \frac{1}{4} \int dx^4 F^a_{\mu\nu} F^a_{\mu\nu}. \tag{26}$$

If one wants to translate this to the lattice, it is convenient to introduce the link variable

$$U_{x\hat{\mu}} \equiv \exp\left[-igaA^b_\mu T^b\right], \tag{27}$$

where we have explicitly displayed the lattice spacing a. In contrast to the gauge field A_μ, which is Lie algebra valued, this link variable is an element of the gauge group. It acts as a parallel transporter from one lattice site to a neighbouring one, thus having a factor of a. From the link variable one can construct the plaquette variable

$$U_p \equiv U_{x,\hat{\mu}} U_{x+\hat{\mu},\hat{\nu}} U_{x+\hat{\mu}+\hat{\nu},-\hat{\mu}} U_{x+\hat{\nu},-\hat{\nu}}, \tag{28}$$

where $\hat{\mu}, \hat{\nu}$ are unit vectors in the corresponding direction and we have set $a = 1$. In terms of this plaquette variable, one can write the action of pure lattice gauge theory as

$$S_g = -\frac{\beta}{2N} \sum_p \left(\mathrm{tr}\, U_p + \mathrm{tr}\, U_p^\dagger \right). \tag{29}$$

This is called Wilson's gauge action. Since the plaquette is a closed path on the lattice and due to the trace operation, this action is gauge invariant. For $a \to 0$ one can show that one arrives at the continuum result of the Yang-Mills action eq. (26). One expresses all link variables in the Wilson action as in eq. (27) and uses the Baker-Campbell-Hausdorff formula to obtain

$$S_g = -\frac{\beta}{4N} \sum_x a^4 \mathrm{tr}\, F_{\mu\nu}(x) F_{\mu\nu}(x) + \mathcal{O}(a^5). \tag{30}$$

For $a \to 0$ this coincides with the Yang-Mills action if one relates continuum coupling g and lattice coupling β via

$$\beta = \frac{2N}{g^2}. \tag{31}$$

In this limit the summation becomes an integral

$$\sum_x a^4 \longrightarrow \int d^4x. \tag{32}$$

There exist other actions, the only requirements being gauge invariance and the right continuum limit. In this work we consider Wilson's action for it is simplicits and dispersiveness. Finally we also want to compare our findings with Monte Carlo results and these have been mostly computed with Wilson's action.

3.3 Fermion action

Fermions on the lattice are a more difficult task. In the continuum the Euclidean free fermion action is given by [23]

$$S = \int d^4x \Big[\overline{\psi}(x)\gamma_\mu \partial_\mu \psi(x) + m\overline{\psi}(x)\psi(x)\Big]. \tag{33}$$

In order to get to a lattice version of this action, one puts the Grassmann variables onto the lattice sites $x = (x_0, x_1, x_2, x_3)$ and replaces the derivatives with finite differences:

$$S_L = \sum_{x,\mu} \overline{\psi}_x \gamma_\mu \Delta_\mu \psi_x + m \sum_x \overline{\psi}_x \psi_x. \tag{34}$$

The lattice version of the partial derivative can be defined as

$$\Delta_\mu \psi_n \equiv \frac{1}{2a}(\psi_{n+\hat{\mu}} - \psi_{n-\hat{\mu}}). \tag{35}$$

In this naive way of formulating a lattice fermion action one encounters the doubling problem. This can be seen by investigating the free fermion propagator [23]

$$\frac{1}{a}S_p = \frac{-i\gamma_\mu \sin(p_\mu a) + ma}{\sum_\mu \sin^2(p_\mu a) + m^2a^2}. \tag{36}$$

This quantity has 16 poles in the Brillouin zone instead of only one at the origin. This proliferation of fermionic degrees of freedom gets severe in an interacting theory, where these - unphysical - doublers are allowed to appear in loop diagrams. The Nielsen-Ninomiya theorem [24] states that it is impossible to have a chirally invariant, doubler-free, local, translation invariant,

bilinear fermion action on the lattice. Thus, by removing the doublers we have to violate one of these other properties.

From now on we only want to consider those two fermion formulations which circumvent the doubling problem and are most widely used: Wilson and staggered fermions. Both have advantages and disadvantages and we refer to the literature [25] for a proper discussion of these issues. Only for the sake of completeness we would like to mention other fermion formulations: Domain wall [26] and overlap fermions [27] share good chiral properties and thus avoid additive mass renormalization. Another formulation are Wilson twisted mass fermions [28], which are automatically $\mathcal{O}(a)$ improved at maximal twist. Only recently a formulation named Creutz fermions [29] has been introduced. It has a minimal number of doublers and these fermions are thus also called minimal doubled fermions. As Wilson and staggered fermions, these formulations have their advantages and drawbacks, but should eventually, in the continuum limit, describe the same physics. All these somewhat newer fermion formulations are technically more involved and thus not well suited for a series expansion approach.

3.3.1 Wilson fermions

Having encountered the doubling problem, Wilson introduced a dimension 5 operator into the action [7], which vanishes in the continuum limit by having an additional factor of a, but gives the doublers a mass term proportional to $\frac{1}{a}$, so that they become infinitely heavy in the continuum limit and thus decouple from physical quantities. Being a quite simple solution to the doubling problem, this trick has the disadvantage of explicitly breaking chiral symmetry. The masses of Wilson quarks are thus subject to additive mass renormalization. Since we will always keep a finite lattice spacing a, we do not have to care about these issues, but should of course keep them in mind. Wilson's formulation of lattice fermions is given as [21]

$$S_q = \sum_{f,x} \left\{ \overline{\psi}_{f,x}\psi_{f,x} - \kappa_f \sum_{\mu} \overline{\psi}_{f,x+\hat{\mu}} \left(1+\gamma_\mu\right) U_{x\mu}\psi_{f,x} \right\}, \tag{37}$$

where we have chosen the Wilson parameter r_f to be equal to 1 for each flavour f and have not displayed spin and colour indices. The full spin and colour structure of the terms reads

$$\begin{aligned} \psi_{f,x} &\equiv \psi_{\alpha,a,f,x}, \\ \overline{\psi}_{f,x} &\equiv \overline{\psi}_{\alpha,a,f,x}, \\ (1+\gamma_\mu) &\equiv (1+\gamma_\mu)_{\alpha\beta}, \\ U_{x\mu} &\equiv U_{ab,x\mu}, \end{aligned} \tag{38}$$

where $\alpha, \beta, \ldots$ are spin indices and $a, b, \ldots$ colour indices. Later we will sometimes drop these indices when there should be no confusion. In case of Wilson fermions we need all indices and in the staggered case all but the Dirac indices.

The Wilson parameter eliminates the doubling problem for the cost of spoiling chiral symmetry and multiplicative renormalizability. The quark mass parameters m_f have been traded for the hopping parameter κ_f by rescaling the fields. Their relation is given by

$$\kappa_f = \frac{1}{2m_f + 8}. \tag{39}$$

3.3.2 Staggered fermions

Another commonly used fermion formulation are staggered fermions. Here one uses a spin diagonalization transformation for naive fermions in order to reduce their number by a factor of 4 from 16 to 4. This transformation is defined by [23]

$$\begin{aligned} \psi_x &\rightarrow \Omega_x \psi'_x \\ \overline{\psi}_x &\rightarrow \overline{\psi}'_x \Omega^\dagger_x \\ \Omega_x &= \gamma_0^{x_0} \gamma_1^{x_1} \gamma_2^{x_2} \gamma_3^{x_3}, \end{aligned} \tag{40}$$

and with

$$\Omega^\dagger_x \gamma_\mu \Omega_{x+\hat{\mu}} = (-1)^{x_0 + \ldots + x_{\mu-1}} \equiv \alpha_{x,\mu} \tag{41}$$

one can write the staggered fermionic action as

$$S = m \sum_x \overline{\psi}_x \psi_x + \frac{1}{2} \sum_{x,\mu} \overline{\psi}_x \alpha_{x,\mu} \Big[U_{x\mu} \overline{\psi}_{x+\hat{\mu}} - U^\dagger_{x-\hat{\mu},\mu} \psi_{x-\hat{\mu}} \Big]. \tag{42}$$

In this way we have diagonalized the action in Dirac indices and have thus four equivalent copies. If we neglect the spinor index and consider only one component, we have reduced the number of continuum fermions from 16 to 4. We will use this fermion formulation only in the last chapter, where we calculate the β correction of the action to the strong coupling limit result of [30–32].

3.4 Calculational techniques

In this section we want to introduce two methods of calculating things on the lattice: Monte Carlo simulations and strong coupling expansions. There are other methods like weak coupling perturbation theory or effective theories, but we will not need them in the following.

3.4.1 Monte Carlo simulations

By far the most important and most widely used lattice techniques are Monte Carlo simulations. This is due to the fact that they provide a nonperturbative approach to quantum field theory and can be used for computing QCD numerically. Thus in principle we can calculate observables with arbitrary precision and we do not have to rely on the smallness of some expansion parameter. For nonabelian gauge theories at zero as well as finite temperature they are beginning to give results compatible to experiments. In a Monte Carlo approach one first integrates over fermions analytically, which can be done since the action is bilinear in the fermion action. This yields the quark determinant. Later we will show explicitly how to do this. The result is a partition function, where we have to integrate solely over gauge degrees of freedom

$$Z = \int [dU]\, e^{-S_g[U]} \det Q[U] = \int [dU]\, e^{-S_{eff}[U]}. \tag{43}$$

Starting with this partition function one generates gauge field configurations and calculates averages of the observable under investigation. This yields an estimate of this observable, whose error decreases with increasing number of different configurations. Thus one usually tries to get a large number of independent configurations. Depending on the observable there can be huge difficulties in doing so, see e.g. [25] for a review.

3.4.2 Strong coupling expansion

In contrast to continuum formulations of quantum field theories, on the lattice it is natural to consider strong coupling expansions rather than weak coupling perturbation theory. As one can see from Wilson's gauge action, for large couplings $g \gg 1$, the leading terms of the Taylor expansion of the exponentiated action should suffice to describe physics in this regime accurately. The major disadvantage of this method is that one wants to describe continuum physics, which is recovered as $g \to 0$, for $a \to 0$, keeping physical quantities fixed.

In the early days of lattice gauge theories, these expansions have been used to gain knowledge at zero as well as at finite temperatures, see e.g. [7, 33–39]. A commonly used simplification was the neglect of spacelike plaquettes and this really led to some qualitatively reasonable results. Nevertheless, this crude approximation made quantitative results to be questionable when leaving the strong coupling region. Throughout this work we will include spatial plaquettes.

3.5 Finite temperature and density on the lattice

In the last sections, we have introduced the lattice regularization and its notations. The lattice provides us with a large, but finite number of degrees of freedom, so that functional integrals are well defined. Here we want to introduce finite temperature and density on the lattice.

With T being the inverse of the imaginary time extent in the continuum, see eq. (18), it is not hard to obtain the lattice version of temperature

$$T = \frac{1}{L_\tau} = \frac{1}{N_\tau a}. \tag{44}$$

The boundary conditions on the lattice are given by

$$\begin{aligned} \text{periodic:} \qquad U_\mu(\tau, \vec{x}) &= U_\mu(\tau + N_\tau, \vec{x}) && (45) \\ \text{anti-periodic} \qquad \psi(\tau, \vec{x}) &= -\psi(\tau + N_\tau, \vec{x}). && (46) \end{aligned}$$

Taking these necessities of finite temperature field theory onto the lattice, it is straightforward to perform Monte Carlo simulations, at least in principle. Besides being quite expensive to simulate QCD, there is a more serious problem of Monte Carlo simulations that is the sign problem. This issue makes it rather impossible to simulate at finite chemical potential μ, when μ is not small compared to the temperature. Chemical potential on the lattice can be introduced as an additional factor on the temporal link variables [40]

$$\begin{aligned} U_0 &\rightarrow U_0 e^{a\mu} \\ U_0^\dagger &\rightarrow U_0^\dagger e^{-a\mu}. \end{aligned} \tag{47}$$

The problem with this simple prescription is that the quark determinant becomes complex, i.e.

$$\det Q = (\det Q)^* \tag{48}$$

does no longer hold in general. In this way the exponentiated quark determinant cannot be interpreted as a probability measure and standard Monte Carlo techniques fail. There are methods to circumvent this problem at small chemical potential and these are summarized e.g. in [11]. On the contrary, in an analytical approach chemical potential enters only as an additional parameter, which can take every value one wants to assign.

4 Free energy density of pure gauge theory

Consider the partition function

$$Z(\beta) = \int [dU] \exp\left(\frac{\beta}{2N} \sum_p \left(\operatorname{tr} U_p + \operatorname{tr} U_p^\dagger\right)\right) \tag{49}$$

of pure lattice gauge theory. We have already seen that we can deduce the free energy density from the logarithm of Z. Furthermore we could do a strong coupling expansion in the coupling β by simply expanding the exponential. Nevertheless, there is a smarter way to expand it and this is the character expansion. Before we do this we have to introduce some aspects of group theory.

4.1 Aspects of group theory

This introduction is a summary of the corresponding chapter of the textbook [21], where one can find a more detailed explanation and references for further reading.

4.1.1 Character expansion

Our groups of interest are the special unitary groups $SU(N)$, which can be represented as $N \times N$ matrices with the following properties

$$U \in SU(N) \quad \Leftrightarrow \quad U^\dagger U = \mathbf{1}, \quad \det U = 1. \tag{50}$$

This is called the defining or fundamental representation of the gauge group. There are other representations r and their corresponding matrices $D^{(r)}(U)$, that obey

$$D^{(r)}(U) D^{(r)}(V) = D^{(r)}(W) \quad \Leftrightarrow \quad UV = W, \tag{51}$$

$$D^{(r)}(\mathbf{1}) = \mathbf{1}_r. \tag{52}$$

Of most importance are the irreducible representations, which are the only ones we will need in the following. In this context irreducible means, that these representations cannot be split into the direct sum of two other representations.

The character of a representation is defined as

$$\chi_r(U) = \operatorname{tr} D^{(r)}(U), \tag{53}$$

with the property

$$\chi_r(\mathbf{1}) = d_r. \tag{54}$$

In order to integrate over the group space, we introduce the Haar measure, with properties

$$\begin{aligned} \int\limits_{SU(N)} dU\, f(U) &= \int\limits_{SU(N)} dU\, f(VU) = \int\limits_{SU(N)} dU\, f(UV) \qquad \forall\ V \in SU(N), \\ \int\limits_{SU(N)} dU &= 1, \end{aligned} \tag{55}$$

i.e. invariance and normalization.

The importance of the characters of irreducible representations lies in the fact that they span a basis in the space of square integrable class functions, that are defined as

$$f(U) = f(VUV^{-1}). \tag{56}$$

Characters share this property

$$\chi_r(U) = \chi_r(VUV^{-1}), \tag{57}$$

as can be seen from the cyclic invariance of the trace operation. Thus we can expand any class function as

$$f(U) = \sum_{r \in G} f_r \chi_r(U), \tag{58}$$

$$f_r = \int dU\, \overline{\chi}_r(U) f(U), \tag{59}$$

where we have defined G to be the set of all irreducible representations. This method will be described in more detail in the next chapter by the example of the pure $SU(2)$ lattice gauge theory.

4.1.2 Group integrals

We have already introduced group integration in the last subsection. Here we would like to give some basic formulas, which will help us later to calculate integrals occurring in the strong coupling expansions of some observables. By far the most important formula for strong coupling expansions is

$$\int dU \chi_r(VU)\chi_s(U^{-1}W) = \frac{\delta_{rs}}{d_r}\chi_r(VW). \tag{60}$$

This formula will help us to integrate over a link which is occupied by two plaquettes in the same or in the complex conjugate representation, depending on the orientation of the plaquettes. This equation (60) is formulated in terms of characters of the group elements. More generally, we have to consider integrals of the type

$$I_{i_1 j_1 \cdots i_n j_n k_1 l_1 \cdots k_m l_m} \equiv \int dU\, U_{i_1 j_1} \cdots U_{i_n j_n} U^\dagger_{k_1 l_1} \cdots U^\dagger_{k_m l_m}. \tag{61}$$

A general method to calculate such integrals has been introduced in [41]. In this paper results were given for the following integrals

$$\begin{aligned}
I_{i_1 j_1 k_1 l_1} &= \frac{1}{N} \delta_{i_1 l_1} \delta_{j_1 k_1}, && (62)\\
I_{i_1 j_1 \cdots i_N j_N} &= \frac{1}{N!} \varepsilon_{i_1 \cdots i_N} \varepsilon_{j_1 \cdots j_N}, && (63)\\
I_{i_1 j_1 i_2 j_2 k_1 l_1 k_2 l_2} &= \frac{1}{N^2-1} \Big(\delta_{i_1 l_1} \delta_{i_2 l_2} \delta_{j_1 k_1} \delta_{j_2 k_2} + \delta_{i_1 l_2} \delta_{i_2 l_1} \delta_{j_1 k_2} \delta_{j_2 k_1} \Big) && (64)\\
&- \frac{1}{N(N^2-1)} \Big(\delta_{i_1 l_1} \delta_{i_2 l_2} \delta_{j_1 k_2} \delta_{j_2 k_1} + \delta_{i_1 l_2} \delta_{i_2 l_1} \delta_{j_1 k_1} \delta_{j_2 k_2} \Big).
\end{aligned}$$

More lenghty formulas are given in the appendix.

Another aspect of group integration is a consequence of eq. (60) and the invariance property. If we set the representation s equal to the trivial representation, we obtain

$$\int dU\, \chi_r(VU) = \int dU\, \chi_r(U) = \delta_{r,0}. \tag{65}$$

Later this integration rule means in practice that at every link the Clebsch-Gordan product of the occurring representations has to contain the trivial representation. Othwerwise the whole integral would vanish.

4.2 Free energy density of $SU(2)$

In the simplest example, the free energy density of pure $SU(2)$ gauge theory, we would like to present the character expansion method in some detail. We start with the partition function at zero temperature

$$Z(\beta) = \int [dU] \exp\left(\frac{\beta}{2} \sum_p \operatorname{tr} U_p \right). \tag{66}$$

Due to the trace operation in the exponential, we are faced with a class function and thus expand the Boltzmann factor in characters

$$\exp\left(\frac{\beta}{2}\mathrm{tr}\, U\right) = c_0(\beta)\left[1 + \sum_{j\neq 0} d_j a_j(\beta)\chi_j(U)\right], \tag{67}$$

where the parameter $c_0(\beta)$ of the trivial representation $\big(\chi_0(U) \equiv \mathbf{1}\big)$ has been factored out for convenience. The character expansion coefficients are given by certain combinations of modified Bessel functions of the first kind

$$c_j(\beta) = \frac{2I_{2j+1}(\beta)}{\beta}, \tag{68}$$

$$a_j(\beta) = \frac{I_{2j+1}(\beta)}{I_1(\beta)}. \tag{69}$$

As we consider $SU(2)$, for the index j we can have $\frac{1}{2}, 1, \frac{3}{2}\ldots$, and we note that for small β the expansion coefficients behave like

$$a_j(\beta) \sim \beta^{2j} + \ldots. \tag{70}$$

In this way we can express the partition function in terms of characters

$$Z(\beta) = c_0^{6\Omega}\int [dU]\prod_p \left[1 + \sum_{j\neq 0} d_{j_p} a_{j_p}(\beta)\chi_{j_p}(U)\right]. \tag{71}$$

In the product every plaquette can occur only once, albeit with an irreducible representation of arbitrarily high j. But in a series expansion in β, higher order representations are supressed as a result of eq. (70). The fact that each plaquette can occur only once is the main advantage of the character expansion in contrast to a direct expansion of the exponential, where each plaquette can contribute an arbitrary number of times.

4.2.1 Graphical expansion

With eq. (71) we can rewrite the partition function as a sum over all graphs G made up out of plaquettes with a non-trivial representation

$$\begin{aligned} Z(\beta) &= c_0^{6\Omega}\sum_G \Phi(G), \\ \Phi(G) &= \int [dU]\prod_{p\in G} d_{j_p} a_{j_p}\chi_{j_p}(U) = \prod_i \Phi(X_i), \end{aligned} \tag{72}$$

which factorise into disconnected components X_i, called polymers. The contribution $\Phi(G)$ of a graph can be calculated with the integration rule eq. (60), by using it link by link.

The occurrence number of a graph is proportional to Ω^n if it consists of n polymers. Using the formalism of moments and cumulants, which is described in more detail in [21], one can isolate the terms linear in the lattice volume Ω, which are the only ones relevant for the free energy density. In fact, the logarithm of the partition function should not grow larger than linear in Ω in order to ensure the existence of a thermodynamic limit. Performing this moment-cumulant method, one arrives at a cluster expansion for our quantity of interest, the free energy density,

$$f(\Omega) \equiv -\frac{1}{\Omega} \ln Z = -6 \ln\, c_0(\beta) - \frac{1}{\Omega} \sum_{C=(X_i^{n_i})} a(C) \prod_i \Phi(X_i)^{n_i}. \tag{73}$$

The sum goes over all clusters C, which are defined as connected polymers X_i, and n_i denotes the multiplicity of a particular polymer in a cluster. The combinatorial factor $a(C)$ is given by

$$a(C) = \frac{[X_1, \ldots, X_1, X_2, \ldots, X_2, \ldots, X_k]}{n_1! n_2! \ldots n_k!} \tag{74}$$

and equals 1 for clusters C which consist of only one polymer X_i. The so-called cumulant [ ] can be expressed in terms of moments $< >$

$$[\alpha, \ldots, \zeta] = \sum_P (-1)^{n-1} (n-1)! < \alpha, \ldots, \beta > \cdots < \gamma, \ldots, \delta > \tag{75}$$

where n is the number of factors on the right hand side and the sum goes over all partitions P. The moments are defined in such a way, that

$$< X_1, \ldots, X_n >= \begin{cases} 1, \text{ if every pair } X_i, X_j \text{ is disconnected} \\ 0, \text{ otherwise} \end{cases} \tag{76}$$

This implies the equivalence between non-zero cumulants and connectedness of graphs,

$$[X_1, \ldots, X_n] \neq 0 \quad \Leftrightarrow \quad X_1 \cup \cdots \cup X_n \quad \text{is connected.} \tag{77}$$

In the graphical expansion of the free energy density, a plaquette is allowed to occur more than one time in a cluster, but again at most once in a given polymer. An example would be two cubes that share the same lattice position and thus form a cluster of two polymers. There each plaquette appears twice, but only once in each cube.

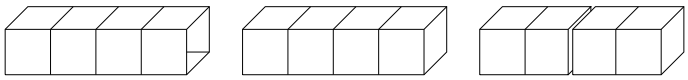

Figure 2: Graphs that appear on the different lattices. Left: Leading order tube for $N_\tau = 4$. Middle: First graph vanishing in the case $N_\tau = 4$. Right: Graph contributing on both, $N_\tau = 4, \infty$, lattices.

The next step consists of introducing finite temperature effects by compactifying the temporal lattice extent. Additionally we have to take into account periodic boundary conditions for bosonic degrees of freedom as we consider pure gauge theory. Another crucial step is the subtraction of zero temperature contributions. Up to now the quantity $f(\Omega)$ was formulated at zero temperature and thus had no direct thermodynamic meaning. Indeed it resembles the divergent vacuum energy in the continuum. Thus our quantity of interest is the physical free energy density

$$f_{phys.} = f(N_\tau) - f(\infty) = -\frac{1}{N_\tau V} \ln Z(N_\tau) + \frac{1}{\Omega} \ln Z(\infty), \tag{78}$$

where the argument denotes the temporal lattice extent. In the calculation of $f(\infty)$, the whole lattice volume goes to infinity, whereas with $f(N_\tau)$ it is only the spatial volume, while the temporal lattice extent stays finite.

4.2.2 Classification of graphs

Because of the subtraction in eq. (78), those graphs contributing in the same way to $f(N_\tau)$ and $f(\infty)$ drop out of the physical free energy. This is true for all polymers with time extent less than N_τ. The calculation thus reduces to graphs with a temporal size of N_τ on the finite N_τ lattice, and graphs spanning or extending N_τ on the infinite lattice. Such graphs contribute either to $f(N_\tau)$ or to $f(\infty)$ (and in some cases to both), and hence to the difference in eq. (78). It is therefore clear from the outset that the strong coupling series for the physical free energy starts at a higher order than the formal zero temperature free energy. Moreover, the order of the leading contribution depends on N_τ. The lowest order graph existing due to the boundary condition on the finite N_τ lattice, but not on the infinite lattice, is a tube of length N_τ with a cross-section of one single plaquette, as shown in fig. (2) (left). It forms a closed torus through the periodic boundary and thus gives a non-vanishing contribution, which is easily calculated to be $\Phi(G_1) = a_f^{4N_\tau}$, where the subscript '$f$' indicates the fundamental representation. We need to sum up all such graphs on the lattice. There are three combinations of spatial directions for the cross section of the tube, giving a factor of 3. Translations in time take the graph into itself and do not give a new contribution,

while we get a factor of V from all spatial translations. Together with the $1/\Omega$ in eq. (73) this gives a factor of $1/N_\tau$. The contribution of all tubes with all plaquettes in the fundamental representation is thus

$$\Phi(G_1) = \frac{3}{N_\tau} a_f^{4N_\tau}, \tag{79}$$

which is - up to a sign - also the leading order result for the physical free energy.

On the other hand, the same tube with both ends closed off by additional plaquettes as in fig. (2) (middle), contributes with $\Phi(G_2) = d_f^2 a_f^{4N_\tau+2}$ on an $N_\tau = \infty$, but not on a finite N_τ lattice. This is because the boundary plaquettes get identified as one doubly occupied plaquette, which is not an allowed graph in the expansion. Therefore, $\Phi(G_2)$ counts with a negative sign relative to $\Phi(G_1)$ towards the physical free energy. Here, translations in time do produce a new graph, so the total contribution is

$$\Phi(G_2) = -3 d_f^2 a_f^{4N_\tau+2}. \tag{80}$$

Fig. (2) (right) shows a variation of these basic graphs, a cluster composed of two double cubes. This is an example of a graph spanning N_τ which contributes to both the finite and infinite N_τ lattices in the same way, thus cancelling out in the physical free energy. (Note that the corresponding tube obtained without the plaquettes at N_τ vanishes, it would correspond to a single polymer with doubly occupied plaquettes at the slit). However, for similar clusters composed of more than two polymers, this cancellation in general no longer holds because of different assignments of combinatoric factors $a(C)$ in the two cases.

4.2.3 Corrections to basic polymers

For fixed N_τ, starting from the basic leading order polymers discussed in the last section, one can now build up the corrections by adding decorations on each of them. These can be either geometric, by adding additional fundamental representation plaquettes as in fig. (3) (left), by inserting plaquettes in higher representations as in fig. (3) (middle) or by adding a whole new polymer as in fig. (3) (right). Of course, these modifications can be combined. Adding plaquettes in higher representations is possible only if at each link the Clebsch-Gordan series of the representation matrices contains the trivial representation, due to eq. (65).

We have already seen in Sec. 4.2.2 that the order in a_f, to which the graphs contribute, depends on N_τ. Thus, the relative importance of different types of graphs changes with N_τ. For our example $N_\tau = 4$ considered in

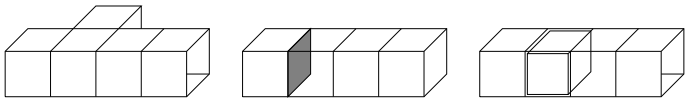

Figure 3: Graphs contributing to the higher order terms of the series.

Sec. 4.2.2, the leading correction to the basic polymer on the N_τ lattice is the insertion of one higher representation plaquette inside the tube, contributing an additional factor $\sim a_f^2$, whereas the lowest order geometric decoration is a shifted plaquette adding a factor $\sim a_f^4$. By contrast, on an $N_\tau = 1$ lattice contributions to the leading order correction $\sim a_f^2$ come from the basic polymer with a cross sectional perimeter of six links. In general, geometric decorations enter earlier the lower N_τ is. Thus the summation of basic polymers and their decorations contains the complete result to some fixed order O only for lattices $N_\tau \geq N_\tau^O$, with some N_τ^O which is obviously growing with O. For lattices $N_\tau < N_\tau^O$ there are additional geometric decorations contributing to $\mathcal{O}(a_f^O)$. In this work, we have calculated corrections to $a_f^{4N_\tau}$ through $\mathcal{O}(a_f^8)$ for which $N_\tau^O = 5$.

4.2.4 Summing basic polymers for $SU(2)$

The contribution of all graphs of length N_τ without geometric decorations and with fundamental plaquettes at the outsides of the tube can be summed up in closed form. To do this we note that an additional plaquette in a representation r as in fig. (3) (middle) gives an additional factor $d_r a_r$. In the case of $SU(2)$, for which we will now describe the calculation, the only possibility is the $j = 1$ representation, because of eq. (65) and

$$\frac{1}{2} \otimes \frac{1}{2} = 0 \oplus 1 \quad \Rightarrow \quad \frac{1}{2} \otimes \frac{1}{2} \otimes 1 = 0 \oplus 1 \oplus 1 \oplus 2 \, . \tag{81}$$

As already explained, the expansion parameters are given by modified Bessel functions and can be expanded in powers of the lattice coupling, e.g. the one of the fundamental representation:

$$a_{1/2} = \frac{I_2(\beta)}{I_1(\beta)} = \frac{1}{4}\beta - \frac{1}{96}\beta^3 + \frac{1}{1536}\beta^5 - \frac{1}{23040}\beta^7 + O(\beta^9). \tag{82}$$

For the following it is convenient to use $u \equiv a_{1/2}$ as the effective expansion parameter instead of β. It is well known from expansions at zero temperature that apparent convergence is better for the series in u [33,34], and we observe the same phenomenon here. We can e.g. expand the expansion parameter of the adjoint representation as

$$v \equiv a_1 = \frac{I_3(\beta)}{I_1(\beta)} = \frac{2}{3}\,u^2 + \frac{2}{9}\,u^4 + \frac{16}{135}\,u^6 + \frac{8}{135}\,u^8 + \mathcal{O}(u^{10}). \tag{83}$$

In addition to this we introduce the combination $c = 1 + 3v - 4u^2$ to shorten some formulas.

In order to sum up the leading contributions, we note that on the N_τ lattice we can have $0 \leq k \leq N_\tau$ additional inner plaquettes at N_τ places which can be distributed in $\binom{N_\tau}{k}$ ways. Summing all possible distributions leads to

$$\Phi_1 = \Phi(G_1) \sum_{k=0}^{N_\tau} \binom{N_\tau}{k} (3v)^k = \Phi(G_1) \left(1 + 3v\right)^{N_\tau} . \tag{84}$$

We can also add slits to get graphs as in fig. (2) (right), consisting of more than one polymer. Each slit gives a factor $d_f^2 u^2 = 4u^2$. The minimum number of slits i is 2 and the combinatorial factor for such graphs is

$$a(C) = (i-1)(-1)^{i-1}. \tag{85}$$

Summing these graphs with possible $j = 1$ plaquettes at the remaining places this yields

$$\begin{aligned} \Phi_2 &= \Phi(G_1) \sum_{i=2}^{N_\tau} \binom{N_t}{i} (i-1)(-1)^{i-1} \left(4u^2\right)^i \sum_{k=0}^{N_\tau - i} \binom{N_\tau - i}{k} (3v)^k \\ &= \Phi(G_1) \left[c^{N_\tau} - (1+3v)^{N_\tau} + 4u^2 N_\tau c^{N_\tau - 1} \right]. \end{aligned} \tag{86}$$

Of course, we can do the same insertions to the graph fig. (2) (middle) on the infinite lattice with the difference that we have at most $N_\tau - 1$ places to add plaquettes. The combinatorial factor now reads

$$a(C) = (-1)^i, \tag{87}$$

where i is again the number of slits and in this case it is unrestricted. The difference in the assignment of the combinatorial factors $a(C)$ on the two lattices is caused by the periodic boundary conditions. On the finite lattice the first and the last polymer touch each other, whereas on the infinite lattice this is not the case. Summing the contributions on the infinite lattice, we get

$$\begin{aligned} \Phi_3 &= \Phi(G_2) \sum_{i=0}^{N_\tau - 1} \binom{N_\tau - 1}{i} (-1)^i \left(4u^2\right)^i \sum_{k=0}^{N_\tau - 1 - i} \binom{N_\tau - 1 - i}{k} (3v)^k \\ &= \Phi(G_2) c^{N_\tau - 1} \\ &= \Phi(G_1)(-4u^2 N_\tau) c^{N_\tau - 1}. \end{aligned} \tag{88}$$

For the final result we have to add the different pieces and obtain

$$\Phi = \Phi_1 + \Phi_2 + \Phi_3 = \frac{3}{N_\tau} u^{4N_\tau} c^{N_\tau}. \tag{89}$$

In higher gauge groups, the summation proceeds in a similar manner with some slight modification due to the fact that there are also complex conjugate representations.

4.2.5 Free energy density of $SU(2)$ up to $\mathcal{O}(u^8)$

We now present our results for the gauge group $SU(2)$. Some examples of contributing graphs in higher orders are given in the appendix. For $N_t \geq 5$, the basic polymers and their decorations can be summed up to give the general result up to higher orders

$$\begin{aligned} &f(N_\tau, u) = \\ &-\frac{3}{N_\tau} u^{4N_\tau} c^{N_\tau} \left[1 + 12 N_\tau u^4 - \frac{1556}{81} N_\tau u^6 + \left(83 N_t^2 + \frac{41417}{243} N_\tau \right) u^8 \right] \end{aligned} \tag{90}$$

For $N_\tau = 1-4$ there are additional geometric decorations, while some graphs contained in the previous result do not contribute on those short lattices. We find up to higher orders

$$f(1,u) = -3\,u^4 - 16\,u^6 - \frac{10913}{54} u^8 - \frac{968642}{405} u^{10}, \tag{91}$$

$$f(2,u) = -\frac{3}{2} u^8 + 6\,u^{10} - 55\,u^{12} + \frac{29236}{135} u^{14} - \frac{78413341}{43740} u^{16}, \tag{92}$$

$$f(3,u) = -u^{12} + 6\,u^{14} - 50\,u^{16} + \frac{37966}{135} u^{18} - \frac{856048}{405} u^{20}, \tag{93}$$

$$f(4,u) = -\frac{3}{4} u^{16} + 6\,u^{18} - 56\,u^{20} + \frac{51376}{135} u^{22} - \frac{2402453}{810} u^{24}. \tag{94}$$

From these expressions all other thermodynamic quantities of interest can be constructed, in particular the pressure $P = -f$ and the energy density e

$$e(\beta) = \frac{1}{6} \frac{d}{d\beta} f(\beta) = \frac{1}{6} \frac{du}{d\beta} \frac{d}{du} f(u). \tag{95}$$

For later comparison with Monte Carlo results, it is convenient to consider the energy density. The curves for consecutive orders in the strong coupling expansion for $N_\tau = 2$ are plotted in fig (4). For $\beta \gtrsim 1$ convergence rapidly becomes poor, announcing the proximity of the convergence radius.

Since the partition function is not directly measurable in Monte-Carlo simulations, the pressure is usually obtained by the integral method [19],

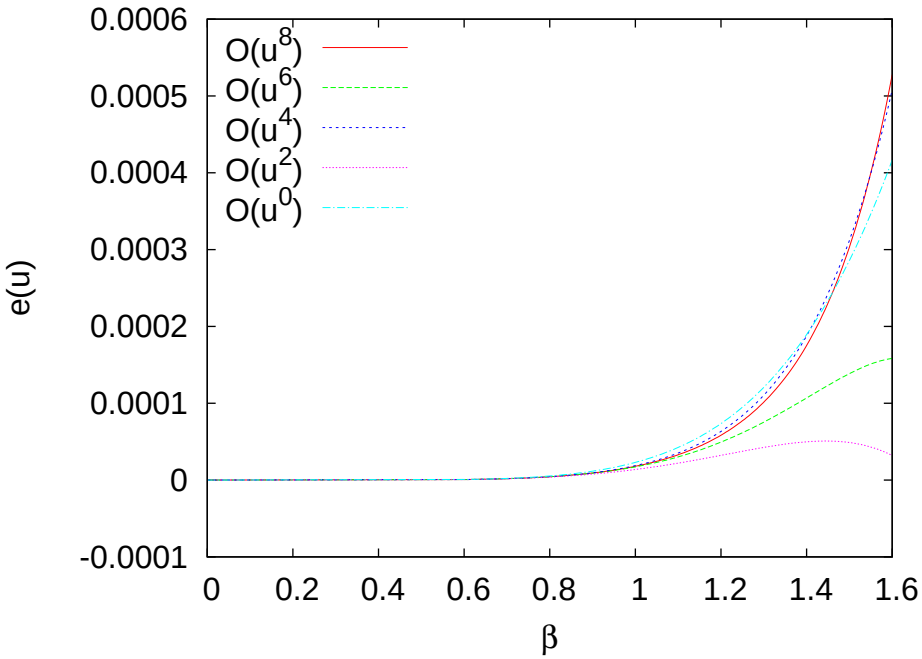

Figure 4: Behaviour of the series expansion of the energy density in different orders.

where the expectation values of derivatives are computed and afterwards integrated out numerically,

$$\left.\frac{P}{T^4}\right|_{\beta_0}^{\beta} = N_\tau^4 \int_{\beta_0}^{\beta} d\beta' \left[6\langle \operatorname{Tr} U_p^0 \rangle - 3\langle \operatorname{Tr} U_p^t + \operatorname{Tr} U_p^s \rangle\right], \tag{96}$$

where $\langle \operatorname{Tr} U_p^0 \rangle$ denotes the plaquette expectation value on symmetric ($T = 0$) lattices, $N_\tau = N_s \to \infty$, and $\langle \operatorname{Tr} U_p^{t,s} \rangle$ are those of space-time and space-space plaquettes for $N_\tau < N_s$. The lower integration limit is usually set to zero by hand, arguing with an exponentially small pressure in the low temperature regime. Our results justify this assumption from first principles and allow to fix that value if desired.

4.2.6 Series analysis: Padé approximants

Strong coupling or high temperature expansions have been worked out to high orders in many spin models, where various tools of series analysis can be applied to improve convergence or extract additional information from the behaviour of the coefficients [9, 34]. Here we introduce a method based on the calculation of Padé approximants.

In particular, we are interested in locating the position of the finite temperature deconfinement transition, which separates the confined hadronic phase from the deconfined phase, where quarks and gluons are the dominant degrees of freedom. The associated critical coupling β_c limits the radius of convergence of the strong coupling series, provided there are no other singularities β_s in the complex β-plane with $|\beta_s| < \beta_c$.

The most straightforward way to estimate the radius of convergence r_n from the nth order series would be via the ratio test of the series coefficients f_{2n},

$$r_n = \left| \frac{f_{2n}}{f_{2n+2}} \right|^{1/2}, \tag{97}$$

and investigate the asymptotic behaviour with n. However, our series eqs (90-94) are still rather short and no convergence in r_n is visible. Moreover, a singularity on the real axis requires the coefficients asymptotically to come with equal signs. This is clearly not the case in our expressions for $N_\tau > 1$, which suggest a nearby imaginary singularity.

A much better tool for our purposes is the analysis of Padé approximants to a function constructed from its series expansion. These are the rational functions

$$[L, M](u) \equiv \frac{a_0 + a_1 u + \cdots + a_L u^L}{1 + b_1 u + \cdots + b_M u^M}, \tag{98}$$

with coefficients a_i, b_i chosen such that they reproduce the power series of the function of interest to the degree $L + M$. As rational functions, Padé approximants are known to give good estimates of isolated pole singularities, whereas branch cuts or algebraic singularities are less well reproduced (for a detailed discussion, see [9]). Furthermore, they give access to several singularities, rather than just the nearest one, if the polynomial in the denominator is of degree larger than 1.

Near the critical point of a second order phase transition one usually encounters singularities of type

$$g(x) \sim (x_c - x)^{-\lambda}, \tag{99}$$

where $g(x)$ is an observable dependent on the physical coupling x and λ is the corresponding critical exponent. Since λ is usually a fractional number it is convenient to consider the logarithmic derivative

$$D_g(x) \equiv \frac{d}{dx} \ln\, g(x) \sim \frac{\lambda}{x_c - x}. \tag{100}$$

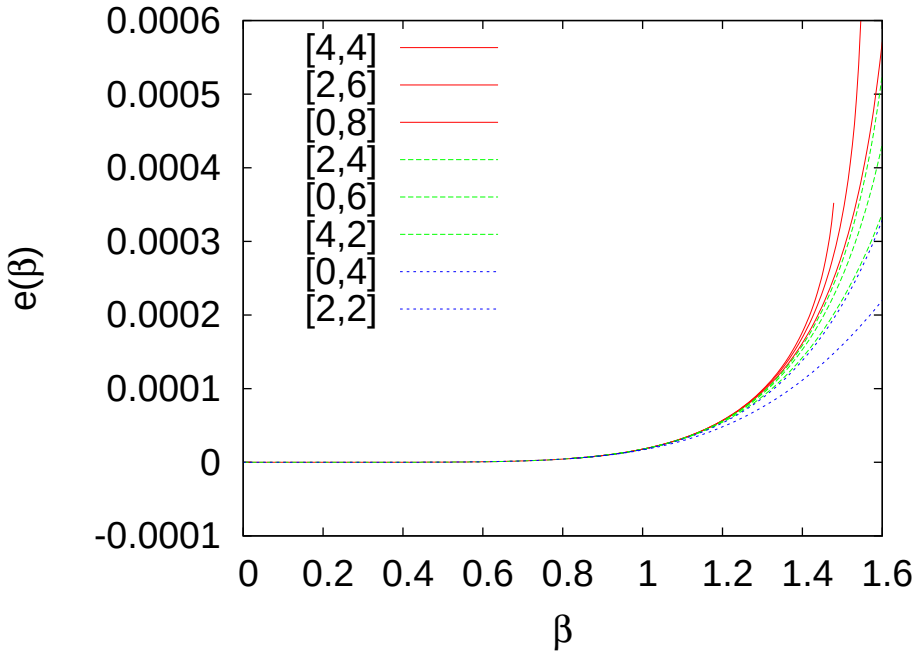

Figure 5: Convergence improvement due to the use of Padé extrapolated sereies expansions.

This quantity, which we call DLog in the following, should be the best quantity to be modelled by Padé approximants, because of the similar pole structure.

4.2.7 Critical couplings from the free energy density

At the finite temperature phase transition the free energy density $f(N_\tau, u_c)$ with $u_c = u(\beta_c)$ is continuous, with a discontinuous first or second derivative, depending on the order of the transition. This type of singularity is difficult to model for Padé approximants. Instead, the 'heat capacity'

$$C(N_\tau, u) = u^2 \frac{d^2}{du^2} f(N_\tau, u) \tag{101}$$

diverges at the phase transition as $C(u) \sim (u_c - u)^{-\alpha}$ with a critical exponent characteristic of the transition. Its logarithmic derivative

$$D_C(N_\tau, u) \equiv \frac{d}{du} \ln C(N_\tau, u) \sim \frac{\alpha}{u_c - u} \tag{102}$$

has a simple pole with residue α and is therefore best suited for an analysis by Padé approximants. We thus consider the DLogs for small N_τ, normalized

to $D_C(N_\tau, 0) = 1$, obtain

$$D_C(1,u) = 1 + \frac{20}{3}u^2 + \frac{54791}{243}u^4 + \frac{1879249}{486}u^6, \quad (103)$$

$$D_C(2,u) = 1 - \frac{45}{28}u^2 + \frac{6445}{196}u^4 - \frac{150331}{92610}u^6 + \frac{31831541863}{21003948}u^8, \quad (104)$$

$$D_C(3,u) = 1 - \frac{91}{66}u^2 + \frac{4573}{242}u^4 - \frac{2653298}{59895}u^6 + \frac{114561591157}{106732890}u^8, \quad (105)$$

$$D_C(4,u) = 1 - \frac{51}{40}u^2 + \frac{29791}{1800}u^4 - \frac{1262057}{27000}u^6 + \frac{1055884297}{1215000}u^8, \quad (106)$$

and model the full functions by Padé approximants. As an example, we show the $L+M = 4, 6, 8$ approximants for the energy density on the $N_\tau = 2$ lattice in fig. (5). Clearly, this sequence of padé approximants shows improved convergence compared to that of the bare series.

The singularities in $D_C(u)$, indicated by zeros of the denominator, along with the zeros of the resulting approximants are shown in Table 1 for $N_\tau = 2, 4$, respectively. Singularities in the immediate neighbourhood of a zero of the same approximant are typically artefacts and unstable under variation of the approximant. However, for $N_\tau = 2$ several approximants show poles around $\beta = 1.5$ without zeroes in the immediate vicinity, indicating that the full function indeed has a singluarity on the real axis in this region. For $N_\tau = 4$, on the other hand, the pole near $\beta = 1.5$ is accompanied by a zero and not to be taken seriously. The next nearest pole on the real axis is instead around $\beta = 2$. A priori it is not possible to judge which approximants are better than others. The scatter in the results is thus a measure for the systematic error associated with the Padé procedure. Moreover, there is also a scatter between approximants based on different orders of the underlying series. With increasing order, the approximants display more and more singularities which should eventually accumulate near the true singularity structure.

To take these systematic effects into account, we estimate β_c by averaging over the lowest lying real singularities obtained from the two highest order approximants, i.e. $L + M = 4, 6$ for $N_\tau = 1$ and $L + M = 6, 8$ for $N_\tau = 2 - 4$. To quantify the scatter due to the systematic uncertainties we quote $(\beta_c^{max} - \beta_c^{min})/2$ as an error estimate. The same procedure is followed for the residues, and the results are collected in table 2. Since the series are still short, the predictions for the critical coupling are not yet very accurate, and those for the critical exponent even less so. In the case of the Polyakov loop susceptibility to be calculated later, we will see that it is indeed possible to accurately determine the values of the critical parameters from a series expansion, at least for small lattices.

Padé	Singularities	Zeroes	Residues
$[0,6]$	$\pm\,1.8356$		0.07486
	$\pm\,(0.2112\,\pm\,1.7192\,i)$		
$[2,4]$	$\pm\,1.6995$	$\pm\,2.8474$	0.05656
	$\pm\,1.5674\,i$		
$[4,2]$	$\pm\,9.9475\,i$	$\pm\,(1.1253\,\pm\,1.2410\,i)$	
$[0,8]$	$\pm\,1.6930$		0.06080
	$\pm\,1.4349\,i$		
	$\pm\,(0.9152\,\pm\,1.6609\,i)$		
$[2,6]$	$\pm\,1.4893$	$\pm\,1.7142$	0.02888
	$\pm\,1.5209\,i$		
	$\pm\,4.2104$		
$[4,4]$	$\pm\,1.5502$	$\pm\,1.9430$	0.03792
	$\pm\,1.4997\,i$	$\pm\,2.2802\,i$	
$[6,2]$	$\pm\,0.1308\,i$	$\pm\,0.1308\,i$	
		$\pm\,(1.1278\,\pm\,1.2384\,i)$	
Padé	Singularities	Zeroes	Residues
$[0,6]$	$\pm\,3.1022$		0.13287
	$\pm\,1.6250\,i$		
$[2,4]$	$\pm\,3.0636$	$\pm\,3.0406$	
	$\pm\,1.6228\,i$		
$[4,2]$	$\pm\,1.9628\,i$	$\pm\,(0.9730\,\pm\,1.7187\,i)$	
$[0,8]$	$\pm\,2.0270$		0.05936
	$\pm\,1.4583\,i$		
	$\pm\,(1.0967\,\pm\,1.5608\,i)$		
$[2,6]$	$\pm\,2.8687$	$\pm\,0.4335\,i$	0.11573
	$\pm\,0.4335i\,i$		
	$\pm\,1.6505i$		
$[4,4]$	$\pm\,1.5084$	$\pm\,1.5762$	
	$\pm\,1.4023\,i$	$\pm\,1.5976\,i$	
$[6,2]$	$\pm\,0.8961\,i$	$\pm\,0.8989\,i$	
		$\pm\,(1.2985\,\pm\,1.5916\,i)$	

Table 1: Singularities, zeros and residues of $L+M=6,8$ Padé approximants for $N_\tau=2$ (top) and $N_\tau=4$ (bottom). Residues are only given for those singularities that enter the estimates for β_c, see Table 2.

N_τ	α	β_c	β_c (Monte Carlo)
1	0.061(38)	0.92(15)	0.85997(10) [42]
2	0.052(19)	1.65(35)	1.880(3) [20]
3	0.078(50)	2.26(63)	2.177(3) [20]
4	0.102(37)	2.66(54)	2.299(6) [20]

Table 2: Estimates for the critical coupling β_c and the critical exponent of the deconfinement phase transition. The exponent for 3d Ising universality is $\alpha = 0.12$.

4.2.8 Comparison to Monte Carlo data

It is now interesting to compare the results from the strong coupling series to Monte Carlo simulations. The thermodynamic quantity most easily accessible by Monte Carlo is the energy density, that is simply the expectation value of the plaquette,

$$e(\beta) = \frac{1}{6}\frac{d}{d\beta} f(\beta) = \langle \operatorname{Tr} U_p \rangle_{N_\tau} - \langle \operatorname{Tr} U_p \rangle_{N_\tau=\infty}, \tag{107}$$

where again the zero temperature (infinite N_t) piece is subtracted for renormalisation. As we have seen, in the low beta region of the deconfined phase, the corresponding values are exponentially small, and very high statistics runs are necessary in order to get significant results for a quantitative comparison. For the infinite volume vacuum lattice we have taken 12^4, and $N_s = 12, N_\tau = 1, 2, 3, 4$ for the finite T lattices. On the $N_\tau = 2$ lattice up to 1.5×10^6 field configurations were generated to achieve sufficient accuracy, for the larger N_τ's this gets scaled down accordingly.

We compare these data with the best estimate based on the strong coupling series, i.e. the Padé approximants to the highest available order in the logarithmic derivative of the heat capacity. The curve for $C(N_\tau, u)$ is reconstructed from the best Padé approximant of $D_C(N_\tau, u)$ via

$$C(N_\tau, u) = \exp\left(\int du\, D_C(N_\tau, u) \right). \tag{108}$$

From this we receive the energy density in the following way

$$\begin{aligned} e(\beta) &= \frac{1}{6}\frac{d}{d\beta} f(\beta) = \frac{1}{6}\frac{du}{d\beta}\frac{d}{du} f(u), \\ \frac{d}{du} f(u) &= \int du \frac{C(N_\tau, u)}{u^2}, \end{aligned} \tag{109}$$

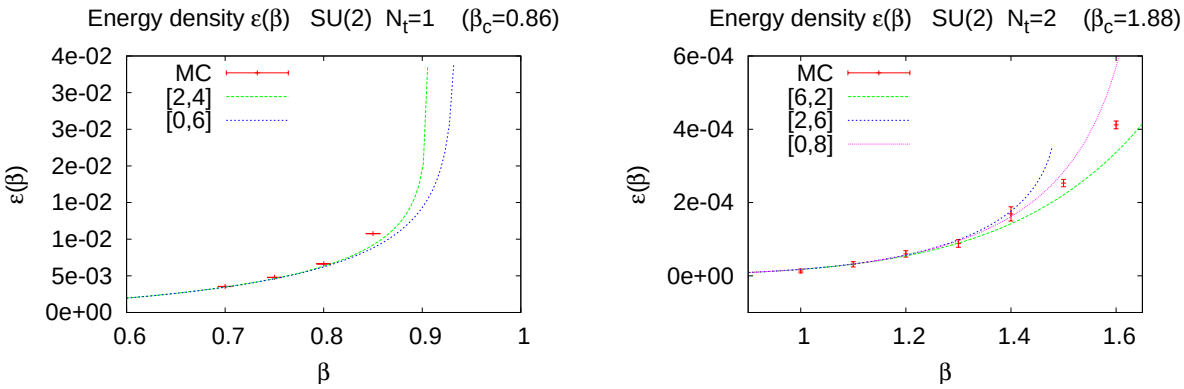

Figure 6: Comparison of Monte Carlo data for $N_t = 2$ (left) and $N_t = 3$ (right) with Padé approximants from the strong coupling series.

and express everything as a function of β. Detailed results for $N_\tau = 1, 2$ are shown in fig. (6). The different curves correspond to different approximants of the same order, and thus serve as an error band quantifying the uncertainties associated with the Padé procedure, giving a valuable error estimate. We observe quantitative agreement with the lattice data all the way up to the lowest estimates of β_c. For $N_\tau = 3, 4$ we have checked at a few points that a similar picture emerges. Hence, the error estimate based on our Padé analysis appears to be reliable and announces the breakdown of the validity of the series.

4.3 Free energy density for $SU(N \geq 3)$

Having discussed the results obtained from the free energy density of $SU(2)$ lattice gauge theory, we now want to consider $N \geq 3$. The summation of the leading terms will proceed similar in this case as before. After having summed the leading order terms, we are going to present the series expansions up to $\mathcal{O}(u^8)$.

4.3.1 Summing basic polymers for $SU(N \geq 3)$

Since the geometry of contributing polymers is independent of the gauge group, the leading order graph for all $N \leq \infty$ is a torus of length N_τ with a number of $4N_\tau$ plaquettes in the fundamental representation f, which is closed due to the periodic boundary conditions in temporal direction. Its contribution in $d = (3+1)$ dimensions and for $N \geq 3$ is given by

$$\phi \;=\; \frac{6}{N_\tau} u^{4N_\tau}, \tag{110}$$

where in contrast to the case of $SU(2)$ an additional factor of 2 appears, accounting for two fundamental representations. The functional form $u(\beta)$ depends on the gauge group. In leading order it is

$$u(\beta) = \frac{1}{N}\int dU \frac{\beta}{2N}\mathrm{tr}\,(U)\mathrm{tr}\,(U^\dagger) + \ldots = \frac{\beta}{2N^2} + \ldots \tag{111}$$

Let us note that, in the limit $N \to \infty$, $u(\beta)$ equals the 't Hooft coupling

$$\lambda = \frac{\beta}{2N^2} \tag{112}$$

and hence remains finite in this limit [34].

The leading corrections to the basic polymer arise from putting spacelike plaquettes in higher dimensional representations inside the torus. In order to have non-vanishing contribution according to the integration formula

$$\int dU \chi_r(U) = \delta_{r,0}, \tag{113}$$

the allowed representations are those whose conjugates appear either in $f \otimes \overline{f}$ or in $f \otimes f$, the Kronecker products of the fundamental representations. The latter representations are forced to appear an even number of times, since they induce a change of orientation of the outer plaquettes and this has to be canceled due to the periodic boundary conditions. If those plaquettes appear n times, we take this fact into account by inserting a factor

$$\frac{1}{2}\left[1 + (-1)^n\right] \tag{114}$$

into the summation of these contributions. Let us denote the parameters of the representations appearing in $f \otimes f$ with v_1 and v_2 and recognize

$$d_{v_1} v_1 = \frac{N(N+1)}{2} v_1 = \frac{1}{2}(Nu)^2 + \ldots \tag{115}$$

$$d_{v_2} v_2 = \frac{N(N-1)}{2} v_2 = \frac{1}{2}(Nu)^2 + \ldots. \tag{116}$$

In the case of $SU(3)$ we have to identify v_2 with the complex conjugate fundamental representation ($3 \otimes 3 = \overline{3} \oplus 6$), thus being of order u rather than u^2. The parameter of the adjoint representation appearing in $f \otimes \overline{f}$ fulfills

$$d_{ad} w = (N^2 - 1)\, w = (Nu)^2 + \mathcal{O}(u^4). \tag{117}$$

As in the case of $SU(2)$ one can add slits, that means inserting two fundamental plaquettes at the same location. This gives an additional factor of $2d_f^2u^2$. The factor of two appears because adding a slit increases the number of polymers by one and this new polymer can contribute in two different orientations. Thus we get a chain of polymers with a nontrivial combinatorial factor $a(C)$ of the resulting cluster C. Now we sum over all possible contributions of the torus with inner decorations and keep in mind the factor (114). So the sum splits into two terms and we find the result

$$\begin{aligned}\phi &= \frac{6}{N_\tau}u^{4N_\tau}\frac{1}{2}\left[c_N^{N_\tau}+b_N^{N_\tau}\right] \\ &= \frac{3}{N_\tau}u^{4N_\tau}\left[c_N^{N_\tau}+b_N^{N_\tau}\right]. \end{aligned} \tag{118}$$

This calculation proceeds in the same way as in the case of $SU(2)$ with the difference of inserting the factor (114). We introduced

$$c_N = 1 + d_{v_1}v_1 + d_{v_2}v_2 + d_{ad}w - 2d_f^2u^2 \tag{119}$$

$$b_N = 1 - d_{v_1}v_1 - d_{v_2}v_2 + d_{ad}w \tag{120}$$

as gauge group dependent factors. In the limit $N \to \infty$ the expansion parameters simplify [34]

$$\begin{aligned} d_{v_1}v_1 &= \frac{1}{2}(Nu)^2, \\ d_{v_2}v_2 &= \frac{1}{2}(Nu)^2, \\ d_{ad}w &= (Nu)^2, \end{aligned} \tag{121}$$

and these gauge group factors become trivial

$$\begin{aligned} c_\infty &= 1 + \frac{1}{2}(Nu)^2 + \frac{1}{2}(Nu)^2 + (Nu)^2 - 2N^2u^2 = 1 \\ b_\infty &= 1 - \frac{1}{2}(Nu)^2 - \frac{1}{2}(Nu)^2 + (Nu)^2 = 1. \end{aligned} \tag{122}$$

As a consequence the contributions of inner plaquettes cancel against each other. This gives a first hint, that in the confined phase the free energy density is a quantity of $\mathcal{O}(N^0)$, when $N \to \infty$.

4.3.2 Free energy density of $SU(3)$ up to $\mathcal{O}(u^8)$

It is in complete analogy to $SU(2)$ to calculate higher order corrections. One can decorate the leading polymer, either geometrically or using higher

dimensional plaquettes, one can add whole new polymers or one can combine these possibilities.

Again we have contributions of some polymers only for large N_τ and some polymers only contribute for small N_τ, since their correction is of order u^{2N_τ} or higher. We would like to mention the interesting cases $N = 3$ and $N \to \infty$.

The results for the free energy density for $SU(3)$ up to higher orders are

$$\begin{aligned}
f(1,u) &= -6\,u^4 - 44\,u^6 + 30\,u^7 - \frac{2251587}{4096}u^8 + \frac{641763}{1024}u^9 \\
&- \frac{124533967}{20480}u^{10}, \\
f(2,u) &= -3\,u^8 - 27\,u^{10} + 135\,u^{11} - \frac{1105}{4}u^{12} + \frac{351}{4}u^{13} - \frac{18058839}{10240}u^{14} \\
&+ \frac{14775291}{2048}u^{15} - \frac{648558969807}{83886080}u^{16}, \\
f(3,u) &= -2\,u^{12} - 54\,u^{14} + 216\,u^{15} - 315\,u^{16} + \frac{1269}{2}u^{17} - \frac{199458821}{30720}u^{18} \\
&+ \frac{89855001}{5120}u^{19} - \frac{671236701}{40960}u^{20}, \\
f(4,u) &= -\frac{3}{2}u^{16} - 81\,u^{18} + 297\,u^{19} - \frac{1989}{4}u^{20} + \frac{9585}{4}u^{21} - \frac{32785323}{2048}u^{22} \\
&+ \frac{375123069}{10240}u^{23} - \frac{2216152967}{40960}u^{24}, \\
f(N_\tau,u) &= -\frac{3}{N_\tau}u^{4N_\tau}\cdot \\
&\Big\{c^{N_\tau}\Big[1 + 12\,N_\tau u^4 + 42\,N_\tau u^5 - \frac{115343}{2048}\,N_\tau u^6 \\
&\qquad - \frac{597663}{2048}\,N_\tau u^7 + \left(83\,{N_\tau}^2 + \frac{72206061}{40960}\,N_\tau\right)u^8\Big] \\
&+ b^{N_\tau}\Big[1 + 12\,N_\tau u^4 + 30\,N_\tau u^5 - \frac{17191}{256}\,N_\tau u^6 \\
&\qquad - 180\,N_\tau u^7 + \left(83\,{N_\tau}^2 + \frac{3819}{10}\,N_\tau\right)u^8\Big]\Big\}.
\end{aligned}$$

As finite temperature $SU(N \geq 3)$ lattice gauge theories undergo first order phase transitions, we did not attempt to locate the critical couplings. In order to get those, one has to rely on scaling relations for different observables, which only show up for a continuous phase transition. For first order phase transitions, the correlation length does not diverge and no scaling relations

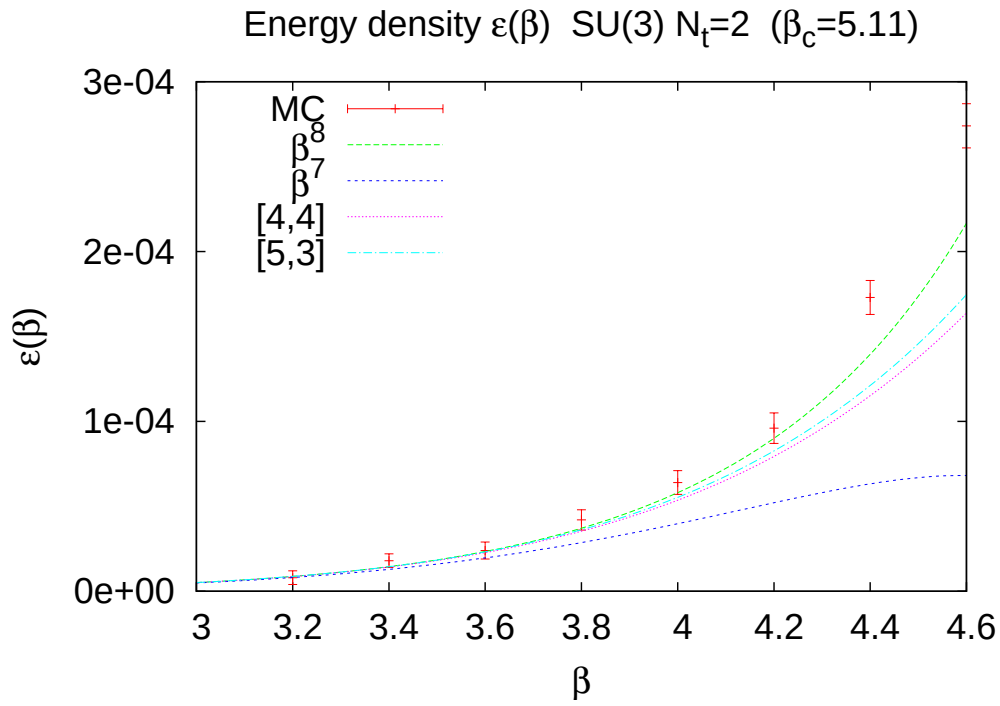

Figure 7: Comparison of Monte Carlo data for $N_t = 2$ with the plain series and Padé approximants in the case of $SU(3)$.

hold. What one can do is to compare the findings of the series expansion approach with a numerical investigation of the energy density, see fig. (7). We have done this in the case of $SU(3)$ and $N_\tau = 2$ and found agreement for the strong coupling region, but also disagreement when approaching the phase transition point. The observed worse convergence properties for $SU(3)$ are quite general in strong coupling expansions and have also encountered e.g. in the study of glueball masses [33].

4.3.3 Free energy density of $SU(N \to \infty)$ up to $\mathcal{O}(u^8)$

Next we will consider the limit $N \to \infty$, where all contributions of polymers of order N or higher cancel, leaving the free energy density in the confined phase a quantity of order N^0. For some typical graphs, we would like to show these cancellations.

Consider the graphs of fig. (8), defined on the N_τ lattice or the infinite lattice. They are of order $\mathcal{O}(u^6)$ in the correction to the basic polymer and

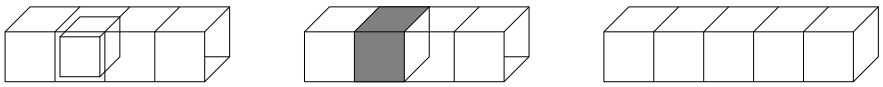

Figure 8: $N_\tau = 4$: Polymers contributing to $\mathcal{O}\left(u^6\right)$ in the correction. Left: One cube has been added to the basic polymer of the compactified lattice. Middle: Four fundamental plaquettes have been changed for plaquettes in higher dimensional representations (gray), whose expansion parameters a_r are proportional to u^2. To fulfill eq. (65) two fundamental plaquettes had to be added at the inside. Right: A graph with temporal extent $N_\tau = 5$, not fitting into the compactified lattice and thus contributing with a negative sign.

their contributions are

$$\begin{aligned}
\text{left:} \qquad \Phi_1 &= \frac{6}{N_\tau} u^{4N_\tau+6}\Big(-2N_\tau d_f^2\Big). \\
\text{middle:} \qquad \Phi_2 &= \frac{6}{N_\tau} u^{4N_\tau+2}\left(\frac{w}{u}\right)^4\Big(N_\tau d_f^2\Big), \\
&+ \frac{6}{N_\tau} u^{4N_\tau+2}\left(\frac{v_1}{u}\right)^4\Big(N_\tau d_f^2\Big), \\
&+ \frac{6}{N_\tau} u^{4N_\tau+2}\left(\frac{v_2}{u}\right)^4\Big(N_\tau d_f^2\Big). \\
\text{right:} \qquad \Phi_3 &= \frac{6}{N_\tau} u^{4N_\tau+6}\Big(-N_\tau d_f^2\Big).
\end{aligned} \tag{123}$$

Noting that in the limit $N \to \infty$ we have

$$w = v_1 = v_2 = u^2, \tag{124}$$

we see that all three contributions cancel against each other,

$$\Phi = \Phi_1 + \Phi_1 + \Phi_3 = 0. \tag{125}$$

One notices that the contributions of the left and the right graphs cancel those of the graph in the middle. We have no general proof, but up to order $\mathcal{O}(u^8)$ in the correction of the leading polymer, we found that all N dependence cancels. We remark that by leaving the limit, these graphs can contribute with $1/N$ corrections. Including all graphs up to $\mathcal{O}(u^8)$ in the

correction we get the following results

$$
\begin{aligned}
f(1,u) &= -6\,u^4 - 44\,u^6 - 495\,u^8 - 5336\,u^{10}, \\
f(2,u) &= -3\,u^8 - 94\,u^{12} - 168\,u^{14} - \frac{1983}{2}u^{16}, \\
f(3,u) &= -2\,u^{12} - 72\,u^{16} - \frac{404}{3}u^{18} - 636\,u^{20}, \\
f(4,u) &= -\frac{3}{2}u^{16} - 72\,u^{20} - 120\,u^{22} - 1121\,u^{24}, \\
f(N_\tau,u) &= -\frac{6}{N_\tau}\,u^{4N_\tau}\Big(1 + 12\,N_\tau u^4 + 20\,N_\tau u^6 + (83\,{N_\tau}^2 - 147\,N_\tau)u^8\Big).
\end{aligned}
$$

We would like to remark two things: First of all one sees that all coefficients have the same sign. This feature should be true for a larger number of orders than those calculated here. We come to this suggestion, since graphs of the infinite lattice, which enter with a positive sign in the free energy density, usually have factors of N^2 or higher and must be cancelled by other graphs to ensure it to be of order N^0. Also single polymers on the compactified lattice with one attached polymer contribute positively to the free energy density, but are either of $\mathcal{O}(N^2)$ or too small in number, to force the sign to switch.

Another observation is that only even powers of u contribute, in contrast to the case of $SU(3)$. This can be understood by noting that graphs with some inner structure cancel against other graphs in this limit, an observation that is true for all calculated graphs. The remaining graphs are made up solely of boundary plaquettes and hence these graphs cannot have an odd number of plaquettes. This observation is related to the fact that the free energy density is of $\mathcal{O}(N^0)$ in these orders. Graphs with inner structure usually have some dependence $\mathcal{O}(N)$ or higher (at least we have no counterexample in the calculated orders) and thus for the free energy density being of $\mathcal{O}(N^0)$, all such graphs must cancel. Although we believe this to be true also in higher orders, let us finally remark that these are just observations from our series expansions and have not been proven in general.

5 Free energy density od QCD

Having calculated the free energy density of pure lattice gauge theories, we now want to go further in the direction of physical theories and include finite quark masses. In a series expansion approach this is most conveniently done by a hopping parameter expansion, which will be described in the following. In doing so we will be tied to strong couplings and heavy quark masses, but our results will confirm the hadron resonance gas model in this regime. This model is used to describe physics in the confined phase up to the phase transition.

5.1 Hopping parameter expansion

As the fermionic action is bilinear in the quark fields it is possible to integrate them out exactly, which we will do for Wilson fermions. Using Grassmann integration [21] we find for an arbitrary flavour

$$S_q^f = -\ln\det(Q_f) = -\mathrm{tr}\ln\,(Q_f)\,, \tag{126}$$

where the quark matrix is given by

$$\begin{aligned}[Q_f]_{ab,\alpha\beta,yx} &= \delta_{ab}\delta_{\alpha\beta}\delta_{yx} - \kappa_f \sum_\mu \delta_{y,x+\hat{\mu}}(1+\gamma_\mu)_{\alpha\beta}U_{ab,x\mu} \\ &\equiv \delta_{ab}\delta_{\alpha\beta}\delta_{yx} - \kappa_f M_{ab,\alpha\beta,yx},\end{aligned} \tag{127}$$

which can be written in matrix notation

$$Q_f = 1 - \kappa_f M, \tag{128}$$

where we have defined the hopping matrix M. This leads to the hopping parameter expansion by expanding the logarithm

$$S_q^f = -\mathrm{tr}\,\ln(1-\kappa_f M) = \sum_l \frac{\kappa_f^l}{l}\mathrm{tr}M^l. \tag{129}$$

The delta functions in the hopping matrix M force the sum to extend solely over closed loops on the lattice. An important remark is, as we consider finite temperature, there will also be closed loops spanning around the temporal dimension of the lattice. Due to the antiperiodic boundary conditions of fermions, this gives an additional factor $(-1)^n$, which depends on the winding number n.

5.2 Hadron masses in the strong coupling and heavy quark mass region

Before considering the free energy density, we would like to calculate hadronic masses in a hopping parameter expansion at $\beta = 0$, for these masses are needed for a hadron resonance gas model description. We are interested only in the leading order term, but in principle this scheme allows also to compute corrections in the hopping parameter κ. The definitions and notations are almost directly taken from [21].

5.2.1 Hadron operators

In order to extract hadron masses, one has to specify suitable operators, which have non-vanishing overlap with the state, whose mass one wants to calculate. An interpolating operator for mesons $A(x)$ can be constructed from a quark and an antiquark and some γ matrices to specify the spin structure, like for the pions, ρ-mesons and kaons

$$\begin{aligned}
\pi_+(x) &\equiv \overline{d}_{\alpha c}(x)\,(\gamma_5)_{\alpha\beta}\,u_{\beta c}(x),\\
\pi_-(x) &\equiv \overline{u}_{\alpha c}(x)\,(\gamma_5)_{\alpha\beta}\,d_{\beta c}(x),\\
\rho_+(x) &\equiv \overline{d}_{\alpha c}(x)\,(\gamma_k)_{\alpha\beta}\,u_{\beta c}(x),\\
\rho_-(x) &\equiv \overline{u}_{\alpha c}(x)\,(\gamma_k)_{\alpha\beta}\,d_{\beta c}(x),\\
K_+(x) &\equiv \overline{s}_{\alpha c}(x)\,(\gamma_5)_{\alpha\beta}\,u_{\beta c}(x),\\
K_-(x) &\equiv \overline{u}_{\alpha c}(x)\,(\gamma_5)_{\alpha\beta}\,s_{\beta c}(x).
\end{aligned} \tag{130}$$

The generalization to mesons with a different quark content and other vector mesons should be obvious.

For baryons or antibaryons we can do the same using three quarks or antiquarks and some γ matrix. For proton and antiproton, we e.g. have

$$\begin{aligned}
p^+_\alpha(x) &\equiv \varepsilon_{cde}\,(C\gamma_5)_{\beta\gamma}\,u_{\alpha c}(x)\big[u_{\beta d}(x)d_{\gamma e}(x) - d_{\beta d}(x)u_{\gamma e}(x)\big],\\
p^-_\delta(y) &\equiv \varepsilon_{fgh}\,(C\gamma_5)_{\varepsilon\varphi}\,\overline{u}_{\delta f}(y)\big[\overline{d}_{\varepsilon g}(y)\overline{u}_{\varphi h}(y) - \overline{u}_{\varepsilon g}(y)\overline{d}_{\varphi h}(y)\big],
\end{aligned} \tag{131}$$

with the charge conjugation Dirac matrix C, satisfying

$$\begin{aligned}
&C\gamma_\mu C^{-1} = -\gamma_\mu^T,\\
&-C = C^T = C^{-1} = C^\dagger.
\end{aligned} \tag{132}$$

Now we are able to calculate the mass of the lightest particle with these quantum numbers from the exponential decay of this interpolating operator

in the following correlation function

$$\begin{aligned} m(A) &= -\lim_{t\to\infty}\frac{1}{t}\ln\langle A(0)A^\dagger(t)\rangle \qquad \text{for mesons,} \\ m(B) &= -\lim_{t\to\infty}\frac{1}{t}\ln\langle B(0)\overline{B}(t)\rangle \qquad \text{for baryons.} \end{aligned} \tag{133}$$

In order to have mass eigenstates, one has to sum over all spacelike coordinates

$$A(t) \equiv \sum_{\vec{x}} A(\vec{x},t), \tag{134}$$

but as we only want to calculate the leading order contribution, we need not care about this.

The curent task remains to calculate the expectation value eq. (133). Therefore we remember how one proceeds in general

$$\langle\mathcal{O}\rangle = \frac{1}{Z}\int \left[dUd\overline{\psi}d\psi\right] \mathrm{e}^{-S\left[U,\overline{\psi},\psi\right]}\mathcal{O}\left[U,\overline{\psi},\psi\right]. \tag{135}$$

As the action is bilinear in the fermion fields, we can perform the Grassmann integration and find for a single quark flavour f

$$\begin{aligned} &\langle\psi_{y_1}\overline{\psi}_{x_1}\psi_{y_2}\overline{\psi}_{x_2}\cdots\psi_{y_n}\overline{\psi}_{x_n}A\left[U\right]\rangle = \\ &\frac{1}{Z}\int\left[dU\right]\mathrm{e}^{-S_{eff}[U]}A\left[U\right]\sum_{z_1,\ldots,z_n}\varepsilon^{z_1\cdots z_n}_{y_1\cdots y_n}P_f\left[U\right]_{z_1x_1}\cdots P_f\left[U\right]_{z_nx_n}, \end{aligned} \tag{136}$$

where we have specified the form of the observable

$$\mathcal{O} = \psi_{y_1}\overline{\psi}_{x_1}\psi_{y_2}\overline{\psi}_{x_2}\cdots\psi_{y_n}\overline{\psi}_{x_n}A\left[U\right]. \tag{137}$$

The quantity $P_f\left[U\right]$ is the quark propagator and given as the inverse of

$$\begin{aligned} Q_f\left[U\right]_{yx} &= \delta_{yx} - \kappa_f\sum_\mu \delta_{yx+\hat{\mu}}(1+\gamma_\mu)U_{x\mu} \\ &= (1-\kappa_f M\left[U\right])_{yx}. \end{aligned} \tag{138}$$

The hopping parameter expansion for the quark propagator is given by

$$P_f\left[U\right]_{yx} = \left(1-\kappa_f M\left[U\right]\right)^{-1}_{yx} = \sum_{l=0}\kappa_f^l M\left[U\right]^l_{yx}. \tag{139}$$

Finally, the generalized ε-tensor is defined as

$$\varepsilon^{j_1\cdots j_n}_{i_1\cdots i_n} \equiv \left\{\begin{array}{c}1\\-1\\0\end{array}\right\}, \text{if } (j_1\cdots j_n) \text{ is } \left\{\begin{array}{c}\text{even}\\\text{odd}\\\text{no}\end{array}\right\} \text{permutation of } (i_1\cdots i_n). \tag{140}$$

5.2.2 Hadron masses

Now we are ready to calculate the hadronic masses in leading order hopping parameter expansion. As an example we want to present the calculations for the positive charged pion, the ρ-meson, the neutral pion and for the proton. The partition function in the strong coupling limit is given by

$$Z(\kappa_f) = \int [dU] \exp\left[\sum_f \sum_{l=1}^{\infty} \frac{\kappa_f^l}{l} \mathrm{tr}\, M^l[U]\right]. \tag{141}$$

Mesons: For the pion correlator $C(t)$, we get

$$C(t) \equiv \left\langle \pi_+(\vec{0},0) \left[\pi_+(\vec{0},t)\right]^\dagger \right\rangle_S = \left\langle \mathrm{tr}\left[\gamma_5 P_d(0,t)\gamma_5 P_u(t,0)\right] \right\rangle_{S_{eff}}, \tag{142}$$

and using γ_5-hermiticity

$$P_f(y,x) = \gamma_5 P_f^\dagger(x,y)\gamma_5, \tag{143}$$

we fing

$$C(t) = \left\langle \mathrm{tr}\left[P_d^\dagger(t,0) P_u(t,0)\right] \right\rangle_{S_{eff}}. \tag{144}$$

Thus we have to compute

$$C(t) = \frac{1}{Z} \int [dU] \exp\left[\sum_f \sum_{l=1}^{\infty} \frac{\kappa_f^l}{l} \mathrm{tr}\, M[U]^l\right] \mathrm{tr}\left[P_d^\dagger(t,0) P_u(t,0)\right]. \tag{145}$$

In the leading order calculation, we can in fact set the effective action as well as Z equal to 1 and obtain

$$\begin{aligned} C(t) &= \kappa_u^t \kappa_d^t \int [dU]\, \mathrm{tr}\left[(1+\gamma_0)^{2t} U_0(t \to 0) U_0^\dagger(t \to 0)\right] \\ &= 2N(2\kappa_u)^t (2\kappa_d)^t. \end{aligned} \tag{146}$$

We have used

$$\gamma_5(1-\gamma_\mu)\gamma_5 = (1+\gamma_\mu) \tag{147}$$

and

$$\mathrm{tr}\,\left[(1+\gamma_\mu)^N\right] = \mathrm{tr}\,\left[2^{N-1}(1+\gamma_\mu)\right] = 2^{N+1}. \tag{148}$$

If we apply eq. (133), we arrive at the following result

$$m(\pi^+) = -\ln(2\kappa_u) - \ln(2\kappa_d). \tag{149}$$

In case of the ρ-meson, which is a vector meson, we get the following correlator

$$C(t) = \left\langle \mathrm{tr}\left[\gamma_k P_d(0,t)\gamma_k P_u(t,0)\right]\right\rangle_{S_{eff}}. \tag{150}$$

If we use

$$\gamma_k(1-\gamma_0)\gamma_k = (1+\gamma_0), \tag{151}$$

instead of eq. (147), we arrive at the same result for the ρ-mass as for the pion masses

$$m(\rho^+) = -\ln(2\kappa_u) - \ln(2\kappa_d). \tag{152}$$

This at first sight surprising result is quite easy to explain. for the calculation we used very high quark masses, i.e. nearly static quarks and thus, as spin is a relativistic concept, have no mass difference between mesons with the same quark content but different spin structure. Another point of view is that we are far away from the chiral limit, indeed expanding about the opposite limit and thus there is no reason for the pseudoscalar mesons to be lighter than the other mesons.

In order to complete the results for the mesons, we consider the neutral pion as it is made of a superposition of quark-antiquark pairs with the same flavours. At this point, there arises a difficulty: As we are far away from the chiral limit, the separation in three light π-mesons and one heavy η_0-meson is no longer justified, since we have to expect similar masses. We have to consider all four possible states made up out of u and d quarks and their antiquarks on equal grounds. Thus we define $\pi_0 \sim \overline{u}\gamma_5 u$ and $\eta_0 \sim \overline{d}\gamma_5 d$, although in the chiral limit we would consider superpositions of these operators as the physical particles. For the neutral pion as defined above, the general expression eq. (136) yields

$$\left\langle \pi_0(x)\pi_0(y)^\dagger \right\rangle = \left\langle \mathrm{tr}\big[\gamma_5 P_u(y,x)\gamma_5 P_u(x,y)\big] - \mathrm{tr}\big[\gamma_5 P_u(x,x)\big]\mathrm{tr}\big[\gamma_5 P_u(y,y)\big]\right\rangle \tag{153}$$

In leading order the second term does not contribute and performing the same steps as mentioned above, we arrive at the following results for the masses of the neutral pseudoscalar mesons

$$\begin{aligned} m(\pi_0) &= -2\ln(2\kappa_u), \\ m(\eta_0) &= -2\ln(2\kappa_d). \end{aligned} \tag{154}$$

With these examples it should be obvious to obtain the leading order hopping parameter expansion of the masses of all other mesons.

Baryons: In the case of baryons, we have to consider interpolating operators made up out of three quarks or antiquarks, as already seen. For the proton mass, we have to consider the expectation value $\langle p_\alpha(x)\overline{p}_\alpha(y)\rangle$, with the following combination of quark propagators quoted from [21]

$$C(t) = \varepsilon_{cde}\varepsilon_{fgh}(C\gamma_5)_{\beta\gamma}(C\gamma_5)_{\varepsilon\varphi}\big[P^u_{\alpha c,\alpha f}(0,t)P^u_{\beta d,\varepsilon g}(0,t)P^d_{\gamma e,\varphi h}(0,t) + (\delta \leftrightarrow \varepsilon)\big].$$

Using the hopping parameter expansion, the leading order of this operator behaves like

$$C(t) \sim (2\kappa_u)^{2t}(2\kappa_d)^t, \tag{155}$$

from which the proton mass can be extracted to yield

$$m(p^+) = -2\ln(2\kappa_u) - \ln(2\kappa_d). \tag{156}$$

In the same way, we get e.g. for the neutron mass

$$m(n) = -\ln(2\kappa_u) - 2\ln(2\kappa_d). \tag{157}$$

As in the meson case, we can calculate every baryon mass with the mentioned recipe.

5.3 Hadron resonance gas model

Before calculating the free energy density of QCD in the strong coupling and heavy quark mass limit, we would like to present a model calculation for the hadronic phase. This model is called the hadron resonance gas model [44].

A starting point is the observation that in high energy experiments a large number of hadrons and resonances are produced. At certain high temperature and/or density, these particles will start to overlap and eventually create a new form of matter, the quark-gluon plasma. The question arises if and how one can understand the critical behaviour of the system in terms of the degrees of freedom in the confined phase.

The hadron resonance gas model is a description of physics in the confined phase as an ideal gas of non-interacting hadrons and resonances. In this way one incorporates all relevant degrees of freedom of the confined phase and implicitly includes interactions that result in resonance formation. It follows that the logarithm of the partition function can be written as a sum over logarithms of one-particle partition functions Z^1_n of all hadrons and resonances

$$\ln\, Z(T) = \sum_n \ln\, Z^1_n(T), \tag{158}$$

which can be directly converted to the free energy density

$$f(T) = \sum_n f_n^1(T). \tag{159}$$

In the continuum and for non-interacting particles the free energy density can be computed

$$\begin{aligned} f_n^1(T) &= \frac{T}{V} \ln Z_n^1, \\ \ln Z_n^1 &= V g_n \int \frac{d^3p}{(2\pi)^3} \ln \left(1 \pm e^{-\omega_n/T}\right)^{\pm 1}, \end{aligned} \tag{160}$$

where the upper sign corresponds to fermions and the lower sign to bosons. The term g_n represents a spin-isospin degeneracy factor. The dispersion relation is given by

$$\omega = \sqrt{p^2 + m^2}, \tag{161}$$

that leads to the following result for the free energy density

$$f_n^1(T) = -g_n \frac{m_n^2 T^2}{2\pi^2} K_2 \left(\frac{m_n}{T}\right), \tag{162}$$

where K_2 is a modified Bessel function. If we assume the particles to move nonrelativistically, i.e. $T \ll m_n$ and use the behaviour of the modified Bessel functions for large arguments x

$$K_n(x) \sim \sqrt{\frac{\pi}{2x}}\, e^{-x}, \tag{163}$$

the one-particle free energy density can be written as

$$f_n^1(T) = -g_n T \left(\frac{m_n T}{2\pi}\right)^{\frac{3}{2}} e^{-m_n/T}. \tag{164}$$

This classical, nonrelatvistic result is true for bosons as well as for fermions. Hence we obtain the following expression for the free energy density from the hadron resonance gas model

$$f(T) = -T \sum_n g_n T \left(\frac{m_n T}{2\pi}\right)^{\frac{3}{2}} e^{-m_n/T}. \tag{165}$$

5.4 The free energy density

Having calculated the leading orders of the hadron masses, we use this knowledge to derive the hadron resonance gas model from first principles in the strong coupling and heavy quark mass sector. For a sufficiently strong coupling, we can omit the gluonic contribution to the partition function and write

$$Z(\kappa_f) = \int [dU] \exp\left[\sum_f \sum_{l=1}^{\infty} \frac{\kappa_f^l}{l} \mathrm{tr}\, M_f[U]^l\right]. \tag{166}$$

In principle the sum extends over all closed loops l on the lattice, which for finite lattice extents can have non-trivial winding numbers. In the finite temperature case, these are e.g. the Polyakov loops. One might wonder, that for temporal lattice sizes $N_\tau \geq 4$ the leading contributions to the effective action are those coming from the plaquette $\sim \kappa^4$. Nevertheless we calculate the free energy density, a quantity that has to be renormalized by subtracting the zero temperature contribution. Thus the leading terms in the observable are those coming from the smallest graphs having a non-trivial winding number, the Polyakov loops

$$L_{\vec{x}} \;=\; \mathrm{tr}\, W_{\vec{x}} = \mathrm{tr} \prod_{\tau=1}^{N_\tau} U_0(\vec{x}, \tau). \tag{167}$$

These terms are $\sim \kappa^{N_\tau}$ in the effective action. Since in the confined phase the Polyakov loop cannot be screened, the leading term in the free energy density will consist of at least two (oppositely oriented) Polyakov loops, giving a factor of $\sim \kappa^{2N_\tau}$. This corresponds to mesonic contributions since we used two static quark lines, one for a quark and one for an antiquark. To get a full hadron resonance gas picture, we also need baryons, which consist of three quarks or antiquarks. Hence we also have to take into account generalized Polyakov loops that wind around the temporal direction two and three times before being traced. If we do so, the effective action leading to the lowest (physical) mass hadrons reads

$$\begin{aligned} S_{eff}^f &= -2(2\kappa_f)^{N_\tau} \sum_{\vec{x}} \left(\mathrm{tr} L_{\vec{x}} + \mathrm{tr} L_{\vec{x}}^\dagger\right) \\ &+ (2\kappa_f)^{2N_\tau} \sum_{\vec{x}} \left(\mathrm{tr} L_{\vec{x}}^2 + \mathrm{tr}(L_{\vec{x}}^2)^\dagger\right) \\ &- \frac{2}{3}(2\kappa_f)^{3N_\tau} \sum_{\vec{x}} \left(\mathrm{tr} L_{\vec{x}}^3 + \mathrm{tr}(L_{\vec{x}}^3)^\dagger\right). \end{aligned} \tag{168}$$

The signs are due to antiperiodic boundary conditions and depend on the winding number n as $(-1)^n$. The effective partition function reads

$$Z = \int [dU] \exp\Big[- S_{eff}(U) \Big] = \int [dU] \exp\Big[- \sum_f S^f_{eff}(U) \Big]. \qquad (169)$$

Expanding all terms up to $\mathcal{O}(\kappa^{3N_\tau})$ and doing the group integrals we get the following result for the free energy density for two flavours up and down

$$\begin{aligned} f &= -\frac{1}{N_\tau}\Big[4(2\kappa_u)^{2N_\tau} + 8(2\kappa_u 2\kappa_d)^{N_\tau} + 4(2\kappa_d)^{2N_\tau}\Big] \\ &- \frac{1}{N_\tau}\Big[8(2\kappa_u)^{3N_\tau} + 12\big[(2\kappa_u)^2 2\kappa_d\big]^{N_\tau} \\ &+ 12\big[2\kappa_u(2\kappa_d)^2\big]^{N_\tau} + 8(2\kappa_d)^{3N_\tau}\Big] \end{aligned} \qquad (170)$$

If we now remember the expressions for the hadron masses, we are able to rewrite this as

$$\begin{aligned} f(N_t;\kappa_f) &= -\frac{1}{N_t}\Big[\sum_{0^-} e^{-m\left(0^-\right)N_t} + 3\sum_{1^-} e^{-m\left(1^-\right)N_t}\Big] \\ &\quad -\frac{1}{N_t}\Big[2\sum_{\frac{1}{2}^+} e^{-m\left(\frac{1}{2}^+\right)N_t} + 4\sum_{\frac{3}{2}^+} e^{-m\left(\frac{3}{2}^+\right)N_t}\Big], \end{aligned} \qquad (171)$$

where the sum over the pseudoscalar mesons includes the pions as well as the η_0. This is due to the fact that we calculate with heavy quark masses. Similar formulas hold for a larger number of flavours.

If we now rewrite $T = 1/N_\tau$, eq. (171) reads

$$\begin{aligned} f(T) &= -T\left[\sum_{0^-} e^{-m\left(0^-\right)/T} + 3\sum_{1^-} e^{-m\left(1^-\right)/T}\right] \\ &\quad -T\left[2\sum_{\frac{1}{2}^+} e^{-m\left(\frac{1}{2}^+\right)/T} + 4\sum_{\frac{3}{2}^+} e^{-m\left(\frac{3}{2}^+\right)/T}\right], \end{aligned} \qquad (172)$$

which one should compare with the formula following from the hadron resonance gas model, eq. (165). One can see that this formula is reproduced with the masses and the corresponding degeneracies up to the factor $(mT/2\pi)^{\frac{3}{2}}$. We believe this factor to be absent due to a modified dispersion relation in the strong coupling limit and the neglect of higher orders in the expansion. Thus in this parameter region, the hadron resonance gas is confirmed from a first principle calculation.

6 Polyakov loop susceptibility

In this chapter we calculate a strong coupling expansion of the susceptibility of the order parameter, the Polyakov loop. There is no major difference between the gauge groups $SU(2)$ and $SU(3)$ in the calculation of the series expansions, but the fact that latter undergoes a first order phase transition spoils our usual analysis method, that relies on scaling properties. Hence we will discuss our calculations in different subchapters.

6.1 Polyakov loop susceptibility of SU(2)

Here we consider the $SU(2)$ Polyakov loop susceptibility

$$\chi_L = V\Big(\langle L^2\rangle - \langle L\rangle^2\Big), \tag{173}$$

where we have defined the Polyakov loop $L_{\vec{x}}$ and its average L as

$$L_{\vec{x}} = \operatorname{tr} W_{\vec{x}} = \operatorname{tr} \prod_{\tau=1}^{N_\tau} U_0(\vec{x},\tau), \tag{174}$$

$$L = \frac{1}{V}\sum_{\vec{x}} L_{\vec{x}}. \tag{175}$$

If we couple the Polyakov loop to an external source J in the action,

$$S(J) = -\frac{\beta}{2}\sum_p \operatorname{tr} U_p - J\sum_{\vec{x}} L_{\vec{x}}, \tag{176}$$

then we can express the susceptibility as

$$\chi_L = \frac{1}{V}\,\frac{\partial^2}{\partial J^2}\ln Z(J)\bigg|_{J=0}. \tag{177}$$

The logarithm of the partition function is an extensive quantity, which can be calculated using the cluster expansion. This is quite similar to the calculation of the free energy density. The factor V^{-1} ensures that χ_L is finite in the thermodynamic limit away from the transition point.

6.1.1 Character expansion

In order to obtain a strong coupling series for eq. (177), we expand the partition function

$$Z(J) = \int [dU]\left[\prod_p \exp\left(\frac{\beta}{2}\operatorname{tr} U_p\right)\right]\left[\prod_{\vec{x}} \exp\left(J\operatorname{tr} W_{\vec{x}}\right)\right] \tag{178}$$

in terms of characters

$$\exp\left(\frac{\beta}{2}\operatorname{tr} U_p\right) = c_0(\beta)\left[1+\sum_{j\neq 0} d_j a_j(\beta)\,\chi_j(U_p)\right] \tag{179}$$

$$\exp\left(J\operatorname{tr} W_{\vec{x}}\right) = c_0(J)\left[1+\sum_{j\neq 0} b_j(J)\chi_j(W_{\vec{x}})\right]. \tag{180}$$

The prefactor $c_0(\beta)$ can be neglected since it does not depend on J, and for $a_j(\beta)$, $b_j(J)$ and $c_0(J)$ we have similar to (69) the expressions

$$a_j(\beta) = \frac{I_{2j+1}(\beta)}{I_1(\beta)}, \tag{181}$$

$$b_j(J) = \frac{d_j I_{2j+1}(2J)}{I_1(2J)}, \tag{182}$$

$$c_0(J) = \frac{I_1(2J)}{J}. \tag{183}$$

As before, we will use the coefficient $u = a_{1/2}$ of the fundamental representation as expansion parameter.

Applying a cluster expansion to the logarithm of the partition function as described in chapter 4, it can be represented as a sum of clusters $\Phi(C)$

$$\frac{1}{V}\ln Z(J) = \ln c_0(J) + \sum_C \Phi(C). \tag{184}$$

The sum contains all clusters C of connected polymers modulo translation, see [21,45] for details. The leading order, i.e. the strong coupling limit $\beta = 0$, can be obtained by neglecting all graphs giving

$$\chi_L = \frac{\partial^2}{\partial J^2}\ln c_0(J)\bigg|_{J=0} = 1. \tag{185}$$

As we will see in the next chapter, corrections are of order $\mathcal{O}(u^{N_\tau})$.

6.1.2 Graphical expansion

The first graph having a non-trivial u-dependence is shown in fig (9), together with the leading correction graph. The left and right boundaries of these graphs are meant to be identified due to the periodic boundary conditions.

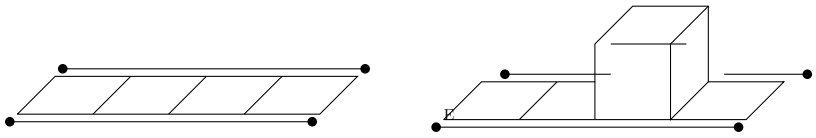

Figure 9: Examples for $N_\tau = 4$. Left: Two Polyakov loops and N_τ plaquettes wind around the temporal dimension. Right: The first correction with additional plaquettes.

The contributions can be calculated with the following group integration formula

$$\int dU \chi_r(U)\chi_s(U) = \frac{\delta_{rs}}{d_{rs}}, \tag{186}$$

so that

$$\Phi_0 = 3u^{N_\tau} \left(b_{1/2}(J)\right)^2 \tag{187}$$

for the leading non-trivial order and

$$\Phi_1 = 12N_\tau u^{N_\tau+4} \left(b_{1/2}(J)\right)^2 \tag{188}$$

for the first correction.

From eq. (177) it is obvious that we solely have to take into account graphs, which contribute to order J^2. That means only graphs with two Polyakov loops in the fundamental or one loop in the adjoint representation are allowed as a consequence of eq. (182). For the first possibility, the loops have to be on different lattice sites. The generation of contributing graphs is not uniform with respect to N_τ and we have to distinguish between small, intermediate and large values of N_τ.

Large N_τ: Large N_τ obtain contributions from nearest-neighbour Polyakov loops as shown in fig. (9) and corrections from adding plaquettes to the leading order graph. Next-to-nearest-neighbour graphs are suppressed in the calculated orders. Of course this is only true for large enough N_τ if we calculate to some fixed order in u.

Small N_τ: The smallest possible N_τ is 1. Typical graphs are shown in fig. (10). These graphs are meant to be spatial projections of graphs like those in fig. (9) on the left side. In higher orders we get some additional spatial plaquettes, too, e.g. by filling the cross-section of the self avoiding polygons, but these contributions are small compared to the increasing number of self-avoiding walks.

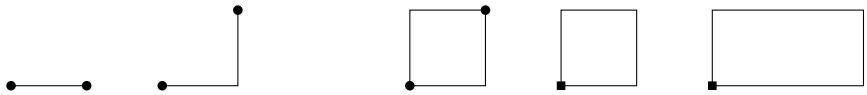

Figure 10: Left: Self avoiding walks with two fundamental Polyakov loops. Right: Self avoiding polygons with one adjoint Polyakov loop or two fundamental ones.

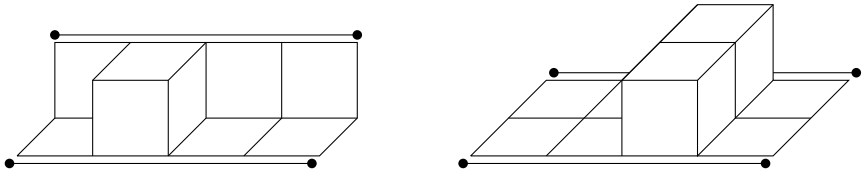

Figure 11: Examples of corrections to self avoiding walks of length $L = 2$ and $N_\tau = 4$.

Intermediate N_τ: For intermediate N_τ $(= 2, 3, 4...)$ we have to take into account graphs of both type. There are also some other corrections as those shown in fig. (11). Thus the expansions for these N_τ are the most labour-intensive ones.

6.1.3 Results

As we restrict ourselves in the analysis to $N_t = 1, \ldots, 4$, we only mention the results for these cases. We have the following series expansions for $\chi_L(N_\tau, u)$:

$$\begin{aligned}
\chi_L(1,u) = \quad & 1 + 6\,u + 30\,u^2 + 150\,u^3 + 738\,u^4 + 3622\,u^5 + \frac{52982}{3}u^6 + \\
& + \frac{773434}{9}u^7 + \frac{11239612}{27}u^8 + \ldots, \\
\chi_L(2,u) = \quad & 1 + 6\,u^2 + 30\,u^4 + 222\,u^6 + 1218\,u^8 + \frac{24602}{3}u^{10} + \ldots, \\
\chi_L(3,u) = \quad & 1 + 6\,u^3 + 30\,u^6 + 72\,u^7 + 72\,u^8 + 78\,u^9 + 576\,u^{10} + 1776\,u^{11} + \\
& + 1770\,u^{12} + \ldots, \\
\chi_L(4,u) = \quad & 1 + 6\,u^4 + 126\,u^8 + 48\,u^{10} + 2830\,u^{12} + \frac{91808}{135}u^{14} + \ldots. \qquad (189)
\end{aligned}$$

One can see that the distribution of non-zero coefficients is not uniform among these N_τ. The leading non-trivial order is always of order u^{N_τ}, while the second one is of order u^{2N_τ}. One thus could think that u^{N_τ} is a more natural expansion parameter and indeed we will see in our analysis of the Polyakov loop effective action, that with some modifications this turns out to be the case.

6.1.4 Series analysis: Biased estimates

As already mentioned in the analysis of the free energy density, there is strong evidence that the finite temperature $SU(2)$ deconfinement transition is of second order and in the 3D Ising universality class. It is possible to use this information in the analysis of our results. Universality tells us that near the critical coupling the Polyakov loop susceptibility should behave like

$$\chi_L \sim \frac{1}{(u_c - u)^{\gamma}}, \tag{190}$$

with $\gamma = \gamma_I = 1.237$ [46] for the 3D-Ising universality class. Taking the logarithmic derivative this should behave like

$$D_\chi(u) \equiv \frac{d}{du} \ln(\chi_L) \sim \frac{\gamma}{(u_c - u)}. \tag{191}$$

For this quantity we can use the analysis introduced in Sec. (4.2.6.)

Since there are precise estimates for the critical couplings from Monte Carlo simulations, it is possible to use them to get better estimates for the critical exponents via

$$(u_c - u) D_\chi(u) = \gamma + \mathcal{O}(u_c - u), \tag{192}$$

which is the more precise the better we know u_c.

In the same way we can use the accurate value γ_I from the 3D Ising model to get more precise Padé estimates for the critical coupling

$$(\chi_L)^{\frac{1}{\gamma}} \sim \frac{1}{(u_c - u)}. \tag{193}$$

For a further discussion of these topics, see [9].

6.1.5 Critical couplings from the Polyakov loop susceptibility

Using Padé approximants and biased estimates we now would like to extract the critical parameters of $SU(2)$ lattice gauge theory from the series expansions of the Polyakov loop susceptibility.

$\mathbf{N_\tau = 1}$: For this N_τ our series shows best convergence behaviour leading to the best estimates we can make. We decided to consider only Padés $[L, M]$ with $L, M > 2$ to have big enough polynomials in the numerator as well as in the denominator, since we have a larger number of coefficients as in other cases. So-called defective approximants with an adjacent zero-pole

Padé	u_c	β_c	γ
$[5,2]$	0.21055	0.86825	1.167
$[3,3]$	0.20967	0.86439	1.138
$[4,2]$	0.20957	0.86396	1.146
$[2,4]$	0.20987	0.86527	1.135
$[3,2]$	0.20927	0.86264	1.126
$[2,2]$	0.20820	0.85796	1.102

Table 3: Unbiased critical couplings and exponents for $N_\tau = 1$.

pair indicated by a small residuum (we chose Res < 0.003 to be defective) are also ruled out. We obtain unbiased results from an analysis of logarithmic derivatives shown in tab. (3).

There exist different values for the critical coupling from Monte Carlo simulations in the literature: $\beta_c = 0.8730(2)$ from [47] and $\beta_c = 0.85997(10)$ or 0.86226(6) from [42]. Our unbiased results seem to favor one of the latter, but with a critical exponent deviating about 10 percent from universality. Additionally, we observe an upwards trend in the coupling as well as in the exponent with increasing order. Thus we consider biased estimates, which should be more accurate. Using $\gamma_I = 1.237$ from [46], we get the results shown in table (4).

Padé	u_c	β_c
$[6,2]$	0.21221	0.87553
$[4,3]$	0.21159	0.87281
$[2,5]$	0.21138	0.87189
$[3,3]$	0.21229	0.87588
$[2,4]$	0.21238	0.87628
$[4,2]$	0.21279	0.87808
$[3,2]$	0.20986	0.86523
$[2,3]$	0.21464	0.88621
$[2,2]$	0.21495	0.88757

Padé	γ_1	γ_2
$[3,4]$	1.1250	1.2378
$[4,3]$	1.1244	1.2331
$[2,5]$	1.1246	1.2157
$[5,2]$	1.1244	1.2208
$[3,3]$	1.1225	1.2579
$[2,4]$	1.1236	1.2661
$[4,2]$	1.1244	1.2950
$[3,2]$	1.1240	1.2308
$[2,3]$	1.1238	1.2215

Table 4: Biased critical couplings and exponents for $N_\tau = 1$.

We calculate the average of β_c to be $\overline{\beta_c} = 0.877(6)$ using all Padés and $\overline{\beta_c} = 0.875(2)$ using only the three highest orders which behave more smoothly. The error mentioned is the standard deviation of the mean value and thus measures rather some scattering in the singularity structure than the true error. But if we take this as an estimate of the real error, then both results are consistent with the Monte Carlo result of [47].

To obtain the biased critical exponent, we used the values $\beta_1 = 0.86226$ and $\beta_2 = 0.873$. The former gives a mean critical exponent of $\overline{\gamma_1} = 1.124(1)$ and the latter $\overline{\gamma_2} = 1.24(2)$. Although the first result is much more stable, it is only the second one which is consistent with universality. Thus we conclude that it is the value $\beta_c = 0.8730(2)$ of [47], which is supported by our series expansions.

$\mathbf{N_\tau = 2, 3, 4}$: For intermediate N_τ our results become less precise the bigger we choose N_τ. This can be understood since we are leaving the strong coupling regime. Nevertheless our results are consistent with Monte Carlo results [20, 42, 47] and universality. We summarize our results in table (5). We have to remark that all given values are biased estimates now, with $\gamma_I = 1.237$ and $\beta_c(N_\tau = 2) = 1.87348$, $\beta_c(N_\tau = 3) = 2.1768$ and $\beta_c(N_\tau = 4) = 2.2991$. The latter values correspond to the latest Monte Carlo estimates [20, 42].

N_τ	γ_I	$\overline{\gamma}$	Padés	β_c^{MC}	$\overline{\beta_c}$	Padés
2	1.237	1.21(2)	5	1.87348(2)	1.871(3)	6
3	1.237	1.3(3)	2	2.1768(30)	2.14(5)	6
4	1.237	1.3(1)	2	2.2991(2)	2.18(3)	4

Table 5: Comparison of expected values for the critical parameters from universality and simulations with our findings.

As already mentioned one can see that results get worse with increasing N_τ. For $N_\tau = 1, 2$ we have nearly the precise Monte Carlo value for the critical coupling and a good estimate for the critical exponent. Error bars become larger for $N_\tau = 3$, but still consistent with the expected values. For $N_\tau = 4$ we got clear signs for leaving the strong coupling regime. Nevertheless, so far these are the best analytic results obtained for the critical parameters, we are aware of. Further improvement on this will be discussed in the next chapter.

6.2 $SU(3)$ and QCD

For pure $SU(3)$ there is a first order phase transition, i.e. the correlation length remains finite even at the critical temperature, thus spoiling our analysis methods, which require scaling behaviour. In this case we define the Polyakov loop as

$$L_{\vec{x}} = \operatorname{tr} W_{\vec{x}} + \operatorname{tr} W_{\vec{x}}^\dagger. \tag{194}$$

If we decrease quark masses m from infinity, there will be a critical value m_c, where the transition should turn second order, but the Polyakov loop loses its property of being an order parameter. Therefore we introduce dynamical quarks in leading order hopping parameter expansion, chemical potential as factors $\exp(\pm\mu)$ to the temporal link variables and get for small temporal lattice extents

$$S_q = h(\kappa,\mu)\mathrm{tr}\, W_{\vec{x}} + h(\kappa,-\mu)\mathrm{tr}\, W^\dagger_{\vec{x}}. \tag{195}$$

The parameter $h(\kappa,\pm\mu)$ depends on the hopping parameter κ and chemical potential μ via

$$h(\kappa,\pm\mu) = 2(2\kappa e^{\pm\mu})^{N_\tau}. \tag{196}$$

Introducing Polyakov loop source terms J and putting everything together, we obtain the following partition function

$$\begin{aligned} Z &= \int [dU] \exp\left[\frac{\beta}{6}\sum_p \left(\mathrm{tr}U_p + \mathrm{tr}U_p^\dagger\right)\right. \\ &+ \left.\sum_{\vec{x}} \left\{\big[h(\kappa,\mu)+J\big]\mathrm{tr}\, W_{\vec{x}} + \big[h(\kappa,-\mu)+J\big]\mathrm{tr}\, W^\dagger_{\vec{x}}\right\}\right]. \end{aligned} \tag{197}$$

Now we can proceed in the same way as in the $SU(2)$ case with the difference that we have to take into account not only the graphs with two Polyakov loop source terms, but all graphs with contributions of the order J^2h^m, for these give finite results after differentiating twice with respect to J and setting $J=0$. At first we rewrite the partition function with two different character expansions and omit the factor $c_0(\beta)$

$$\begin{aligned} Z &= \int [dU] \prod_p \left[1 + \sum_{r\neq 0} d_r a_r(\beta)\chi_r(U_p)\right] \\ &\times \prod_{\vec{x}} b_0(h,J)\left[1 + \sum_{r\neq 0} b_r(h,J)\chi_r(W_{\vec{x}})\right]. \end{aligned} \tag{198}$$

Let us note that for non-vanishing chemical potential μ the expansion parameters $b_r\big(h,J\big)$ are different for complex conjugate representations r and $\bar{r}$ and related via

$$b_r\big(h(\kappa,\mu),J\big) = b_{\bar{r}}\big(h(\kappa,-\mu),J\big). \tag{199}$$

In order to get the proper series expansion we now have to draw all possible diagrams to a given order in u and the number of Polyakov loop terms m. An

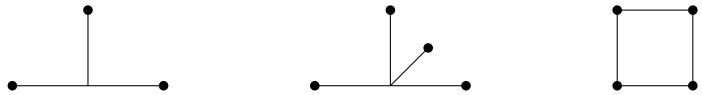

Figure 12: Examples of terms with a larger number of Polyakov loop source terms.

important fact is that for a given order in u, there is only a finite number of graphs. For example in order u^n, we can have only graphs fulfilling $m \leq 2n$. The higher powers in (h, J) in a given order in u are all emerging from the expansion of the parameters $b_r(h, J)$. This remains true even if we include higher order hopping parameter terms in the action, but then of course the number of diagrams increases even more rapidly than in our approximation.

6.2.1 Series expansion

As already mentioned we now have to take into account also terms with higher powers in (h, J). Some examples for graphs of the case $N_\tau = 1$ are given in fig. (12). We have derived the series expansion of the Polyakov loop susceptibility up to orders $u^n h^m$, with $n + m \leq 6$. The result for the $N_\tau = 1$ series, arranged in increasing orders of u, reads

$$\begin{aligned}
\chi_L(u,h) \;=\; & \left[1 + ch + \left(-\frac{4}{3}c^3 + \frac{1}{2}c\right)h^3 + \left(-\frac{5}{3}c^4 + \frac{4}{3}c^2 - \frac{7}{24}\right)h^4 \right. \\
& \left. + \left(\frac{2}{15}c^5 + \frac{1}{3}c^3 - \frac{1}{8}c\right)h^5 + \left(\frac{28}{15}c^6 - \frac{7}{5}c^4 - \frac{7}{120}c^2 + \frac{119}{720}\right)h^6\right] \\
& + \left[6 + 18ch + \left(6c^2 + 3\right)h^2 + \left(-40c^3 + 15c\right)h^3 \right. \\
& \left. + \left(-90c^4 + 66c^2 - \frac{69}{4}\right)h^4 + \left(-\frac{32}{5}c^5 - 8c^3 + 6c\right)h^5\right]u \\
& + \left[30 + 180ch + \left(144c^2 + 72\right)h^2 + \left(-760c^3 + 285c\right)h^3 \right. \\
& \left. + \left(-\frac{5985}{2}c^4 + \frac{8985}{4}c^2 - \frac{4485}{8}\right)h^4\right]u^2 \\
& + \left[150 + 1470ch + \left(\frac{4113}{2}c^2 + \frac{4113}{4}\right)h^2 \right. \\
& \left. + \left(-6856c^3 + 2571c\right)h^3\right]u^3 \\
& + \left[786 + 10752ch + \left(\frac{1131747}{32}c^2 + \frac{1088547}{64}\right)\right]u^4 \\
& + \left[4011 + 73521ch\right]u^5 + \frac{152247}{8}u^6, \qquad (200)
\end{aligned}$$

where we used the abbreviation $c \equiv \cosh(\mu)$. Since the only μ-dependence appears in $\cosh(\mu)$ terms, one can immediately see that the Polyakov loop susceptibility is invariant under $\mu \leftrightarrow -\mu$ as it should be.

6.2.2 Results and analysis: $\mu = 0$

In order to locate the critical point $(\beta_c, \kappa_c)(\mu)$ we have to adjust our analysis methods to multiple variables. Since we assume the critical point to be a second order phase transition point, we try to construct a scaling axis, which passes through this point. As our series are expanded around the origin $(\beta = 0, \kappa = 0)$, we rescale our expansion variables as

$$\begin{aligned} u &= n \cdot t, \\ h &= \frac{1}{n} \cdot t. \end{aligned} \tag{201}$$

The slopes of the two curves are the inverse of each other, since they have to describe the same axis in a (u, h) diagram. Along this scaling axis, we expect a behaviour

$$\chi_L(t) \sim \frac{1}{(t_c - t)^\lambda}, \tag{202}$$

with some critical exponent λ. The critical point is believed to be in the 3d Ising universality class, thus one could assume $\lambda = \gamma_I = 1.237$. But as mentioned, the Polyakov loop is no longer an order parameter with finite quark masses, so why should χ_L scale in this way? At the critical point the dynamics are supposed to be controlled by an effective Ising-like Hamiltonian H, which can be expressed in terms of two operators E and M [48]. These energy-like and magnetic-field-like operators couple to two relevant scaling fields τ and ξ according to

$$H = \tau E + \xi M. \tag{203}$$

The operators E and M must be related to the fields entering the action, the plaquette term S_G and the Polyakov loop term S_L. Generally one would expect some superposition, so that the susceptibility χ_L will receive contributions from both χ_E and χ_M. Thus also the exponent could be some mixture of γ and α. As a result and to keep the analysis general, we will not calculate biased estimates, but use the logarithmic derivative method with scaling parameter t.

Our argumentation for the observation of the critical point will be as follows: According to eq. (201) we let n, which parametrizes the slope of

our scaling axis, run between some values and calculate DLog-Padés and singularities. If the axis misses the critical point, we will expect a vast scattering in the distribution of the singularities depending on the distance to the critical point. Otherwise if we meet this point, the logarithmic derivative in t shall give a quite narrow window where the singularities accumulate. Additionally the residues should approach at this point.

As a result, we define our estimate of the critical value t_c as the mean value over all Padé singularities evaluated at the point where the standard deviation of this mean value gets minimal. With this method we find at $\mu = 0$

$$\begin{aligned} n &= 0.730, \\ \overline{t_c} &= 0.1716(1), \\ \overline{\lambda} &= 1.0296(26), \end{aligned} \tag{204}$$

where the errors in brackets are the standard deviations from the mean value. Let us note that both standard deviations reach their minimum for the same slope parameter n. We also see that the critical exponent obtained with this method differs from the Ising exponents γ and α. By using n and t_c we can calculate the critical couplings with eq. (201), and obtain

$$\begin{aligned} u_c &= 0.1253(1), \\ h_c &= 0.2351(1). \end{aligned} \tag{205}$$

6.2.3 Results and analysis: $\mu \neq 0$

Now we would like to turn on a chemical potential. The result (200) given in the last section has already been obtained with finite chemical potential. All we have to do now is to repeat the same steps as described in the analysis for $\mu = 0$ for various choices of the chemical potential. Of particular interest is the movement of the critical point with μ. From a Potts model investigation and mean field theory [49, 50], one expects a shrinking of the first order region, i.e.

$$\left.\frac{dh_c(\mu^2)}{d\mu^2}\right|_{\mu=0} < 0. \tag{206}$$

We have calculated this function at several points and plotted it in fig. (13). One can see the shrinking of the critical region with increasing μ. For small μ we performed a fit to a low order polynomial to get a rough picture of the behaviour of the signs of the different coefficients. We got the following

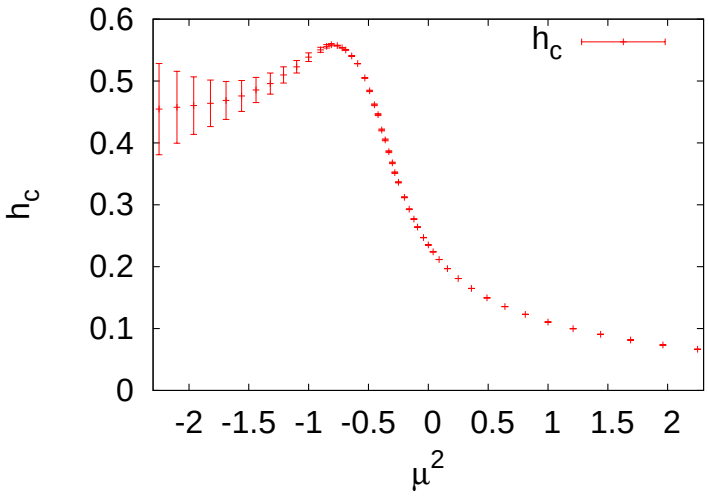

Figure 13: Behaviour of the critical h_c as a function of μ^2 for real and imaginary chemical potential.

result

$$\frac{h_c(\mu^2)}{h_c(0)} = 1 - 1.24(2)\mu^2 + 1.59(13)\mu^4 - 1.38(35)\mu^6 + \ldots, \tag{207}$$

where the error bars occurs from the fitting procedure. These alternating signs indicate the convergence limiting singularity to be on the negative μ^2 axis, i.e. at imaginary chemical potential. thus it is interesting to study the behaviour of $h_c(\mu^2)$ also at negative values of the argument. There will be no problem with the series expansion approach, as we merely have to set $\mu \to i\mu$ to do this. In eq. (200), this means that c abbreviates now $\cos(\mu)$ instead of $\cosh(\mu)$. If we do so, we get the curve shown in fig. (13). One can see that starting at about $\mu^2 \simeq -1$ the standard deviation grows larger and larger. We interpret this as the point where the convergence radius limiting singularity is located. Theoretical arguments show that indeed there should be a singularity indicating the Roberge-Weiss transition point [51].

7 Polyakov loop effective action

In the preceding chapters we saw that strong coupling expansions are able to give both qualitatively as well as quantitatively reasonable results. The drawback is that this is limited to the strong coupling region. In case of the Polyakov loop susceptibility this means $N_\tau \lesssim 4$. In order to get to larger temporal lattice extents, we should calculate more terms, but this is very limited in applicability. A possible way out is to try to resum a large number of terms. Resummation techniques are also used in weak coupling perturbation theory, e.g. in hard thermal loop (HTL) resummed perturbation theory in order to improve convergence [52]. The price we have to pay is that we spoil the exactness of the strong coupling expansion after some N_τ-dependent order. We will see that the obtained results will justify this procedure.

7.1 Effective action for $SU(2)$

In contrast to the preceding chapter, we will now employ a different strategy. We remark that we can rewrite the pure gauge partition function as

$$\begin{aligned} Z &= \int [dU] \exp\left(-S_g\left[U\right]\right) = \int [dU_0] \exp(-S_{eff}\left[L\right]), \\ S_{eff}\left[L\right] &\equiv -\ln \int [dU_i] \exp\left(-S_g\left[U\right]\right), \end{aligned} \tag{208}$$

where we have split the integration measure and will perform the spatial link integrations first. The crucial observation is that the remaining effective action is a function of only the Polyakov loop, as it is the only remaining gauge invariant observable. In this way we are able to formulate an effective theory for the order parameter of finite temperature deconfinement and this should be the best quantity to study, when one is interested in the phase transition. Let us say that this procedure is exactly compatible with the approach proposed in [53]: One first integrates out the spatial degrees of freedom and is left with an effective theory of the order parameter, which resembles some spin model. This dimensionally reduced effective model is easier to solve and matching of its parameters to the original ones should serve to obtain critical parameters.

On e should remark that at this stage, there has been no approximation in eq. (208). The approximations we will do are to consider only a finite number of Polyakov loop interaction terms (indeed only the nearest neighbour interaction) and to truncate the strong coupling expansion of this interaction terms after some order. The strong coupling expansion will give us the matching of the different model parameters. The fact that we will consider

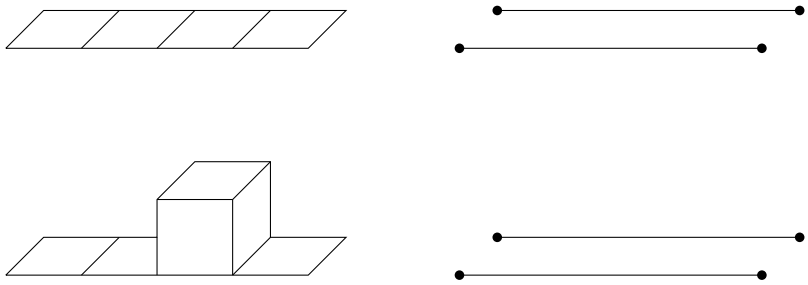

Figure 14: Examples for $N_\tau = 4$. Upper left: N_τ plaquettes wind around the temporal dimension. Lower left: $N_\tau + 4$ plaquettes wind around. Both rights: Two Polyakov loops remain after spatial integration.

only nearest neighbour interactions is the reason why we spoil an exact strong coupling expansion after some order. For example, in the case $N_\tau = 4$, next-to-nearest neighbour interactions occur with $\mathcal{O}(u^8 = u^{2N_\tau})$. As we have calculated the leading order term up to $\mathcal{O}(u^{12})$ in its correction, this is what we mean with a non-exact strong coupling expansion.

7.1.1 Graphical expansion

In order to obtain the effective action, we follow the same methods as before in this thesis; a character expansion, followed by a cluster expansion. If we do so, by omitting the factor $c_0(\beta)$ of the trivial representation we will obtain

$$\begin{aligned} S_{eff} &= -\ln \int [dU_i] \prod_p \Big[1 + \sum_{r\neq 0} d_r a_r(\beta)\chi_r(U_p)\Big] \\ &= -\ln \Big[1 + 4N_\tau V d_f^2 u^6 + \ldots + u^{N_\tau} \sum_{\vec{x},\vec{e}_i} L_{\vec{x}} L_{\vec{x}+\vec{e}_i} + \ldots\Big]. \end{aligned} \quad (209)$$

In the logarithm, the factor $4N_\tau V d_f^2 u^6$ corresponds to simple cubes, with a contribution of $d_f^2 u^6$ and an occurrence number of $4N_\tau V$. As they do not wind around the temporal direction (we consider lattices large enough), we were able to integrate them out completely. However, after expanding the logarithm, one has to take these and analogously higher order terms of this kind into account, since

$$\ln(1 + x + y) = x + y - xy + \ldots. \quad (210)$$

The most convenient way to take along these terms is the method of moments and cumulants as already explained in earlier chapters. This method allows to consider only connected graphs. The second non-trivial term in the logarithm corresponds to fig. (14). There, one can integrate out the spatial links, too, but one remains with a system of two Polyakov loops. Again we get higher

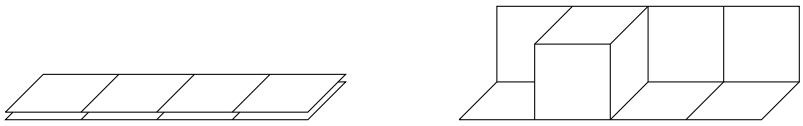

Figure 15: Graphs that have been neglected in the effective action. Left: Four Polyakov loop interaction term. Right: Next-to-nearest neighbour coupling.

order terms, which change the nearest-neighbour Polyakov loop coupling

$$u^{N_\tau} \sum_{\vec{x},\vec{e}_i} L_{\vec{x}} L_{\vec{x}+\vec{e}_i} \longrightarrow u^{N_\tau}(1 + 4N_\tau u^4 + \ldots) \sum_{\vec{x},\vec{e}_i} L_{\vec{x}} L_{\vec{x}+\vec{e}_i}. \tag{211}$$

As already mentioned, we neglect some higher order terms, like the ones in fig. (15). A reason for this is the simplified series expansion without these graphs. One can argue that neglecting these terms gives only a small systematic error. Next-to-nearest-neighbour terms and terms involving more than two Polyakov loops are suppressed by powers of u^{N_τ} compared to the nearest-neighbour terms in the fundamental representation, and hence are at least in the strong coupling range suppressed. If we now put everything together, we will arrive at the following expression

$$S_{eff} \;=\; -\lambda(N_\tau, u) \sum_{\vec{x},\vec{e}} L_{\vec{x}} L_{\vec{x}+\vec{e}}, \tag{212}$$

for the leading term of the effective action. Our purpose is to calculate the new effective coupling constant $\lambda(N_\tau, u)$ in a strong coupling expansion for each N_τ. Since next-to-nearest neighbour couplings are suppressed by $\mathcal{O}(u^{N_\tau})$ and $0 \leq u \leq 1$, we expect this approximation to work better the larger the temporal lattice extent is. As we saw that the strict strong coupling expansions worked quite well for $N_\tau \leq 2$, we only want to discuss the Polyakov loop effective action for $N_\tau \geq 3$.

Some graphs contributing to the effective coupling $\lambda(N_\tau, u)$ are given in fig. (14). One recognises the similarities in shape to those of the Polyakov loop susceptibility, see fig. (9), the difference being that we do not have to introduce Polyakov loop source terms. If we perform the series expansion,

we get the following results:

$$\begin{aligned}
\lambda(3,u) &= 1 + 12u^4 - 12u^6 + 200u^8 - \frac{55484}{135}u^{10} + \frac{1519624}{405}u^{12} + \ldots, \\
\lambda(4,u) &= 1 + 16u^4 - 16u^6 + \frac{944}{3}u^8 - \frac{254336}{405}u^{10} + \frac{8155336}{1215}u^{12} + \ldots, \\
\lambda(5,u) &= 1 + 20u^4 - 20u^6 + \frac{1300}{3}u^8 - \frac{68444}{81}u^{10} + \frac{2365264}{243}u^{12} + \ldots, \\
\lambda(N_\tau,u) &= 1 + 4N_\tau u^4 - 4N_\tau u^6 + \left(8N_\tau^2 + \frac{140}{3}\right)u^8 \\
&- \left(16N_\tau^2 + \frac{36044}{405}\right)u^{10} \\
&+ \left(\frac{32}{2}N_\tau^3 + \frac{584}{3}N_\tau^2 + \frac{863524}{1215}\right)u^{12} + \ldots. \qquad (213)
\end{aligned}$$

As we have calculated up to $\mathcal{O}(u^{12})$, there is one formula for all $N_\tau \geq 6$. For smaller N_τ, there are some graphs of the larger N_τ missing, since they do not fit into these small lattices.

From the general expression $\lambda(N_\tau, u)$, one recognizes that terms of higher order in N_τ are just coming from exponentiation of lower order terms, like

$$\begin{aligned}
8N_\tau^2 u^8 &= \frac{1}{2!}\left(4N_\tau u^4\right)^2, \\
-16N_\tau^2 u^{10} &= 4N_\tau u^4 \cdot (-4N_\tau u^6), \\
\frac{32}{3}N_\tau^3 u^{12} &= \frac{1}{3!}\left(4N_\tau u^4\right)^3. \qquad (214)
\end{aligned}$$

Thus it seems natural to exponentiate the N_τ-dependence and write

$$\lambda(N_\tau,u) = \exp\left[N_\tau\left(4u^4 - 4u^6 + \frac{140}{3}u^8 - \frac{36044}{405}u^{10} + \frac{863524}{1215}u^{12}\right)\right]. \qquad (215)$$

In doing so we should model the N_τ-dependence more accurately. This is the first part of the resummation, for in this way we have already included all terms which appear only as repetitions of lower order terms at different places. For the smaller N_τ we do the same and get up to higher orders

$$\begin{aligned}
\lambda(3,u) &= \exp\left[12u^4 - 12u^6 + 128u^8 - \frac{36044}{135}u^{10} + \frac{751744}{405}u^{12}\right], \\
\lambda(4,u) &= \exp\left[16u^4 - 16u^6 + \frac{560}{3}u^8 - \frac{150656}{405}u^{10} + \frac{3541576}{1215}u^{12}\right], \\
\lambda(5,u) &= \exp\left[20u^4 - 20u^6 + \frac{700}{3}u^8 - \frac{36044}{81}u^{10} + \frac{858664}{243}u^{12}\right]. \qquad (216)
\end{aligned}$$

In order to improve convergence of the series expansions in the exponential, we will use Padé approximants.

7.1.2 Solving the effective action

With eqs (215) and (216), we can convert a critical coupling λ_c of the effective action

$$S_{eff} \;=\; -\lambda(N_\tau, u) \sum_{\vec{x},\vec{e}} L_{\vec{x}} L_{\vec{x}+\vec{e}} \tag{217}$$

into a critical coupling u_c of the original theory for a given N_τ. There are several ways to obtain the critical coupling of this model. One could use mean field theory [37] or numerical methods [54]. Here we would like to use the series expansion approach and compare them with numerical results. Mean field theory turns out to be simple but not very accurate.

In order to calculate a critical coupling we use the same method as we did for the Wilson action. We couple a Polyakov loop source term into the action

$$S_{eff}(\lambda, J) = -\lambda \sum_{\vec{x},\vec{e}} L_{\vec{x}} L_{\vec{x}+\vec{e}} - J \sum_{\vec{x}} L_{\vec{x}} \tag{218}$$

and derive a series expansion for the Polyakov loop susceptibility

$$\chi(\lambda) = \frac{\partial^2}{\partial J^2} \ln\, Z(\lambda, J)\Big|_{J=0}, \tag{219}$$

where the partition function is given by

$$Z(\lambda, J) = \int [dW] \exp\big[- S_{eff}(\lambda, J)\big]. \tag{220}$$

Let us note that in this case the Polyakov loop interaction term is not a class function and we are thus not able to perform a character expansion. Nevertheless it is of course possible to directly expand the exponential in order to get a series expansion in λ. This limits the number of achievable coefficients, but we will see that we can extract the critical coupling with a sufficent accuracy. After doing so we get the following series expansion for the Polyakov loop susceptibility of the effective theory

$$\chi(\lambda) = 1 + 6\lambda + 33\lambda^2 + 181\lambda^3 + 969.25\lambda^4 + 5277\lambda^5 \ldots \tag{221}$$

Now we argue why this whole scheme is a resummation: λ is of order u^{N_τ}, thus we have actually calculated the Polyakov loop susceptiblity to order u^{5N_τ}. Since we have also included the spatial structure by including terms as $u^{N_\tau}(1 + \ldots)$ up to order u^{12}, we have extended this to order $u^{5(N_\tau+12)}$. By

writing the N_τ-dependence as an exponential and extrapolating the remaining u-dependence with Padé-approximants, we have resummed an infinite number of terms with a finite number of graphs which we calculated. Of course, reexpressing the Polyakov loop susceptibility $\chi_L(\lambda)$ as a function of u would give us wrong coefficients above some certain order.

Padé	λ_c
$[3,2]$	0.1959
$[2,3]$	0.1916
$[1,4]$	0.1963
$[2,2]$	0.1971
$[1,3]$	0.1973

Table 6: Critical couplings of the effective action from different Padé approximants.

As the effective theory must be in the same universality class as the original theory we use biased estimates to get the critical value λ_c. Like in the case of the Wilson action, we biase with the Ising model exponent for the susceptibility $\gamma_I = 1.237$. As we can see in table (6), the different approximants are quite stable around the mean value $\lambda_c = 0.1956$.

7.1.3 Critical couplings from the Polyakov loop effective action

We get the values shown in table (7) from different orders of our series expansion for the effective coupling λ and different N_τ. There one can see that convergence in u is rather slow, which is connected to the alternating sign in eq. (216). Nevertheless, one can see what kind of improvement can be achieved if one includes spatial plaquettes by comparing e.g. the orders u^0, which corresponds to neglecting all spacelike plaquettes and u^4, that is the first "spatial" correction.

Due to the slow convergence, we try to improve by using different Padé approximants. The results are shown in table (8). We see that with Padé extrapolation, the results are much more stable and deviate from Monte Carlo results less than 1 percent up to $N_\tau = 8$. These deviations should be due to neglecting higher order terms. In the case of larger N_τ this neglect should become a better approximation, but the behaviour of the results in comparison to Monte Carlo results is worse. Thus we conclude that there we are leaving the region where we can extrapolate from strong coupling expansions with resummations and weak coupling influences have to be added, if we wish to further improve the results.

N_τ	$\mathcal{O}(u^0)$	$\mathcal{O}(u^4)$	$\mathcal{O}(u^6)$	$\mathcal{O}(u^8)$	$\mathcal{O}(u^{10})$	$\mathcal{O}(u^{12})$	MC
3	3.121	2.266	2.364	2.180	2.297	2.157	2.1768(30)
4	4.102	2.512	2.677	2.345	2.458	2.288	2.2991(2)
5	5.050	2.664	2.885	2.444	2.587	2.368	2.3726(45)
6	5.985	2.766	3.034	2.507	2.679	2.417	2.4265(30)
8	7.839	2.895	3.235	2.584	2.795	2.475	2.5104(2)
12	11.531	3.027	3.454	2.657	2.915	2.528	2.6355(10)
16	15.217	3.094	3.572	2.692	2.977	2.554	2.7310(20)

Table 7: Comparison of the critical couplings β_c derived from different orders of the calculated effective coupling

N_τ	$[4,4]$	$[4,6]$	$[6,4]$	$[6,6]$	$\overline{\beta}_c$	β_c^{MC}
3	2.175	2.182	2.182	2.168	2.177	2.1768(30)
4	2.312	2.318	2.318	2.308	2.314	2.2991(2)
5	2.393	2.392	2.392	2.389	2.392	2.3726(45)
6	2.441	2.440	2.440	2.438	2.440	2.4265(30)
8	2.496	2.495	2.495	2.496	2.496	2.5104(2)
12	2.546	2.545	2.545	2.546	2.546	2.6355(10)
16	2.569	2.568	2.568	2.569	2.569	2.7310(20)

Table 8: Comparison of the critical couplings β_c derived from different Padés of the calculated effective coupling, their mean value and numerical results from Monte Carlo simulations [20, 42, 43, 47]

7.2 Effective action for $SU(3)$

In case of $SU(3)$ we can do the same as for $SU(2)$ and construct an effective action by integrating out the spatial degrees of freedom. Nevertheless we have to take into account that we now have to deal with two fundamental representations and care about the orientation of the Polyakov loop. The nearest neighbour effective action is thus of the generic form

$$S_{eff} = -\eta(N_\tau, u) \sum_{\vec{x},\vec{e}} \left(L_{\vec{x}} L^\dagger_{\vec{x}+\vec{e}} + L^\dagger_{\vec{x}} L_{\vec{x}+\vec{e}} \right), \tag{222}$$

with some effective coupling η. In case of $SU(3)$, we have calculated up to $\mathcal{O}(u^{10})$, due to the somwehat more complicated group structure. We saw that in case of $SU(2)$ this order suffices to reproduce the critical couplings obtained from numerical simulations quite accurately. Hence we get for the

effective coupling in the exponentiated form

$$\begin{aligned}
\eta(N_\tau, u) &= \exp\Bigg[N_\tau\Big(4u^4 + 12u^5 - 14u^6 - 36u^7 + \frac{295}{2}u^8 \\
&\quad + \frac{1671}{10}u^9 + \frac{543707}{5120}u^{10}\Big)\Bigg], \\
\eta(4, u) &= \exp\Bigg[16u^4 + 48u^5 - 56u^6 - 144u^7 + 590u^8 \\
&\quad + \frac{3342}{5}u^9 + \frac{523317}{1280}u^{10}\Bigg], \\
\eta(3, u) &= \exp\Bigg[12u^4 + 36u^5 - 42u^6 - 108u^7 + \frac{861}{2}u^8 \\
&\quad + \frac{5013}{10}u^9 + \frac{1262751}{5120}u^{10}\Bigg].
\end{aligned} \tag{223}$$

We notice that the behaviour of the series expansion coefficients is quite different as in the $SU(2)$ case. The three highest orders go with equal sign, indicating a quite good convergence behaviour.

7.2.1 Solving the effective action

The solution to this effective action is straightforward with mean field techniques and has already been done. But the series expansion approach is not applicable, as this action is supposed to have a first order phase transition, like its origin, pure $SU(3)$ gauge theory. The mean field solution [37] for the critical coupling is

$$\eta_c = 0.134. \tag{224}$$

7.2.2 Critical couplings for $SU(3)$

Using the mean field value of the critical effective coupling, we can calculate the critical values u_c of $SU(3)$ gauge theory, inverting the transformations (223). In this case, the behaviour of the coefficients' signs makes it possible to use the series expansions directly instead of extrapolating with Padé approximants. In fact, a Padé analysis gave inconsistent results. Thus we used the three highest orders of the series expansion for the exponential to invert. This gives the results displayed in table (9).

We observe that the agreement with Monte Carlo is not as good as for $SU(2)$, but within $\sim 10\%$ error. A possible reason for this could be that in $SU(3)$ neglecting higher order diagrams gives a worse approximation than

N_τ	$\mathcal{O}(u^8)$	$\mathcal{O}(u^9)$	$\mathcal{O}(u^{10})$	MC
3	5.78	5.66	5.64	5.5500(100)
4	6.22	6.03	5.99	5.6925(2)
6	6.61	6.35	6.29	5.8941(5)
8	6.79	6.49	6.43	6.0010(250)
10	6.89	6.57	6.51	6.1600(70)
12	6.96	6.63	6.56	6.2680(120)
14	7.01	6.66	6.59	6.3830(100)
16	7.04	6.69	6.62	6.4500(500)

Table 9: Comparison of the critical couplings β_c derived from different orders of the calculated effective coupling with numerical results, [20].

for $SU(2)$. Also there should be some error due to the use of a mean field value for the critical coupling λ_c of the effective theory.

8 Corrections to lattice QCD with staggered fermions in the strong coupling limit

Up to now our strategy in dealing with lattice QCD was to integrate out the fermionic degrees of freedom and then to do the group integrals. Of course, we can reverse this procedure and do the gauge integrals first. The easiest way to do this is to consider the strong coupling limit first, where the link integrals become independent, due to neglecting the plaquette term. In order to get closer to nature, one can perform β corrections, e.g. as in [55–60]. Nevertheless all these calculations have been done using at least one additional expansion, e.g. in a large number of spatial dimensions d or colors N, and we are not aware of a complete calculation of the linear term in β. This calculation shall be presented here.

8.1 Strong coupling limit

At first we would like to present the calculations in the strong coupling limit, which have been done a long time ago [30–32]. In this limit $\beta = 0$, one can neglect the plaquette action and the remaining staggered fermion partition function can be written as

$$Z = \int [dU] \exp\left[m \sum_x \overline{\psi}_x \psi_x + \frac{1}{2} \sum_{x,\mu} \overline{\psi}_x \alpha_{x,\mu} \left[U_{x\mu} \overline{\psi}_{x+\hat{\mu}} - U^\dagger_{x-\hat{\mu},\mu} \psi_{x-\hat{\mu}} \right] \right] \quad (225)$$

The integrals over link variables become independent and it is thus possible to integrate them exactly. We consider the following generic link integral

$$I = \int dU \exp\left[\overline{\varphi} U \chi + \overline{\chi} U^\dagger \varphi \right],$$

which appears in the strong coupling limit and has been solved [30, 61] to give

$$I = \sum_{k=0}^{3} \frac{(3-k)!}{3!k!} (-M_\chi M_\varphi)^k + \overline{B}_\chi B_\varphi + \overline{B}_\varphi B_\chi,$$

with the abbreviations

$$\begin{aligned} M_\chi &= \overline{\chi}_k \chi_k, \\ B_\chi &= \frac{1}{6} \varepsilon_{ijk} \chi_i \chi_j \chi_k = \chi_1 \chi_2 \chi_3, \\ \overline{B}_\varphi &= \frac{1}{6} \varepsilon_{ijk} \overline{\varphi}_k \overline{\varphi}_j \overline{\varphi}_i = \overline{\varphi}_3 \overline{\varphi}_2 \overline{\varphi}_1. \end{aligned}$$

In search for the finite temperature chiral symmetry restoration transition, this partition function has been investigated numerically. One rewrites the partition function as collection of monomers, dimers and baryonic loops and computes the average of different configurations of these ingredients [31, 32].

8.2 Leading correction in β

Corrections in β to the strong coupling limit have been computed shortly after the limit calculation. As a simplification one considers the approximation of a large number of spatial dimensions and neglects terms which are suppressed by powers of d. In order to correctly implement a monomer, dimer and baryonic loop description one should have the full β correction, regardless which d behaviour the terms have.

Here we want to present the calculation leading to this full β correction. Some lengthy integrals are given in the appendix. Notations are adjusted to the papers [31, 61].

8.2.1 Link integral

For an expansion in β, we need the link integral

$$J_{ik} \;=\; \int dU \exp\left[\overline{\varphi} U \chi + \overline{\chi} U^\dagger \varphi\right] U_{ik},$$

for which we find (see Appendix)

$$\begin{aligned} J_{ik} &= \frac{1}{3}\overline{\chi}_k\varphi_i - \frac{1}{6}M_\chi M_\varphi \overline{\chi}_k\varphi_i + \frac{1}{12}M_\chi^2 M_\varphi^2 \overline{\chi}_k\varphi_i - \frac{1}{12}\varepsilon_{ii_1i_2}\varepsilon_{kk_1k_2}\overline{\varphi}_{i_1}\overline{\varphi}_{i_2}\chi_{k_1}\chi_{k_2} \\ &+ \frac{1}{32}\varepsilon_{ii_1i_2}\varepsilon_{kk_1k_2}M_\chi M_\varphi \overline{\varphi}_{i_1}\overline{\varphi}_{i_2}\chi_{k_1}\chi_{k_2} + \frac{7}{24}\overline{B}_\varphi B_\chi \overline{\chi}_k\varphi_i \\ &+ \frac{1}{48}\varepsilon_{ii_1i_2}M_\varphi B_\chi \overline{\varphi}_{i_1}\overline{\varphi}_{i_2}\overline{\chi}_k + \frac{1}{48}\varepsilon_{kk_1k_2}M_\chi \overline{B}_\varphi \chi_{k_1}\chi_{k_2}\varphi_i. \end{aligned}$$

One recognises that the link terms carry colour indices and are thus not gauge invariant. Combining four of these terms to a plaquette and tracing them must yield a full gauge invariant result. We will see this in the next chapter.

8.2.2 Plaquette integral

Finally we want to calculate the following plaquette integral

$$P = J_{ik}J_{kl}J_{lm}J_{mi}.$$

The eight terms in the result for the link integration can be separated into five terms with different quark content

$$\begin{aligned}
L_1(\chi,\varphi) &= \frac{1}{3}\overline{\chi}_k\varphi_i, \\
L_2(\chi,\varphi) &= -\frac{1}{12}\varepsilon_{ii_1i_2}\varepsilon_{kk_1k_2}\overline{\varphi}_{i_1}\overline{\varphi}_{i_2}\chi_{k1}\chi_{k2}, \\
L_3(\chi,\varphi) &= -\frac{1}{6}M_\chi M_\varphi\overline{\chi}_k\varphi_i, \\
L_4(\chi,\varphi) &= \frac{1}{32}\varepsilon_{ii_1i_2}\varepsilon_{kk_1k_2}M_\chi M_\varphi\overline{\varphi}_{i_1}\overline{\varphi}_{i_2}\chi_{k_1}\chi_{k_2} + \frac{7}{24}\overline{B}_\varphi B_\chi\overline{\chi}_k\varphi_i \\
&+ \frac{1}{48}\varepsilon_{ii_1i_2}M_\varphi B_\chi\overline{\varphi}_{i_1}\overline{\varphi}_{i_2}\overline{\chi}_k + \frac{1}{48}\varepsilon_{kk_1k_2}M_\chi\overline{B}_\varphi\chi_{k_1}\chi_{k_2}\varphi_i, \\
L_5(\chi,\varphi) &= \frac{1}{12}M_\chi^2M_\varphi^2\overline{\chi}_k\varphi_i.
\end{aligned}$$

To get the final result for the plaquette integration, we have to arrange the link integrals around the plaquette in such a way, that at no site there are more than 3 quarks or antiquarks, due to the nilpotency of Grassmann variables and $N = 3$. This leads to 18 different (up to rotations) terms for the plaquette integration, where the corners are labelled by x, $x+\mu$, $x+\mu+\nu$ and $x+\nu$. In brackets there are terms that follow from adopting the notation of [31]. These terms carry the staggered sign factor α_{x_μ} and the dependence of chemical potential.

1. $\underline{L_1L_1L_1L_1:}$

   $I = -\frac{1}{81}M_xM_{x+\mu}M_{x+\mu+\nu}M_{x+\nu}$
   $[\zeta_{x,x+\mu}\zeta_{x+\mu,x+\mu+\nu}\zeta_{x+\mu+\nu,x+\nu}\zeta_{x+\nu,x}]$

2. $\underline{L_1L_1L_1L_2:}$ + 3 rotations

   $I = \frac{1}{9}B_xM_{x+\mu}M_{x+\mu+\nu}\overline{B}_{x+\nu}$
   $\left[\zeta_{x,x+\mu}\zeta_{x+\mu,x+\mu+\nu}\zeta_{x+\mu+\nu,x+\nu}\zeta^2_{x,x+\nu}\right]$

3. $\underline{L_1L_1L_2L_2:}$ + 3 rotations

   $I = -\frac{1}{18}B_xM_{x+\mu}\overline{B}_{x+\mu+\nu}M^2_{x+\nu}$
   $\left[\zeta_{x,x+\mu}\zeta_{x+\mu,x+\mu+\nu}\zeta^2_{x+\nu,x+\mu+\nu}\zeta^2_{x,x+\nu}\right]$

4. $\underline{L_1L_2L_1L_2:}$ + 1 rotation

   $I = B_x\overline{B}_{x+\mu}B_{x+\mu+\nu}\overline{B}_{x+\nu}$
   $\left[\zeta_{x,x+\mu}\zeta^2_{x+\mu+\nu,x+\mu}\zeta_{x+\mu+\nu,x+\nu}\zeta^2_{x,x+\nu}\right]$

5. $\underline{L_1L_2L_2L_2:}$ + 3 rotations

$I = \frac{1}{36} B_x \overline{B}_{x+\mu} M^2_{x+\mu+\nu} M^2_{x+\nu}$
$\left[\zeta_{x,x+\mu}\zeta^2_{x+\mu+\nu,x+\mu}\zeta^2_{x+\nu,x+\mu+\nu}\zeta^2_{x,x+\nu}\right]$

6. $\underline{L_2L_2L_2L_2:}$

$I = \frac{1}{1296} M^2_x M^2_{x+\mu} M^2_{x+\mu+\nu} M^2_{x+\nu}$
$\left[\zeta^2_{x+\mu,x}\zeta^2_{x+\mu+\nu,x+\mu}\zeta^2_{x+\nu,x+\mu+\nu}\zeta^2_{x,x+\nu}\right]$

7. $\underline{L_1L_1L_1L_3:}$ + 3 rotations

$I = \frac{1}{162} M^2_x M_{x+\mu} M_{x+\mu+\nu} M^2_{x+\nu}$
$\left[\zeta_{x,x+\mu}\zeta_{x+\mu,x+\mu+\nu}\zeta_{x+\mu+\nu,x+\nu}\zeta^2_{x+\nu,x}\zeta_{x,x+\nu}\right]$

8. $\underline{L_1L_2L_1L_3:}$ + 3 rotations

$I = \frac{1}{18} M^2_x \overline{B}_{x+\mu} B_{x+\mu+\nu} M^2_{x+\nu}$
$\left[\zeta_{x,x+\mu}\zeta^2_{x+\mu+\nu,x+\mu}\zeta_{x+\mu+\nu,x+\nu}\zeta^2_{x+\nu,x}\zeta_{x,x+\nu}\right]$

9. $\underline{L_1L_3L_1L_3:}$ + 1 rotation

$I = -\frac{1}{324} M^2_x M^2_{x+\mu} M^2_{x+\mu+\nu} M^2_{x+\nu}$
$\left[\zeta_{x,x+\mu}\zeta^2_{x+\mu,x+\mu+\nu}\zeta_{x+\mu+\nu,x+\mu}\zeta_{x+\mu+\nu,x+\nu}\zeta^2_{x+\nu,x}\zeta_{x,x+\nu}\right]$

10. $\underline{L_1L_3L_3L_3:}$ + 3 rotations

$I = \frac{1}{648} M^2_x M^2_{x+\mu} M^3_{x+\mu+\nu} M^3_{x+\nu}$
$\left[\zeta_{x,x+\mu}\zeta^2_{x+\mu,x+\mu+\nu}\zeta_{x+\mu+\nu,x+\mu}\zeta^2_{x+\mu+\nu,x+\nu}\zeta_{x+\nu,x+\mu+\nu}\zeta^2_{x+\nu,x}\zeta_{x,x+\nu}\right]$

11. $\underline{L_3L_3L_3L_3:}$

$I = -\frac{1}{1296} M^3_x M^3_{x+\mu} M^3_{x+\mu+\nu} M^3_{x+\nu}$
$\left[\zeta^2_{x,x+\mu}\zeta_{x+\mu,x}\zeta^2_{x+\mu,x+\mu+\nu}\zeta_{x+\mu+\nu,x+\mu}\zeta^2_{x+\mu+\nu,x+\nu}\zeta_{x+\nu,x+\mu+\nu}\zeta^2_{x+\nu,x}\zeta_{x,x+\nu}\right]$

12. $\underline{L_1L_1L_1L_5:}$ + 3 rotations

$I = -\frac{1}{324} M^3_x M_{x+\mu} M_{x+\mu+\nu} M^3_{x+\nu}$
$\left[\zeta_{x,x+\mu}\zeta_{x+\mu,x+\mu+\nu}\zeta_{x+\mu+\nu,x+\nu}\zeta^3_{x+\nu,x}\zeta^2_{x,x+\nu}\right]$

13. $\underline{L_1L_2L_1L_5:}$ + 3 rotations

$I = -\frac{1}{36} M_x^3 \overline{B}_{x+\mu} B_{x+\mu+\nu} M_{x+\nu}^3$
$\left[\zeta_{x,x+\mu} \zeta_{x+\mu+\nu,x+\mu}^2 \zeta_{x+\mu+\nu,x+\nu} \zeta_{x+\nu,x}^3 \zeta_{x,x+\nu}^2\right]$

14. $\underline{L_1 L_3 L_1 L_5 :}$ + 3 rotations

$I = \frac{1}{648} M_x^3 M_{x+\mu}^2 M_{x+\mu+\nu}^2 M_{x+\nu}^3$
$\left[\zeta_{x,x+\mu} \zeta_{x+\mu,x+\mu+\nu}^2 \zeta_{x+\mu+\nu,x+\mu} \zeta_{x+\mu+\nu,x+\nu} \zeta_{x+\nu,x}^3 \zeta_{x,x+\nu}^2\right]$

15. $\underline{L_1 L_5 L_1 L_5 :}$ + 1 rotation

$I = -\frac{1}{1296} M_x^3 M_{x+\mu}^3 M_{x+\mu+\nu}^3 M_{x+\nu}^3$
$\left[\zeta_{x,x+\mu}^3 \zeta_{x+\mu,x+\mu+\nu}^3 \zeta_{x+\mu+\nu,x+\mu}^2 \zeta_{x+\mu+\nu,x+\nu} \zeta_{x+\nu,x}^3 \zeta_{x,x+\nu}^2\right]$

16. $\underline{L_2 L_1 L_2 L_4 :}$ + 3 rotations

$I = \left[\frac{7}{8} B_x \overline{B}_x B_{x+\mu} \overline{B}_{x+\mu+\nu} B_{x+\nu} \overline{B}_{x+\nu} - \frac{1}{96} M_x^3 B_{x+\mu} \overline{B}_{x+\mu+\nu} M_{x+\nu}^3 \right.$
$\left. -\frac{1}{48} M_x^3 B_{x+\mu} \overline{B}_{x+\mu+\nu} B_{x+\nu} \overline{B}_{x+\nu} + \frac{1}{48} B_x \overline{B}_x B_{x+\mu} \overline{B}_{x+\mu+\nu} M_{x+\nu}^3\right]$
$\left[\zeta_{x+\mu,x}^2 \zeta_{x+\mu,x+\mu+\nu} \zeta_{x+\nu,x+\mu+\nu}^2 \zeta_{x+\nu,x} \zeta_{x,x+\nu}^3\right]$

17. $\underline{L_2 L_2 L_2 L_4 :}$ + 3 rotations

$I = \left[\frac{7}{288} B_x \overline{B}_x M_{x+\mu}^2 M_{x+\mu+\nu}^2 B_{x+\nu} \overline{B}_{x+\nu} - \frac{1}{3456} M_x^3 M_{x+\mu}^2 M_{x+\mu+\nu}^2 M_{x+\nu}^3 \right.$
$\left. -\frac{1}{1728} M_x^3 M_{x+\mu}^2 M_{x+\mu+\nu}^2 B_{x+\nu} \overline{B}_{x+\nu} + \frac{1}{1728} B_x \overline{B}_x M_{x+\mu}^2 M_{x+\mu+\nu}^2 M_{x+\nu}^3\right]$
$\left[\zeta_{x+\mu,x}^2 \zeta_{x+\mu+\nu,x+\mu}^2 \zeta_{x+\nu,x+\mu+\nu}^2 \zeta_{x+\nu,x} \zeta_{x,x+\nu}^3\right]$

18. $\underline{L_2 L_4 L_2 L_4 :}$ +1 rotation

$I = \left[\frac{49}{64} B_x \overline{B}_x B_{x+\mu} \overline{B}_{x+\mu} B_{x+\mu+\nu} \overline{B}_{x+\mu+\nu} B_{x+\nu} \overline{B}_{x+\nu} \right.$
$- \frac{7}{768} B_x \overline{B}_x M_{x+\mu}^3 M_{x+\mu+\nu}^3 B_{x+\nu} \overline{B}_{x+\nu}$
$+ \frac{7}{384} B_x \overline{B}_x M_{x+\mu}^3 B_{x+\mu+\nu} \overline{B}_{x+\mu+\nu} B_{x+\nu} \overline{B}_{x+\nu}$
$- \frac{7}{384} B_x \overline{B}_x B_{x+\mu} \overline{B}_{x+\mu} M_{x+\mu+\nu}^3 B_{x+\nu} \overline{B}_{x+\nu}$
$- \frac{7}{768} M_x^3 B_{x+\mu} \overline{B}_{x+\mu} B_{x+\mu+\nu} \overline{B}_{x+\mu+\nu} M_{x+\nu}^3$
$+ \frac{1}{9216} M_x^3 M_{x+\mu}^3 M_{x+\mu+\nu}^3 M_{x+\nu}^3$
$- \frac{1}{4608} M_x^3 M_{x+\mu}^3 B_{x+\mu+\nu} \overline{B}_{x+\mu+\nu} M_{x+\nu}^3$
$+ \frac{1}{4608} M_x^3 B_{x+\mu} \overline{B}_{x+\mu} M_{x+\mu+\nu}^3 M_{x+\nu}^3$
$+ \frac{7}{384} B_x \overline{B}_x B_{x+\mu} \overline{B}_{x+\mu} B_{x+\mu+\nu} \overline{B}_{x+\mu+\nu} M_{x+\nu}^3$
$- \frac{1}{4608} B_x \overline{B}_x M_{x+\mu}^3 M_{x+\mu+\nu}^3 M_{x+\nu}^3$
$+ \frac{1}{2304} B_x \overline{B}_x M_{x+\mu}^3 B_{x+\mu+\nu} \overline{B}_{x+\mu+\nu} M_{x+\nu}^3$
$- \frac{1}{2304} B_x \overline{B}_x B_{x+\mu} \overline{B}_{x+\mu} M_{x+\mu+\nu}^3 M_{x+\nu}^3$
$- \frac{7}{384} M_x^3 B_{x+\mu} \overline{B}_{x+\mu} B_{x+\mu+\nu} \overline{B}_{x+\mu+\nu} B_{x+\nu} \overline{B}_{x+\nu}$
$+ \frac{1}{4608} M_x^3 M_{x+\mu}^3 M_{x+\mu+\nu}^3 B_{x+\nu} \overline{B}_{x+\nu}$

$$
\begin{aligned}
&- \tfrac{1}{2304} M_x^3 M_{x+\mu}^3 B_{x+\mu+\nu} \overline{B}_{x+\mu+\nu} B_{x+\nu} \overline{B}_{x+\nu} \\
&+ \tfrac{1}{2304} M_x^3 B_{x+\mu} \overline{B}_{x+\mu} M_{x+\mu+\nu}^3 B_{x+\nu} \overline{B}_{x+\nu} \Big] \\
&\Big[\zeta_{x+\mu,x}^2 \zeta_{x+\mu,x+\mu+\nu} \zeta_{x+\mu+\nu,x+\mu}^3 \zeta_{x+\nu,x+\mu+\nu}^2 \zeta_{x+\nu,x} \zeta_{x,x+\nu}^3 \Big]
\end{aligned}
$$

The final result of $\mathcal{O}(\beta)$ is given by adding all these contributions and their rotations and to consider the hermitian conjugate plaquette. The latter one gives the same contributions, but in reversed order

$$
x \to x + \nu \to x + \nu + \mu \to x + \mu. \tag{226}
$$

9 Conclusions

In this last chapter, we want to conclude the overall picture that emerges from this thesis. A fundamental result is, that strong coupling expansions at finite temperature are suitable to provide qualitatively as well as quantitatively accurate results. Although maybe not fully competitive to numerical simulations, it is a complementary approach which is even able to provide information about phase transitions. In case of $SU(2)$ we were able to accurately reproduce the critical couplings already measured in Monte Carlo simulations. If one could use automated series generation methods to get more expansion coefficients, this method would gain even more predictive power for observables, which are hard to calculate numerically, like quantities at a finite chemical potential. We have shown first steps in this direction.

A serious drawback so far was the inability to deal with first order phase transitions. This is a place, where future work can be done. A possiblity could be to consider finite volumes and get finite-size-scaling calculations.

The conclusion for the single observables is as follows:

Free energy density: Concerning this quantity we conclude that most work using strong coupling expansions has been done. The series expansions have been worked out to relatively high orders and are in fairly good correspondence with numerical data. In the case of $SU(2)$ more coefficients certainly will reduce the errors in the estimates of the critical parameters, but we have already shown how to get them out quite accurately.

Nevertheless, we also want to say, that with this quantity we observed the most interesting qualitative feature, the confirmation of the hadron resonance gas model in the strong coupling and heavy quark mass region. As we have calculated only the strong coupling limit and the leading order of the hopping parameter expansion in the case of QCD, higher orders could help gaining more insights to the relevance and validity of this model.

Polyakov loop susceptibility: Strong coupling expansions of this observable using Wilson's gauge action gave us the most accurate estimates for critical parameters even competitive to recent Monte Carlo simulations in case of $SU(2)$ and $N_\tau = 1$ [42]. As already mentioned above, the major drawback was the limitation to go to larger temporal lattice sizes with strong coupling methods.

For future work we believe the case of QCD with heavy quarks to deliver some more topics to work on. In this thesis we have considered only the case $N_\tau = 1$ and it is necessary to go to larger temporal lattice extents

to compare with simulations and possibly gain insights about continuum physics. With some more series coefficents one would be able to use two variable extrapolation techniques like partial differential approximants [62].

Polyakov loop effective action: The most promising approach presented here are effective actions, derived directly from the lattice QCD-Lagrangian. As we have shown, they give quantitatively reasonable results even for lattices which belong to the largest ones used in modern Monte Carlo calculations. These effective actions can be solved either analytically or numerically with much less computer power needed than the original theory.

Work in this area could be done in incorporating finite quark masses and chemical potential. Although we have seen that in case of the gauge group $SU(3)$ values of critical couplings becomes less accurate, it should be possible to gain insights into the behaviour of the critical values with decreasing quark masses and increasing chemical potential.

Corrections to strong coupling lattice QCD: Another interesting application of strong coupling expansions is the incorporation of β corrections to the strong coupling limit of lattice QCD with staggered fermions. When written in a monomer-dimer-baryonic-loop formulation one could be able to investigate lattice QCD at small quark masses, quite large chemical potentials and away from the strong coupling limit. This would allow to investigate also the chiral phase transiton, which has been omitted in this thesis.

A Group integrals

The group integrations calculated here have been derived with a method given in [41]. To calculate the integral J_{ik} of chapter (8.2) we need two group integrals which we will calculate in the following.

Integrating six U-matrices: A group integral with six U-matrices in $SU(3)$ corresponds to the lowest diagram of fig. (6) in [41] with $N = 3$ and $p = 2$. With the mentioned formulas we get $\frac{1}{72}$ for the prefactor and 10 for the number of different ε-tensor permutations. This yields

$$\begin{aligned} I_6 &= \int dU U_{i_1 j_1} U_{i_2 j_2} U_{i_3 j_3} U_{i_4 j_4} U_{i_5 j_5} U_{i_6 j_6} \\ &= \frac{1}{72} \left[\varepsilon_{i_1 i_2 i_3} \varepsilon_{i_4 i_5 i_6} \varepsilon_{j_1 j_2 j_3} \varepsilon_{j_4 j_5 j_6} + \varepsilon_{i_1 i_2 i_4} \varepsilon_{i_3 i_5 i_6} \varepsilon_{j_1 j_2 j_4} \varepsilon_{j_3 j_5 j_6} \right. \\ &+ \varepsilon_{i_1 i_2 i_5} \varepsilon_{i_3 i_4 i_6} \varepsilon_{j_1 j_2 j_5} \varepsilon_{j_3 j_4 j_6} + \varepsilon_{i_1 i_2 i_6} \varepsilon_{i_3 i_4 i_5} \varepsilon_{j_1 j_2 j_6} \varepsilon_{j_3 j_4 j_5} \\ &+ \varepsilon_{i_1 i_3 i_4} \varepsilon_{i_2 i_5 i_6} \varepsilon_{j_1 j_3 j_4} \varepsilon_{j_2 j_5 j_6} + \varepsilon_{i_1 i_3 i_5} \varepsilon_{i_2 i_4 i_6} \varepsilon_{j_1 j_3 j_5} \varepsilon_{j_2 j_4 j_6} \\ &+ \varepsilon_{i_1 i_3 i_6} \varepsilon_{i_2 i_4 i_5} \varepsilon_{j_1 j_3 j_6} \varepsilon_{j_2 j_4 j_5} + \varepsilon_{i_1 i_4 i_5} \varepsilon_{i_2 i_3 i_6} \varepsilon_{j_1 j_4 j_5} \varepsilon_{j_2 j_3 j_6} \\ &+ \left. \varepsilon_{i_1 i_4 i_6} \varepsilon_{i_2 i_3 i_5} \varepsilon_{j_1 j_4 j_6} \varepsilon_{j_2 j_3 j_5} + \varepsilon_{i_1 i_5 i_6} \varepsilon_{i_2 i_3 i_4} \varepsilon_{j_1 j_5 j_6} \varepsilon_{j_2 j_3 j_4} \right]. \end{aligned}$$

Integrating four U-matrices and one $U^\dagger$-matrix: Using the first result we can get this integral by expressing U^{-1} in terms of the cofactor of U:

$$(U^{-1})_{ij} = (cof\, U)_{ji} = \frac{1}{2} \varepsilon_{j i_1 i_2} \varepsilon_{i j_1 j_2} U_{i_1 j_1} U_{i_2 j_2}.$$

$$
\begin{aligned}
I_{4,1} &= \int dU U_{i_1 j_1} U_{i_2 j_2} U_{i_3 j_3} U_{i_4 j_4} U^{-1}_{kl} = \frac{1}{2}\varepsilon_{li_5i_6}\varepsilon_{kj_5j_6} I_6 \\
&= \frac{1}{144}\,[\varepsilon_{li_5i_6}\varepsilon_{kj_5j_6}\,(\varepsilon_{i_1i_2i_3}\varepsilon_{i_4i_5i_6}\varepsilon_{j_1j_2j_3}\varepsilon_{j_4j_5j_6} + \varepsilon_{i_1i_2i_4}\varepsilon_{i_3i_5i_6}\varepsilon_{j_1j_2j_4}\varepsilon_{j_3j_5j_6} \\
&+ \varepsilon_{i_1i_3i_4}\varepsilon_{i_2i_5i_6}\varepsilon_{j_1j_3j_4}\varepsilon_{j_2j_5j_6} + \varepsilon_{i_1i_5i_6}\varepsilon_{i_2i_3i_4}\varepsilon_{j_1j_5j_6}\varepsilon_{j_2j_3j_4} \\
&+ \varepsilon_{i_1i_2i_5}\varepsilon_{i_3i_4i_6}\varepsilon_{j_1j_2j_5}\varepsilon_{j_3j_4j_6} + \varepsilon_{i_1i_2i_6}\varepsilon_{i_3i_4i_5}\varepsilon_{j_1j_2j_6}\varepsilon_{j_3j_4j_5} \\
&+ \varepsilon_{i_1i_3i_5}\varepsilon_{i_2i_4i_6}\varepsilon_{j_1j_3j_5}\varepsilon_{j_2j_4j_6} + \varepsilon_{i_1i_3i_6}\varepsilon_{i_2i_4i_5}\varepsilon_{j_1j_3j_6}\varepsilon_{j_2j_4j_5} \\
&+ \varepsilon_{i_1i_4i_5}\varepsilon_{i_2i_3i_6}\varepsilon_{j_1j_4j_5}\varepsilon_{j_2j_3j_6} + \varepsilon_{i_1i_4i_6}\varepsilon_{i_2i_3i_5}\varepsilon_{j_1j_4j_6}\varepsilon_{j_2j_3j_5})] \\
&= \frac{1}{144}\,[4\,(\delta_{li_1}\delta_{kj_1}\varepsilon_{i_2i_3i_4}\varepsilon_{j_2j_3j_4} + \delta_{li_2}\delta_{kj_2}\varepsilon_{i_1i_3i_4}\varepsilon_{j_1j_3j_4} \\
&\qquad + \delta_{li_3}\delta_{kj_3}\varepsilon_{i_1i_2i_4}\varepsilon_{j_1j_2j_4} + \delta_{li_4}\delta_{kj_4}\varepsilon_{i_1i_2i_3}\varepsilon_{j_1j_2j_3}) \\
&+ \varepsilon_{i_1i_2i_5}\varepsilon_{j_1j_2j_5}(\delta_{li_3}\delta_{i_5i_4} - \delta_{li_4}\delta_{i_5i_3})(\delta_{kj_3}\delta_{j_5j_4} - \delta_{kj_4}\delta_{j_5j_3}) \\
&+ \varepsilon_{i_1i_3i_5}\varepsilon_{j_1j_3j_5}(\delta_{li_2}\delta_{i_5i_4} - \delta_{li_4}\delta_{i_5i_2})(\delta_{kj_2}\delta_{j_5j_4} - \delta_{kj_4}\delta_{j_5j_2}) \\
&+ \varepsilon_{i_1i_4i_5}\varepsilon_{j_1j_4j_5}(\delta_{li_2}\delta_{i_5i_3} - \delta_{li_3}\delta_{i_5i_2})(\delta_{kj_2}\delta_{j_5j_3} - \delta_{kj_3}\delta_{j_5j_2}) \\
&+ \varepsilon_{i_3i_4i_5}\varepsilon_{j_3j_4j_5}(\delta_{li_1}\delta_{i_5i_2} - \delta_{li_2}\delta_{i_5i_1})(\delta_{kj_1}\delta_{j_5j_2} - \delta_{kj_2}\delta_{j_5j_1}) \\
&+ \varepsilon_{i_2i_4i_5}\varepsilon_{j_2j_4j_5}(\delta_{li_1}\delta_{i_5i_3} - \delta_{li_3}\delta_{i_5i_1})(\delta_{kj_1}\delta_{j_5j_3} - \delta_{kj_3}\delta_{j_5j_1}) \\
&+ \varepsilon_{i_2i_3i_5}\varepsilon_{j_2j_3j_5}(\delta_{li_1}\delta_{i_5i_4} - \delta_{li_4}\delta_{i_5i_1})(\delta_{kj_1}\delta_{j_5j_4} - \delta_{kj_4}\delta_{j_5j_1})] \\
&= \frac{1}{144}\,[4\,(\delta_{li_1}\delta_{kj_1}\varepsilon_{i_2i_3i_4}\varepsilon_{j_2j_3j_4} + \delta_{li_2}\delta_{kj_2}\varepsilon_{i_1i_3i_4}\varepsilon_{j_1j_3j_4} \\
&\qquad + \delta_{li_3}\delta_{kj_3}\varepsilon_{i_1i_2i_4}\varepsilon_{j_1j_2j_4} + \delta_{li_4}\delta_{kj_4}\varepsilon_{i_1i_2i_3}\varepsilon_{j_1j_2j_3}) \\
&+ (\delta_{li_3}\varepsilon_{i_1i_2i_4} - \delta_{li_4}\varepsilon_{i_1i_2i_3})(\delta_{kj_3}\varepsilon_{j_1j_2j_4} - \delta_{kj_4}\varepsilon_{j_1j_2j_3}) \\
&+ (\delta_{li_2}\varepsilon_{i_1i_3i_4} - \delta_{li_4}\varepsilon_{i_1i_3i_2})(\delta_{kj_2}\varepsilon_{j_1j_3j_4} - \delta_{kj_4}\varepsilon_{j_1j_3j_2}) \\
&+ (\delta_{li_2}\varepsilon_{i_1i_4i_3} - \delta_{li_3}\varepsilon_{i_1i_4i_2})(\delta_{kj_2}\varepsilon_{j_1j_4j_3} - \delta_{kj_3}\varepsilon_{j_1j_4j_2}) \\
&+ (\delta_{li_1}\varepsilon_{i_3i_4i_2} - \delta_{li_2}\varepsilon_{i_3i_4i_1})(\delta_{kj_1}\varepsilon_{j_3j_4j_2} - \delta_{kj_2}\varepsilon_{j_3j_4j_1}) \\
&+ (\delta_{li_1}\varepsilon_{i_2i_4i_3} - \delta_{li_3}\varepsilon_{i_2i_4i_1})(\delta_{kj_1}\varepsilon_{j_2j_4j_3} - \delta_{kj_3}\varepsilon_{j_2j_4j_1}) \\
&+ (\delta_{li_1}\varepsilon_{i_2i_3i_4} - \delta_{li_4}\varepsilon_{i_2i_3i_1})(\delta_{kj_1}\varepsilon_{j_2j_3j_4} - \delta_{kj_4}\varepsilon_{j_2j_3j_1})] \\
&= \frac{1}{144}\,[\delta_{li_1}\varepsilon_{i_2i_3i_4}(7\delta_{kj_1}\varepsilon_{j_2j_3j_4} - \delta_{kj_2}\varepsilon_{j_1j_3j_4} + \delta_{kj_3}\varepsilon_{j_1j_2j_4} - \delta_{kj_4}\varepsilon_{j_1j_2j_3}) \\
&+ \delta_{li_2}\varepsilon_{i_1i_3i_4}(7\delta_{kj_2}\varepsilon_{j_1j_3j_4} - \delta_{kj_1}\varepsilon_{j_2j_3j_4} - \delta_{kj_3}\varepsilon_{j_1j_2j_4} + \delta_{kj_4}\varepsilon_{j_1j_2j_3}) \\
&+ \delta_{li_3}\varepsilon_{i_1i_2i_4}(7\delta_{kj_3}\varepsilon_{j_1j_2j_4} + \delta_{kj_1}\varepsilon_{j_2j_3j_4} - \delta_{kj_2}\varepsilon_{j_1j_3j_4} - \delta_{kj_4}\varepsilon_{j_1j_2j_3}) \\
&+ \delta_{li_4}\varepsilon_{i_1i_2i_3}(7\delta_{kj_4}\varepsilon_{j_1j_2j_3} - \delta_{kj_1}\varepsilon_{j_2j_3j_4} + \delta_{kj_2}\varepsilon_{j_1j_3j_4} - \delta_{kj_3}\varepsilon_{j_1j_2j_4})]
\end{aligned}
$$

A.1 Integration of J_{ik}

This integral can (partly) be solved by introducing c-number sources C_{ik} and then differentiate with respect to them [61] giving

$$J^1 = \sum_{m=1}^{3} \frac{(3-m)!}{3!m!} m(-M_\chi M_\varphi)^{m-1} \overline{\chi}_k \varphi_i - \frac{1}{12} \varepsilon_{ii_1i_2} \varepsilon_{kk_1k_2} \overline{\varphi}_{i1} \overline{\varphi}_{i2} \chi_{k_1} \chi_{k_2}.$$

But with this procedure one misses another allowed term, which corresponds to the integral $I_{4,1}$ and gives

$$\begin{aligned}
J^2 &= \int dU (\overline{\varphi}_{i_1} U_{i_1 j_1} \chi_{j_1})(\overline{\varphi}_{i_2} U_{i_2 j_2} \chi_{j_2})(\overline{\varphi}_{i_3} U_{i_3 j_3} \chi_{j_3})(\overline{\chi}_k U^\dagger_{kl} \varphi_l) U_{i_4 j_4} \\
&= \frac{1}{144} \overline{\varphi}_{i_1} \chi_{j_1} \overline{\varphi}_{i_2} \chi_{j_2} \overline{\varphi}_{i_3} \chi_{j_3} \overline{\chi}_k \varphi_l \\
&\cdot \; [\delta_{li_1} \varepsilon_{i_2 i_3 i_4} (7\delta_{kj_1} \varepsilon_{j_2 j_3 j_4} - \delta_{kj_2} \varepsilon_{j_1 j_3 j_4} + \delta_{kj_3} \varepsilon_{j_1 j_2 j_4} - \delta_{kj_4} \varepsilon_{j_1 j_2 j_3}) \\
&+ \; \delta_{li_2} \varepsilon_{i_1 i_3 i_4} (7\delta_{kj_2} \varepsilon_{j_1 j_3 j_4} - \delta_{kj_1} \varepsilon_{j_2 j_3 j_4} - \delta_{kj_3} \varepsilon_{j_1 j_2 j_4} + \delta_{kj_4} \varepsilon_{j_1 j_2 j_3}) \\
&+ \; \delta_{li_3} \varepsilon_{i_1 i_2 i_4} (7\delta_{kj_3} \varepsilon_{j_1 j_2 j_4} + \delta_{kj_1} \varepsilon_{j_2 j_3 j_4} - \delta_{kj_2} \varepsilon_{j_1 j_3 j_4} - \delta_{kj_4} \varepsilon_{j_1 j_2 j_3}) \\
&+ \; \delta_{li_4} \varepsilon_{i_1 i_2 i_3} (7\delta_{kj_4} \varepsilon_{j_1 j_2 j_3} - \delta_{kj_1} \varepsilon_{j_2 j_3 j_4} + \delta_{kj_2} \varepsilon_{j_1 j_3 j_4} - \delta_{kj_3} \varepsilon_{j_1 j_2 j_4})] \\
&= \frac{1}{144} \big[\varepsilon_{i_2 i_3 i_4} (7\varepsilon_{j_2 j_3 j_4} \overline{\varphi}_l \chi_k \overline{\varphi}_{i_2} \chi_{j_2} \overline{\varphi}_{i_3} \chi_{j_3} - \varepsilon_{j_1 j_3 j_4} \overline{\varphi}_l \chi_{j_1} \overline{\varphi}_{i_2} \chi_k \overline{\varphi}_{i_3} \chi_{j_3} \\
&+ \; \varepsilon_{j_1 j_2 j_4} \overline{\varphi}_l \chi_{j_1} \overline{\varphi}_{i_2} \chi_{j_2} \overline{\varphi}_{i_3} \chi_k - \varepsilon_{j_1 j_2 j_3} \overline{\varphi}_l \chi_{j_1} \overline{\varphi}_{i_2} \chi_{j_2} \overline{\varphi}_{i_3} \chi_{j_3} \delta_{kj_4}) \overline{\chi}_k \varphi_l \\
&+ \; \varepsilon_{i_1 i_3 i_4} (7\varepsilon_{j_1 j_3 j_4} \overline{\varphi}_{i_1} \chi_{j_1} \overline{\varphi}_l \chi_k \overline{\varphi}_{i_3} \chi_{j_3} - \varepsilon_{j_2 j_3 j_4} \overline{\varphi}_{i_1} \chi_k \overline{\varphi}_l \chi_{j_2} \overline{\varphi}_{i_3} \chi_{j_3} \\
&- \; \varepsilon_{j_1 j_2 j_4} \overline{\varphi}_{i_1} \chi_{j_1} \overline{\varphi}_l \chi_{j_2} \overline{\varphi}_{i_3} \chi_k + \varepsilon_{j_1 j_2 j_3} \overline{\varphi}_{i_1} \chi_{j_1} \overline{\varphi}_l \chi_{j_2} \overline{\varphi}_{i_3} \chi_{j_3} \delta_{kj_4}) \overline{\chi}_k \varphi_l \\
&+ \; \varepsilon_{i_1 i_2 i_4} (7\varepsilon_{j_1 j_2 j_4} \overline{\varphi}_{i_1} \chi_{j_1} \overline{\varphi}_{i_2} \chi_{j_2} \overline{\varphi}_l \chi_k + \varepsilon_{j_2 j_3 j_4} \overline{\varphi}_{i_1} \chi_k \overline{\varphi}_{i_2} \chi_{j_2} \overline{\varphi}_l \chi_{j_3} \\
&- \; \varepsilon_{j_1 j_3 j_4} \overline{\varphi}_{i_1} \chi_{j_1} \overline{\varphi}_{i_2} \chi_k \overline{\varphi}_l \chi_{j_3} - \varepsilon_{j_1 j_2 j_3} \overline{\varphi}_{i_1} \chi_{j_1} \overline{\varphi}_{i_2} \chi_{j_2} \overline{\varphi}_l \chi_{j_3} \delta_{kj_4}) \overline{\chi}_k \varphi_l \\
&+ \; \varepsilon_{i_1 i_2 i_3} (7\varepsilon_{j_1 j_2 j_3} \overline{\varphi}_{i_1} \chi_{j_1} \overline{\varphi}_{i_2} \chi_{j_2} \overline{\varphi}_{i_3} \chi_{j_3} \delta_{kj_4} - \varepsilon_{j_2 j_3 j_4} \overline{\varphi}_{i_1} \chi_k \overline{\varphi}_{i_2} \chi_{j_2} \overline{\varphi}_{i_3} \chi_{j_3} \\
&+ \; \varepsilon_{j_1 j_3 j_4} \overline{\varphi}_{i_1} \chi_{j_1} \overline{\varphi}_{i_2} \chi_k \overline{\varphi}_{i_3} \chi_{j_3} - \varepsilon_{j_1 j_2 j_4} \overline{\varphi}_{i_1} \chi_{j_1} \overline{\varphi}_{i_2} \chi_{j_2} \overline{\varphi}_{i_3} \chi_k) \overline{\chi}_k \varphi_{i_4} \big] .
\end{aligned}$$

Combining similar terms (e.g. the first three terms with a coefficient of 7) and changing summation indices, we get

$$
\begin{aligned}
J^2 &= \frac{1}{144}\big[21\varepsilon_{i_1i_2i_4}\varepsilon_{j_1j_2j_4}\overline{\varphi}_l\varphi_l\overline{\chi}_k\chi_k\overline{\varphi}_{i_1}\overline{\varphi}_{i_2}\chi_{j_1}\chi_{j_2} \\
&- 7\varepsilon_{i_1i_2i_3}\varepsilon_{j_1j_2j_3}\overline{\varphi}_{i_1}\overline{\varphi}_{i_2}\overline{\varphi}_{i_3}\chi_{j_1}\chi_{j_2}\chi_{j_3}\overline{\chi}_{j_4}\varphi_{i_4} \\
&+ 2\varepsilon_{i_2i_3i_4}\varepsilon_{j_1j_2j_4}\overline{\varphi}_l\chi_{j_1}\overline{\varphi}_{i_2}\chi_{j_2}\overline{\varphi}_{i_3}\chi_k\overline{\chi}_k\varphi_l \\
&- 2\varepsilon_{i_1i_3i_4}\varepsilon_{j_1j_2j_4}\overline{\varphi}_{i_1}\chi_{j_1}\overline{\varphi}_l\chi_{j_2}\overline{\varphi}_{i_3}\chi_k\overline{\chi}_k\varphi_l \\
&- 2\varepsilon_{i_1i_2i_4}\varepsilon_{j_1j_2j_4}\overline{\varphi}_{i_1}\chi_{j_1}\overline{\varphi}_{i_2}\chi_k\overline{\varphi}_l\chi_{j_2}\overline{\chi}_k\varphi_l \\
&+ 3\varepsilon_{i_1i_3i_4}\varepsilon_{j_1j_2j_3}\overline{\varphi}_{i_1}\chi_{j_1}\overline{\varphi}_l\chi_{j_2}\overline{\varphi}_{i_3}\chi_{j_3}\overline{\chi}_{j_4}\varphi_l \\
&+ 3\varepsilon_{i_1i_2i_3}\varepsilon_{j_1j_3j_4}\overline{\varphi}_{i_1}\chi_{j_1}\overline{\varphi}_{i_2}\chi_k\overline{\varphi}_{i_3}\chi_{j_3}\overline{\chi}_k\varphi_{i_4}\big] \\
&= \frac{1}{144}\big[21\varepsilon_{i_1i_2i_4}\varepsilon_{j_1j_2j_4}\overline{\varphi}_l\varphi_l\overline{\chi}_k\chi_k\overline{\varphi}_{i_1}\overline{\varphi}_{i_2}\chi_{j_1}\chi_{j_2} \\
&- 7\varepsilon_{i_1i_2i_3}\varepsilon_{j_1j_2j_3}\overline{\varphi}_{i_1}\overline{\varphi}_{i_2}\overline{\varphi}_{i_3}\chi_{j_1}\chi_{j_2}\chi_{j_3}\overline{\chi}_{j_4}\varphi_{i_4} \\
&+ 2\varepsilon_{i_1i_2i_4}\varepsilon_{j_1j_2j_4}\overline{\varphi}_l\chi_{j_1}\overline{\varphi}_{i_1}\chi_{j_2}\overline{\varphi}_{i_2}\chi_k\overline{\chi}_k\varphi_l \\
&- 2\varepsilon_{i_1i_2i_4}\varepsilon_{j_1j_2j_4}\overline{\varphi}_{i_1}\chi_{j_1}\overline{\varphi}_l\chi_{j_2}\overline{\varphi}_{i_2}\chi_k\overline{\chi}_k\varphi_l \\
&- 2\varepsilon_{i_1i_2i_4}\varepsilon_{j_1j_2j_4}\overline{\varphi}_{i_1}\chi_{j_1}\overline{\varphi}_{i_2}\chi_k\overline{\varphi}_l\chi_{j_2}\overline{\chi}_k\varphi_l \\
&+ 3\varepsilon_{i_1i_2i_4}\varepsilon_{j_1j_2j_3}\overline{\varphi}_{i_1}\chi_{j_1}\overline{\varphi}_l\chi_{j_2}\overline{\varphi}_{i_2}\chi_{j_3}\overline{\chi}_{j_4}\varphi_l \\
&+ 3\varepsilon_{i_1i_2i_3}\varepsilon_{j_1j_2j_4}\overline{\varphi}_{i_1}\chi_{j_1}\overline{\varphi}_{i_2}\chi_k\overline{\varphi}_{i_3}\chi_{j_2}\overline{\chi}_k\varphi_{i_4}\big] \\
&= \frac{1}{144}\big[27\varepsilon_{i_1i_2i_4}\varepsilon_{j_1j_2j_4}M_\varphi M_\chi\overline{\varphi}_{i_1}\overline{\varphi}_{i_2}\chi_{j_1}\chi_{j_2} \\
&+ 252\overline{B}_\varphi B_\chi\overline{\chi}_{j_4}\varphi_{i_4} + 18\varepsilon_{i_1i_2i_4}M_\varphi B_\chi\overline{\varphi}_{i_1}\overline{\varphi}_{i_2}\overline{\chi}_{j_4} \\
&+ 18\varepsilon_{j_1j_2j_4}M_\chi\overline{B}_\varphi\chi_{j_1}\chi_{j_2}\varphi_{i_4}
\end{aligned}
$$

Adding J^1 and J^2 we obtain the complete result for J_{ik}.

B Graphs

Finally we want to comment on the generation of the different graphs appearing during this thesis. Instead of just showing all graphs needed for this work, we want to show how to get from the lowest order graphs to higher order graphs. This will hold for the series expansion of the free energy density as well as for the Polyakov loop susceptibility and the Polyakov loop effective action. As already explained in chapter (4), there are different kinds of modification.

Geometric decoration: The first and simplest modification is the shift of a plaquette or another connected path along a leading order polymer as shown in fig. (16). The order of the correction is proportional to the perimeter of the shifted path. We call this a geometric decoration.

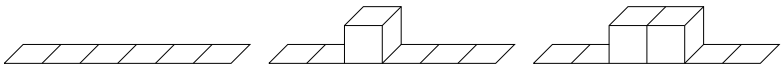

Figure 16: Generation of an $\mathcal{O}(u^4)$ and an $\mathcal{O}(u^6)$ correction to a leading order graph by shifting plaquettes.

Insertion: With shifted graphs we can explain another type of modifications. It is the insertion of plaquettes in some representation into a smaller order polymer. Examples of this are shown in fig. (17) and we call them an insertion.

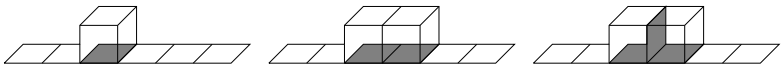

Figure 17: Higher order corrections by decorating lower order polymers with additional plaquettes in possibly higher dimensional representations.

Adding a polymer: The next type of decorations emerges from adding a complete polymer, that in our small order series usually is a cube or some double cube. Examples are shown in fig. (18). Of course it is possible to combine all three kinds of modifications.

In the following we will only show graphs, which are purely geometric decorations as all other graphs emerge from them by insertions of plaquettes or adding polymers. We will also not distingiush between different gauge

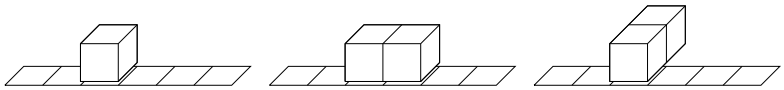

Figure 18: Clusters consisting of two polymers. The leading order graph and attached cubes or double cubes.

groups, since the only effect is a more complicated assignment of representations in the case of higher dimensional gauge groups.

B.1 Free energy density

In the corresponding chapter (4) we have seen that these graphs consist of bundles of plaquettes spanning around the temporal direction. Up to now we addressed only graphs with a cross-sectional perimeter of $l = 4$, but we also have to consider larger perimeters for the smaller N_τ.

B.1.1 Perimeter $l = 4$:

According to the discussion in the corresponding chapter it is possible to sum up the contributions of the leading order graphs. This can also be done if there is a geometric decoration. Thus we will only show graphs with different geometric decorations. It is obvious that other contributing graphs can be obtained by inserting either plaquettes or slits or both.

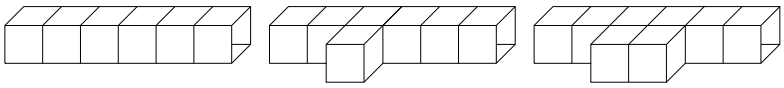

Figure 19: Left: Leading order polymer, the tube of $\mathcal{O}(u^{4N_\tau})$. Middle: One shifted plaquette, correction $\mathcal{O}(u^4)$. Right: Two adjacent shifted plaquettes, correction $\mathcal{O}(u^6)$.

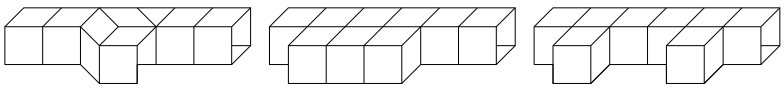

Figure 20: Left: Two adjacent plaquettes shifted from the tube, correction $\mathcal{O}(u^6)$. Middle: Three adjacent plaquettes shifted, correction $\mathcal{O}(u^8)$. Right: Two non-adjacent plaquettes shifted, correction $\mathcal{O}(u^8)$.

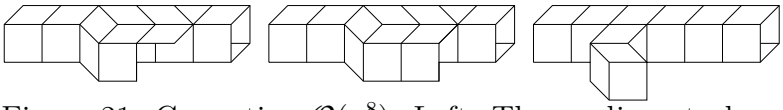

Figure 21: Correction $\mathcal{O}(u^8)$: Left: Three adjacent plaquettes shifted. Middle: Four adjacent plaquettes shifted. Right: One plaquette shifted from a $\mathcal{O}(u^4)$ correction polymer.

B.1.2 Perimeter $l = 6, 8$:

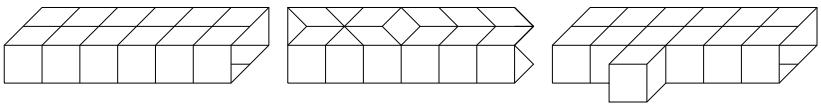

Figure 22: Left: Correction $\mathcal{O}(u^{2N_\tau})$. Middle: Two unfolded and two added plaquettes to a $\mathcal{O}(u^{6N_\tau})$ polymer. Right: One shifted plaquette from a $\mathcal{O}(u^{6N_\tau})$ polymer.

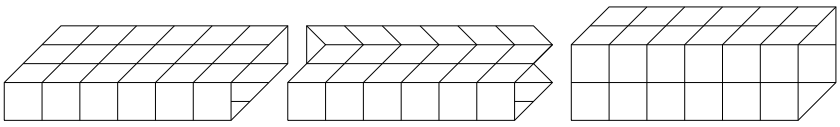

Figure 23: Correction $\mathcal{O}(u^{4N_\tau})$: Three examples of polymers with a perimeter $l = 8$.

B.2 Polyakov loop susceptibility

In this case we have to insert Polyakov loop source terms at different lattice sites. Polyakov loops at distance $x \geq 1$ have a leading order contribution $\Phi \sim u^{xN_\tau}$ and thus larger distances are suppressed for higher N_τ. Consequently we will display examples of the contributing graphs sorted by their distance. To keep the drawing simple we will omit the lines for the Polyakov loop sources as it is obvious that they have to be placed at the edges of the graphs.

B.2.1 Distance $x = 1$:

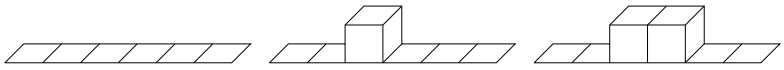

Figure 24: Left: Leading order polymer $\mathcal{O}(u^{N_\tau})$. Middle: One plaquette shifted, correction $\mathcal{O}(u^4)$. Right: Two adjacent plaquettes shifted, correction $\mathcal{O}(u^6)$.

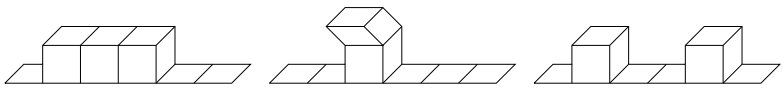

Figure 25: Correction $\mathcal{O}(u^8)$. Left: Three adjacent plaquettes shifted. Middle and right: One plaquette shifted from a $\mathcal{O}(u^4)$ polymer.

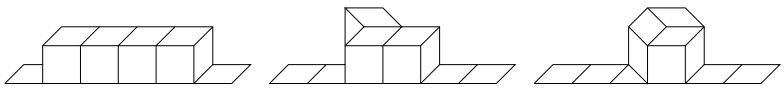

Figure 26: Correction $\mathcal{O}(u^{10})$. Left: Four adjacent plaquettes shifted. Middle: One plaquette shifted from a $\mathcal{O}(u^6)$ polymer. Right: Two angled plaquettes shifted from a $\mathcal{O}(u^4)$ polymer.

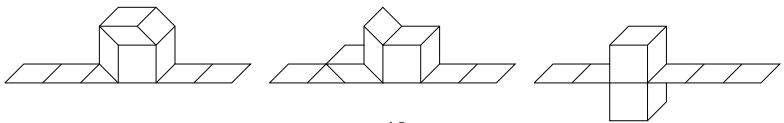

Figure 27: Correction $\mathcal{O}(u^{10})$. Left and middle: Two angled plaquettes shifted from a $\mathcal{O}(u^4)$ polymer. Right: Two plaquettes shifted at the same position in different directions. This graph is without insertion only allowed for $SU(3)$.

B.2.2 Distance $x = 2$:

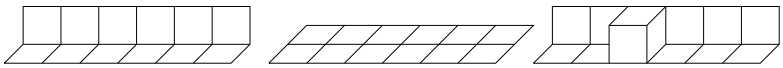

Figure 28: Left and middle: Polymers with correction of $\mathcal{O}(u^{N_\tau})$. Right: Correction of $\mathcal{O}(u^{N_\tau+2})$ by unfolding two and adding two plaquettes.

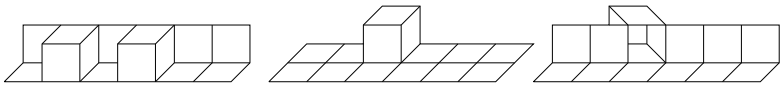

Figure 29: Corrections $\mathcal{O}(u^{N_\tau+4})$. Left: Four unfolded and four added plaquettes. Middle and right: One plaquette shifted from $\mathcal{O}(u^{2N_\tau})$ polymers.

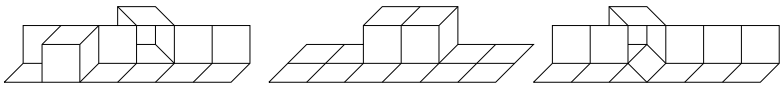

Figure 30: Corrections $\mathcal{O}(u^{N_\tau+6})$. Left: Combination of unfolding, adding and shifting plaquettes. Middle and right: Two plaquettes shifted from $\mathcal{O}(u^{2N_\tau})$ polymers.

B.2.3 Distance $x = 3, 4, 5$:

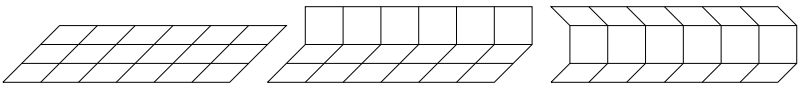

Figure 31: Corrections $\mathcal{O}(u^{2N_\tau})$. The temporal projections of these polymers correspond to self avoiding walks.

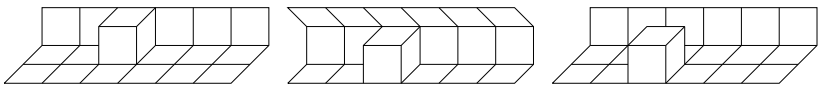

Figure 32: Left and middle: Corrections of $\mathcal{O}(u^{2N_\tau+2})$ by folding and adding plaquettes. Right: One plaquette shifted to give a correction of $\mathcal{O}(u^{2N_\tau+4})$.

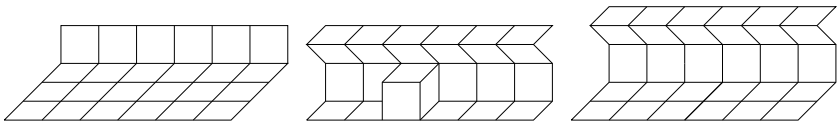

Figure 33: Examples of corrections of $\mathcal{O}(u^{3N_\tau})$ (left), $\mathcal{O}(u^{3N_\tau+2})$ (middle) and $\mathcal{O}(u^{4N_\tau})$ (right).

B.3 Polyakov loop effective action

The graphs needed for this calculation are identical to those of the Polyakov loop susceptibility with distance $x = 1$. Thus we will show here examples of the $\mathcal{O}(u^{12})$, which were included only in the calculation of the effective coupling for the Polyakov loop effective action.

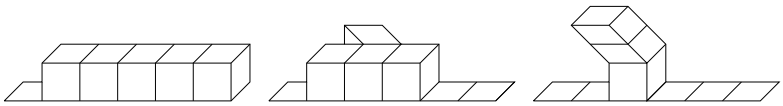

Figure 34: Correction $\mathcal{O}(u^{12})$. Left: Five adjacent plaquettes shifted. Middle and right: One plaquette shifted from $\mathcal{O}(u^8)$ polymers.

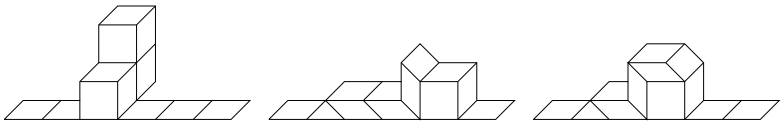

Figure 35: Correction $\mathcal{O}(u^{12})$. Left: One plaquette shifted from a $\mathcal{O}(u^8)$ polymer. Middle and right: Three adjacent plaquettes shifted from $\mathcal{O}(u^4)$ polymers.

References

[1] H. Fritzsch, M. Gell-Mann and H. Leutwyler,
Phys. Lett. B **47** (1973) 365.

[2] D. J. Gross and F. Wilczek,
Phys. Rev. Lett. **30** (1973) 1343.

[3] H. D. Politzer,
Phys. Rev. Lett. **30** (1973) 1346.

[4] A. M. Polyakov,
Phys. Lett. B **72** (1978) 477.

[5] L. Susskind,
Phys. Rev. D **20** (1979) 2610.

[6] E. V. Shuryak,
Phys. Lett. B **78** (1978) 150 [Sov. J. Nucl. Phys. **28** (1978 YAFIA,28,796-808.1978) 408.1978 YAFIA,28,796].

[7] K. G. Wilson,
Phys. Rev. D **10** (1974) 2445.

[8] Y. Aoki, G. Endrodi, Z. Fodor, S. D. Katz and K. K. Szabo,
Nature **443** (2006) 675.

[9] A. J. Guttman, in *Phase Transitions and Critical Phenomena*,
Vol. 13, p.1, eds. C. Domb and J. L. Lebowitz, Academic Press, London, 1989.

[10] P. de Forcrand and O. Philipsen,
JHEP **0811** (2008) 012.

[11] O. Philipsen,
Eur. Phys. J. ST **152** (2007) 29.

[12] M. E. Peskin and D. V. Schroeder,
An Introduction to Quantum Field Theory
(Reading, USA: Addison-Wesley (1995) 842 p).

[13] J. I. Kapusta and C. Gale,
Finite-temperature field theory: Principles and applications,
(Cambridge University Press, Cambridge, 2006).

[14] L. D. Faddeev and V. N. Popov,
Phys. Lett. B **25** (1967) 29.

[15] A. D. Linde,
Phys. Lett. B **100** (1981) 37.

[16] L. D. Landau and E. M. Lifschitz,
Lehrbuch der Theoretischen Physik V: Statistische Physik,
Akademie Verlag, Berlin (1970).

[17] K. Huang,
Statistical Mechanics
John Wiley & Sons, New York (1987) 493 p.

[18] P. de Forcrand, S. Kim and O. Philipsen,
PoS **LAT2007** (2007) 178.

[19] G. Boyd, J. Engels, F. Karsch, E. Laermann, C. Legeland, M. Lutgemeier and B. Petersson,
Nucl. Phys. B **469**, 419 (1996).

[20] J. Fingberg, U. M. Heller and F. Karsch,
Nucl. Phys. B **392** (1993) 493.

[21] I. Montvay and G. Münster,
Quantum Fields on a Lattice,
Cambridge University Press, Cambridge, 1994

[22] S. Capitani,
Phys. Rept. **382** (2003) 113.

[23] T. DeGrand and C. E. Detar,
Lattice Nethods for Quantum Chromodynamics,
New Jersey, USA: World Scientific (2006) 345 p.

[24] H. B. Nielsen and M. Ninomiya,
Phys. Lett. B **105** (1981) 219.

[25] K. Jansen,
arXiv:0810.5634 [hep-lat].

[26] D. B. Kaplan,
Phys. Lett. B **288** (1992) 342.

[27] H. Neuberger,
Phys. Lett. B **417** (1998) 141.

[28] R. Frezzotti, P. A. Grassi, S. Sint and P. Weisz [Alpha collaboration],
JHEP **0108** (2001) 058.

[29] M. Creutz,
JHEP **0804** (2008) 017.

[30] P. Rossi and U. Wolff,
Nucl. Phys. B **248** (1984) 105.

[31] F. Karsch and K. H. Mutter,
Nucl. Phys. B **313** (1989) 541.

[32] M. Fromm and P. de Forcrand,
arXiv:0811.1931 [hep-lat].

[33] G. Münster,
Nucl. Phys. B **190** (1981) 439 [Erratum-ibid. B **200** (1982 ERRAT,B205,648.1982) 536].

[34] J. M. Drouffe and J. B. Zuber,
Phys. Rept. **102** (1983) 1.

[35] J. Polonyi and K. Szlachanyi,
Phys. Lett. B **110**, 395 (1982).

[36] F. Green,
Nucl. Phys. B **215** (1983) 83.

[37] F. Green and F. Karsch,
Nucl. Phys. B **238**, 297 (1984).

[38] M. Gross and J. F. Wheater,
Nucl. Phys. B **240** (1984) 253.

[39] M. Billo, M. Caselle, A. D'Adda and S. Panzeri,
Nucl. Phys. B **472**, 163 (1996).

[40] P. Hasenfratz and F. Karsch,
Phys. Lett. B **125** (1983) 308.

[41] M. Creutz,
J. Math. Phys. **19** (1978) 2043.

[42] A. Velytsky,
Int. J. Mod. Phys. C **19** (2008) 1079.

[43] I. L. Bogolubsky, V. K. Mitrjushkin, A. V. Sergeev, M. Muller-Preussker and H. Stuben,
Nucl. Phys. Proc. Suppl. **129** (2004) 611.

[44] F. Karsch, K. Redlich and A. Tawfik,
Eur. Phys. J. C **29** (2003) 549.

[45] J. Langelage, G. Münster and O. Philipsen,
JHEP **0807** (2008) 036.

[46] M. Campostrini, A. Pelissetto, P. Rossi and E. Vicari,
Phys. Rev. E **65** (2002) 066127.

[47] R. Ben-Av, H. G. Evertz, M. Marcu and S. Solomon,
Phys. Rev. D **44** (1991) 2953.

[48] F. Karsch, E. Laermann and C. Schmidt,
Phys. Lett. B **520** (2001) 41

[49] S. Kim, Ph. de Forcrand, S. Kratochvila and T. Takaishi,
PoS **LAT2005**, 166 (2006)

[50] T. Celik, T. Firat, Y. Gunduc and M. Onder,
Phys. Rev. D **35**, 3958 (1987).

[51] A. Roberge and N. Weiss,
Nucl. Phys. B **275** (1986) 734.

[52] E. Braaten and R. D. Pisarski,
Nucl. Phys. B **337** (1990) 569.

[53] B. Svetitsky and L. G. Yaffe,
Nucl. Phys. B **210** (1982) 423.

[54] M. Tassler,
PhD thesis.

[55] T. Jolicoeur, H. Kluberg-Stern, M. Lev, A. Morel and B. Petersson,
Nucl. Phys. B **235**, 455 (1984).

[56] J. Hoek and J. Smit,
Nucl. Phys. B **263**, 129 (1986).

[57] A. Ohnishi, N. Kawamoto and K. Miura,
J. Phys. G **34**, S655 (2007).

[58] K. Miura, T. Z. Nakano, A. Ohnishi and N. Kawamoto,
arXiv:0907.4245 [hep-lat].

[59] G. Faldt and B. Petersson,
Nucl. Phys. B **265** (1986) 197.

[60] P. H. Damgaard, N. Kawamoto and K. Shigemoto,
Nucl. Phys. B **264** (1986) 1.

[61] S. I. Azakov and E. S. Aliev,
Phys. Scripta **38** (1988) 769.

[62] M. E. Fisher,
Physica (Utrecht) 86-98, 590 (1977).